An Analysis of *Agrobacterium tumefaciens* Attachment to Leaf Tissues and Subsequent Plant Transformation

By

CHRISTOPHER WILLIAM SIMMONS
B.S. (University of California, Davis) 2005
M.S. (University of California, Davis) 2007

DISSERTATION

Submitted in partial satisfaction of the requirements for the degree of

DOCTOR OF PHILOSOPHY

in

Biological Systems Engineering

in the

OFFICE OF GRADUATE STUDIES

of the

UNIVERSITY OF CALIFORNIA

DAVIS

Approved:

____

Prof. Jean VanderGheynst, Chair

____

Prof. Karen McDonald

____

Prof. Nitin Nitin

Committee in Charge

2011

Abstract

Plant-based expression systems offer a number of benefits compared to traditional microbial expression systems for producing recombinant proteins, including the ability to perform certain post-translational protein modifications and the potential to reduce energy inputs due to their autotrophic nature. While most commercially available transgenic crops are stable transformants expressing genes that confer agronomic traits to the plant, the possibility exists for high-level plant-based production of recombinant proteins that have inherent value not just to growers, but to consumers and other industries directly. Transient expression of transgenes *in planta* can provide higher levels of recombinant protein in a fraction of the time needed to generate stably transformed plants. Furthermore, the rapid nature of transient expression facilitates recombinant protein production in harvested plant tissues. The bacterium *Agrobacterium tumefaciens* is commonly used to induce transient expression in plant tissue via its endogenous ability to transform plants. However, certain aspects of the *A. tumefaciens* infection process are not well understood. Specifically, the fate of the bacteria after entering leaf tissue is largely unknown in part due to lack of knowledge regarding what factors affect the attachment of bacteria to leaf cells. Understanding how bacteria distribute themselves within leaf tissue, infiltration factors that influence bacterial attachment, and the relationship between attachment levels and *in planta* transgene expression may provide avenues for improving transformation efficiency and expression levels.

To quantify *A. tumefaciens* attached to leaf cells, a rapid *in situ* assay was developed. The use of fluorescent stains was investigated for labeling bacteria in lieu of transforming cells to express a fluorescent protein. Several vital dyes and nucleic acid

stains were tested for their ability to yield a detectable signal against a leaf tissue background using fluorescent confocal microscopy. The fluorescent nucleic acid stain Syto16 was found to perform best. Furthermore, Syto16 was found to have no significant affect on the viability or virulence of *A. tumefaciens*, as indicated by plate counting and agroinfiltration assays. Subsequently, a protocol was developed for quantifying bound bacteria in micrographs of sections of infiltrated leaf tissue, yielding measurements of attached bacteria per volume leaf tissue.

The *in situ* bacterial attachment assay was used to study *A. tumefaciens* attachment in response to infiltration factors including bacterial density, vacuum intensity, and surfactant concentration in both lettuce and switchgrass harvested leaf tissue. While vacuum level influenced the volume of bacterial suspension that entered leaf tissue, no significant effect on bacterial attachment levels was observed in either lettuce or switchgrass in response to varying vacuum intensity levels. For lettuce, surfactant concentration in the bacterial suspension had a positive effect on both the volume of suspension that entered leaf tissue and the amount of bacteria that attached to leaf cells. Alternately, addition of surfactant did not correspond to larger volumes of suspension infiltrated into switchgrass leaf tissue and there was no effect on bacterial binding. For both lettuce and switchgrass, bacterial adhesion was most sensitive to changes in the density at which the bacteria were infiltrated into leaf tissue. Levels of attached bacteria in lettuce leaves versus the density of infiltrated bacteria exhibited a saturation trend. Likewise, there was a positive relationship between bacterial density and attachment rates in switchgrass, although the relationship was linear with no indication of saturation at the highest bacterial density. In light of its dominant effect on

adhesion levels, infiltrated bacterial density was varied and *in planta* transient expression levels of an agroinfiltrated β-glucuronidase gene were measured in lettuce and switchgrass leaves. For the range of bacterial densities tested in lettuce, lower bacterial densities yielded a constant expression level. However, expression levels fell dramatically at the highest observed attachment level. These results show that infiltration parameters can be used to control *Agrobacterium* attachment density and that attachment levels can influence transgene transient expression levels in lettuce. However, the results also reveal that optimizing expression levels is not simply a matter of promoting maximal bacterial attachment, as attachment levels beyond a threshold correspond to plant responses that ultimately lower transgene transient expression levels. Alternately, two methods for measuring β-glucuronidase activity in agroinfiltrated switchgrass demonstrated that *in planta* transgene transient expression levels remain low regardless of *Agrobacterium* attachment levels. Spectrophotometric activity assays performed on leaf extracts revealed no significant β-glucuronidase activity while staining for β-glucuronidase activity showed extremely low-levels of activity signified by microscopic stained regions. The lack of high-level transgene transient expression in response to altered *Agrobacterium* attachment levels suggests that recalcitrance of switchgrass to agroinfiltration does not lie at the level of *Agrobacterium* attachment.

Acknowledgements

I thank my advisor, Prof. Jean VanderGheynst, for her profound mentorship over the course of my higher education. Her tireless dedication to education and creating opportunities for her students has afforded me invaluable professional training that has shaped me as an engineer and aspiring educator. I am proud to have learned under her. I am also grateful to my qualifying exam and dissertation committees, collectively comprised of Profs. Julia Fan, Bryan Jenkins, John Labavitch, Karen McDonald, Nitin Nitin, Shrini Upadhyaya, and Jean VanderGheynst, for their encouragement and guidance. I also thank my labmates and other graduate student friends for their comradery and support. I appreciate my family for their unending abetment and taking pride in what I do. Finally, I am incalculably grateful to my loving, caring fiancé, Maelene, for whom I do all things.

Table of Contents

List of Tables

List of Figures

Chapter 1 – Development of *Agrobacterium tumefaciens* imaging methodology

1.1 Introduction

Bacterial imaging traditionally involves labeling of cells with a fluorescent or chemiluminescent tag to emit a detectable signal. Labeling options are limited when the vitality of bacteria, in addition to the native behavior of pathways of interest, must be preserved post-labeling. Recombinant expression of fluorescent proteins (e.g., green fluorescent protein) or enzymes that catalyze chemiluminescent reactions (e.g., luciferase) have commonly been used in these applications. As an alternative, certain stains may also be useful under these criteria. Staining protocols frequently require less time compared to the cloning needed to establish bacteria expressing recombinant proteins. As a result, staining may offer higher throughput in certain applications. These tags encompass many forms, from stains that have affinity for general molecular groups, such as nucleic acids and polypeptides, to those that have more targeted binding, such as labeled antibodies and nucleic acid probes that associate with specific amino- and nucleic-acid arrangements, respectively.

Several staining modalities exist for fluorescently labeling live bacteria. These include nucleic acid stains, protein stains, and vital dyes, which diffuse through intact membranes, but don’t necessarily bind any cellular components. A representative stain from each of these classes was examined for compatibility with *Agrobacterium tumefaciens*. Stains were evaluated based on their *in vivo* signal intensity against a leaf tissue background. Following this screening, stained bacteria were assayed for virulence, as indicated by their ability to transfer T-strands to plant cells, in comparison to unstained bacteria. In this way, a methodology was developed to facilitate *in situ* imagining of *A. tumefaciens* within leaf tissue while preserving the native virulence of the bacteria.

Such a technique is useful for monitoring bacterial attachment to leaf tissue during *A. tumefaciens* infection. Previous methods of monitoring *A. tumefaciens* attachment to plant tissue have relied on plating homogenates of infected plant cells and counting colonies (Matthysse et al., 1978; Matthysse, 1987; Reuhs et al., 1997) in addition to light and electron microscopy of bacteria bound to plant cells (Matthysse et al., 1978; Douglas et al., 1982; Graves et al., 1988; Matthysse et al., 2005; Clauce-Coupel et al., 2008; Verma et al., 2008) Assays based on viable bacterial counts from plated homogenized plant matter provide no information regarding the distribution of *A. tumefaciens* within the plant tissue. As a result, it is an inadequate approach for determining potential bacterial preferences for specific cells types within plant tissue or for gauging the ability of the bacteria to penetrate into intact tissue. Light and electron microscopy are best suited for visualizing attachment of *A. tumefaciens* to single plant cells and smooth surfaces and are unable to distinguish bacteria that are attached beyond the exposed surface of porous plant tissue samples. Electron microscopy, in particular, may alter apparent bacterial attachment by disturbing cells during sample preparation (Matthysse, 1986). Moreover, the wealth of attachment studies looking solely at plant cell cultures as hosts for *A. tumefaciens* neglect the three-dimensional structural aspects that may affect bacterial attachment in applications where intact plant tissue is agroinfiltrated. Fluorescence microscopy overcomes many of the drawbacks associated with light and electron microscopy. For instance, bacteria emitting a fluorescent signal can be distinguished from the background more easily and in a more reproducible quantitative fashion compared to light and electron microscopy, where it is largely up to the viewer to determine what elements of an image represent bacteria. Additionally, it may be possible to probe deeper into tissue with fluorescence microscopy relative to these other imaging modalities due to fluorescent signals' ability to pass through plant tissue that would normally obscure bacteria during light or electron microscopy.

Agrobacterium tumefaciens expressing GFP has been used to visualize bacteria bound to a variety of plant tissues and surfaces (Finer and Finer, 2000; Ramey et al., 2004; Merritt et al., 2007). However, fluorescent labeling of *A. tumefaciens* via staining has not been studied for examining *A. tumefaciens* binding. Furthermore, imaging and quantifying fluorescently labeled *A. tumefaciens* within plant tissue, as would be relevant in leaves vacuum-infiltrated with bacteria, has not been performed.

1.2 Materials and Methods

1.2.1 Bacterial strains and culture

Agrobacterium tumefaciens strain C58C1 (Wroblewski et al., 2005) was used. C58C1 harbors the binary vector pTFS40 (British Sugar Corporation, Norwich, UK) derived from the host vector pSLJ1006 (Jones et al., 1992), which contains an intronated-*uidA* gene on its T-strand. Furthermore, the strain contains the helper plasmid pCH32 (Hamilton, 1997), which constitutively expresses VirG and VirE proteins, eliminating the need for chemical induction of virulence in the bacteria. These proteins are transcription factors that promote the expression of all *A. tumefaciens* virulence operons. pTFS40 and pCH32 contain kanamycin and tetracycline resistance selection markers, respectively. C58C1 was grown in YEP media (10 g/l yeast extract, 10 g/l peptone, 5 g/l NaCl) with 50 mg/l kanamycin and 5 mg/l tetracycline at 28 °C with 150 rpm agitation. For plated bacteria, 50 µl of 500 CFU/ml suspension was inoculated onto YEP agar plates (YEP with 10 g/L agarose) supplemented with kanamycin and tetratcycline. Plates were sealed and incubated at 28 °C.

1.2.2 Plant materials

Leaves from Romaine lettuce (*Lactuca sativa* valmaine) were used for all experiments. Seeds from each species were germinated by sealing them in Petri dishes lined with paper towels moistened with distilled deionized water. Seeds were incubated in plates for three to four days in darkness at room temperature. Following germination, seedlings were transferred to pots containing a soil mix (1 part ground Canadian sphagnum, 1 part uniform coarse sand, 1 part white pumice, 1 part redwood compost, 1.78 kg/m^3 oyster shell, 1.78 kg/m^3 dolomite, 1.78 kg/m^3 single super phosphate). Potted seedlings were grown in a greenhouse where average temperature and relative humidity varied between 27.2 °C and 14.4 °C and 83% and 30%, respectively. Seedlings were watered hourly for eight to nine hours each day via two minutes of misting with reverse osmosis-purified water containing 0.6 g/l Grow More 4-18-38 fertilizer (Grow More, Inc., Gardena, CA), 1.59 g/l calcium nitrate, and 0.6 g/l magnesium sulfate. The pH of the water ranged between 5 and 6. After one to two weeks, plants were transferred to a drip irrigation system where they were watered to saturation twice daily with the previously described fertilized water. Lettuce leaves were harvested from the second and third whorls (counting from the outermost leaves) after 4 to 6 weeks of growth. Leaves were washed with distilled deionized water and stored at 4 °C at 100% relative humidity until use. Leaves were not stored for more than two hours before use.

1.2.3 Preparation of leaf explants

A 1 cm cork borer was used to punch disks from lettuce leaf tissue. Disks were obtained from the second quarter of the leaf (from the top), taking care to avoid the leaf edges and midrib (Figure 1.1).

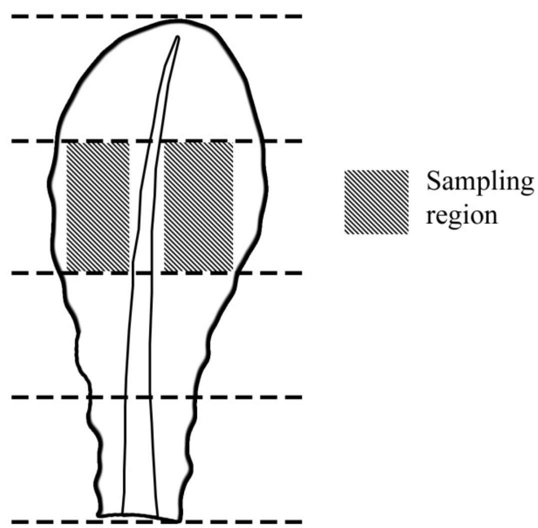

Figure 1.1. Leaf regions used for obtaining leaf disk samples.

1.2.4 Staining of Agrobacterium tumefaciens

50 ml aliquots of C58C1 in YEP medium were centrifuged at 7,000×g for 10 minutes at 4 °C. Pellets were resuspended in sterile distilled water to achieve 10^{10} CFU/ml using a previously determined equation relating the absorbance of a bacterial culture to its bacterial density ($[CFU/ml] = 4\times10^{9}[A_{590}] - 10^{8}$, where A_{590} is the absorbance of light at 590 nm of a suspension of *A. tumefaciens* in water with a path

length of 0.72 cm). Several stains were examined, including Syto 16 green fluorescent nucleic acid stain (Invitrogen, Carlsbad, CA), a double-stranded DNA stain; Alexa Fluor 488 carboxylic acid, succinimidyl ester (Alexa 488 CA SE) (Invitrogen), a protein stain; and carboxyfluoroscein diacetate succinimidyl ester (CFDA SE), a vital dye, from Sigma-Alrich (St. Louis, MO). Stain was added to 1 ml aliquots of 10^{10} CFU/ml suspension to achieve a concentration of 10 μM. Cells were incubated with stain for 2 hours at room temperature in darkness. Stained cells were washed three times in water. Each wash consisted of centrifugation at 10,000×g for 10 minutes at 4 °C followed by resuspension of the pellet in 14 ml of sterile distilled water. Following the final wash, cells were resuspended to achieve 10^9 CFU/ml. For treatments containing surfactant, Break-Thru S 240 (Goldschmidt Chemical, Hopewell, VA) was added to the washed cells to varying concentrations depending on the specific experiment.

1.2.5 Infiltration of Agrobacterium tumefaciens into leaf tissue

Suspensions of *A. tumefaciens* were vacuum-infiltrated into leaf tissue as previously described (Joh et al., 2005; Simmons et al., 2009). Leaf explants were weighed prior to vacuum application and then placed in 15 ml tubes containing 4 to 5 ml of bacterial suspension. Wads of polyester mesh were inserted in the tubes to ensure that leaf tissue was completely submerged. Uncapped tubes were placed in a vacuum chamber connected to a vacuum pump. The submerged leaves were subjected to various reduced pressures for 7.5 minutes. Following vacuum, leaves were removed from tubes, blotted dry, weighed, and sealed within Petri dishes lined with moistened gauze.

Infiltrated leaves were incubated at 20 to 22 °C in darkness. The volume of infiltrated suspension was taken to be the difference between the pre- and post-vacuum leaf masses.

1.2.6 Measurement of viable bacteria in infiltrated leaf tissue

Four aliquots of five *L. sativa* leaf explants were infiltrated with Syto 16-stained *A. tumefaciens* at 25 kPa. Infiltrated aliquots were incubated as described in section 1.2.4 for 0, 24, 48, and 72 hours. Following incubation, aliquots were washed three times in 40 mL sterile distilled deionized (dd) water by vortexing. Washed leaf explants were lysed by grinding in an ice-cooled mortar and pestle with 5 ml PBS (140 mM NaCl, 3 mM KCl, 8 mM sodium phosphate, 1.5 mM potassium phosphate, pH 7.5). Extracts were diluted 1/3000 in PBS and 50 μl of dilution were plated onto YEPKT agar plates as described in section 1.2.1. Colonies were counted 48 hours after plating.

1.2.7 Sectioning of leaf tissue

A Vibratome 1000P manual vibrating microtome from Leica Microsystems, Inc. (Bannockburn, IL) was used to section leaf tissue. For live tissue, leaf explants were braced by sliding them into a slit cut into a cube of carrot root. Leaf tissues that underwent histochemical staining were embedded in a cube of apple to provide support during sectioning. Leaf tissue was submerged in distilled water during sectioning. Blade vibration amplitude and advancement speed were both set to 5 on the machine. Sections were removed from the Vibratome and placed into tissue culture plate wells filled with distilled water. The sections were washed to remove unbound bacteria by gently stirring them in water using a soft-bristled brush.

1.2.8 Histochemical staining of leaf tissue

A histochemical assay to detect GUS activity (Jefferson, 1987; Joh et al., 2005) was used to map areas of recombinant GUS expression in agroinfiltrated leaf tissue. Following agroinfiltration, leaf tissue was submerged in 4 to 5 ml of histochemical staining buffer (100 mM sodium phosphate, pH 7.0; 10 mM EDTA, pH 8.0; 0.5 mM potassium ferrocyanide, 0.5 mM potassium ferricyanide, 0.006% Triton X-100) containing 1 mg/ml 5-bromo-4-chloro-3-indolyl-β-D-glucuronic acid, cyclohexylammonium salt (X-gluc). In brief, GUS acts to cleave X-gluc, resulting in 5-bromo-4-chloro-3-indolyl as a primary product. Once oxidized, as catalyzed by the oxidizing agents potassium ferri- and ferro-cyanide, this product dimerizes to form a vibrant indigo precipitate. Submerged leaves were subjected to 25 kPa for 5 minutes to infiltrate the staining solution into leaves. Leaves were incubated in staining solution for 8 hours. Stained leaves were soaked in 70% ethanol to remove chlorophyll and enhance the contrast of stained areas.

1.2.9 Imaging of labeled Agrobacterium tumefaciens and leaf tissue

An IX71 fluorescent microscope equipped with an IX2-UCB control box, U-RFL-T power supply with 100 W mercury burner, IX2-DSU disk scanning unit, and TH4-100 power supply with halogen lamp, all from Olympus (Tokyo, Japan), in addition to an ORCA-ER camera from Hamamatsu Photonics (Hamamatsu, Japan), was used for imaging labeled *A. tumefaciens* and leaf tissue at micro scales. Methamorph Basic version 7.6.5.0 from Olympus was used to operate the microscope and analyze signal intensities within images. The microscope was equipped with various excitation filters in addition to dichroic mirrors and emission filters. These elements were used in concert to measure particular emission wavelengths from samples excited with light of specific wavelengths (Table 1.1).

Table 1.1. Combinations of excitation and emission wavelengths examined.

Excitation wavelength (nm)	Emission wavelength (nm)
355	460
488	520
550	576
650	666

For macroscopic imaging of histochemical stained leaves, a MultiImage II FluorChem Xplor imager with AlphaView software (version 2.0.1.2) from Alpha Innotech (Santa Clara, CA) was used. Leaves were illuminated with the imager's XplorBright illuminator and images were exposed for 1040 ms. Photoshop CS3 version 10.0.1 from Adobe Systems Inc. (San Jose, CA) was used to measure the area of stained tissue in leaves. Images of stained leaves were converted to binary by setting a threshold of 100 (8-bit). The area of signal in each leaf disk was measured and normalized against the volume of bacterial suspension infiltrated into the leaves. Additionally, Photoshop was used to adjust the brightness and contrast of micrographs in order to optimize their appearance in print.

1.2.10 Parameter fitting and statistical analysis

MATLAB R2009a version 7.8.0.347 from MathWorks (Natick, MA) was used to fit parameters in non-linear models describing data. JMP version 8.0 from SAS Institute Inc. (Cary, NC) was used to compare means and test hypotheses. Student's t-test was used to test sample mean and slope value differences from hypothesized values. Tukey's Honestly Significant Difference test was used for pairwise comparisons of means.

1.3 Results

1.3.1 Measurement of leaf autofluorescence

A 200 µm section of lettuce leaf tissue was imaged (40x, widefield) at three separate regions. At each region, the tissue was excited with light at various wavelengths. Autofluorescence at particular emission wavelengths was measured (see Table 1.1). An exposure time of 100 ms was used for all images. The autofluorescence of the tissue at each region was characterized by the average pixel intensity across the entire image for a given excitation wavelength. For each excitation wavelength used at a particular region, the ratio of the autofluorescence was determined relative to that measured at other excitation wavelengths. Mean autofluorescence ratios were calculated from the ratios corresponding to each of the three sample regions (Table 1.2, Appendix 1.1).

Table 1.2. Relative leaf autofluorescence at various excitation and emission wavelengths.

	Ex: 355 nm Em: 460 nm	Ex: 488 nm Em: 520 nm	Ex: 550 nm Em: 576 nm	Ex: 650 nm Em: 666 nm
Ex: 355 nm, Em: 460 nm	1 (0)	1.67 (0.10)	1.52 (0.13)	0.22 (0.04)
Ex: 488 nm, Em: 520 nm	0.60 (0.04)	1 (0)	0.91 (0.03)	0.13 (0.03)
Ex: 550 nm, Em: 576 nm	0.66 (0.06)	1.10 (0.03)	1 (0)	0.15 (0.04)
Ex: 650 nm, Em: 666 nm	4.60 (0.69)	7.73 (1.56)	7.03 (1.53)	1(0)

Values represent mean ratios of average pixel intensities with standard deviations given in parentheses. Values were calculated as the mean ratio of the average pixel intensity of autofluorescence at the wavelengths given in the vertical axis to the average pixel intensity at the wavelengths given in the horizontal axis. $n = 3$ for each autofluorescence measurement.

The data show that, of the excitation wavelengths examined, 488 nm resulted in the lowest amount of autofluorescence by the leaf tissue. This is indicated by the fact that autofluorescence ratios at 488 nm relative to all other wavelengths are all significantly below 1 ($\alpha = 0.05$).

1.3.2 Screening of stains for labeling Agrobacterium tumefaciens

Aliquots of *A. tumefaciens* strain C58C1 were stained with 10 μM Syto 16 nucleic acid stain, Alexa 488 CA SE, and CFDA SE. 10 μl of stained cells were mounted on slides and imaged at 40x magnification using confocal microscopy. Three separate images were obtained for each group of stained cells using an exposure time of 5 seconds. The average pixel intensity (12-bit) of each image was measured (Table 1.3, Appendix 1.2).

Table 1.3. Mean average pixel intensity values for images of *A. tumefaciens* labeled with various stains. n = 3.

Stain	mean average pixel intensity (standard deviation)*
Syto 16 nucleic acid stain	228.19 (0.40) A
CFDA SE	213.28 (0.11) BC
Alexa 488 CA SE	212.59 (0.93) B
none	214.95 (0.85) C

*Values not connected by the same letter are significantly different ($\alpha = 0.05$).

Of the dyes tested, only Syto 16 nucleic acid stain yielded an average pixel intensity that is significantly higher than background.

1.3.3 Optimization of staining conditions

A. tumefaciens was stained with various concentrations of Syto 16 nucleic acid stain. 10 μl of bacterial suspension from each staining treatment was mounted on slides and imaged at 40x using confocal microscopy. Each slide was imaged in three random locations. For each image, a signal threshold was selected to best isolate cells from the background and eliminate ghost signals stemming from bacterial movement during the exposure period. Moreover, signals were filtered to only accept those with a shape factor between 0.8 and 1.0, further reducing the confounding effects of ghost signals. The average pixel intensity of each cell in an image was measured. The average of these values for all cells in a given image was calculated to determine the cell mean average pixel intensity for that image. Additionally, the average pixel intensity of the cell with the greatest signal in each image was recorded as the cell maximum average pixel intensity value (Figure 1.2, Appendix 1.3).

A saturation function was fitted to the data (Appendix 1.4)

$$I = \frac{I_{max}S}{S_{1/2}+S} \qquad \text{(eq. 1.1)}$$

where I is the 12-bit average pixel intensity per cell (either maximum or mean), I_{max} is the maximum 12-bit average pixel intensity per cell, S is the concentration of dye used during staining of cells, and $S_{1/2}$ is the dye concentration necessary for achieving half the theoretical maximum signal intensity in stained cells. The values of I_{max} and $S_{1/2}$ were estimated by non-linear regression. For the cell mean average pixel intensity versus stain concentration data set, I_{max} and $S_{1/2}$ were estimated to be 3227.1 and 9.9 μM, respectively. Likewise, for the cell maximum average pixel intensity versus stain concentration data set, I_{max} and $S_{1/2}$ were estimated to be 4736.0 and 9.3 μM, respectively.

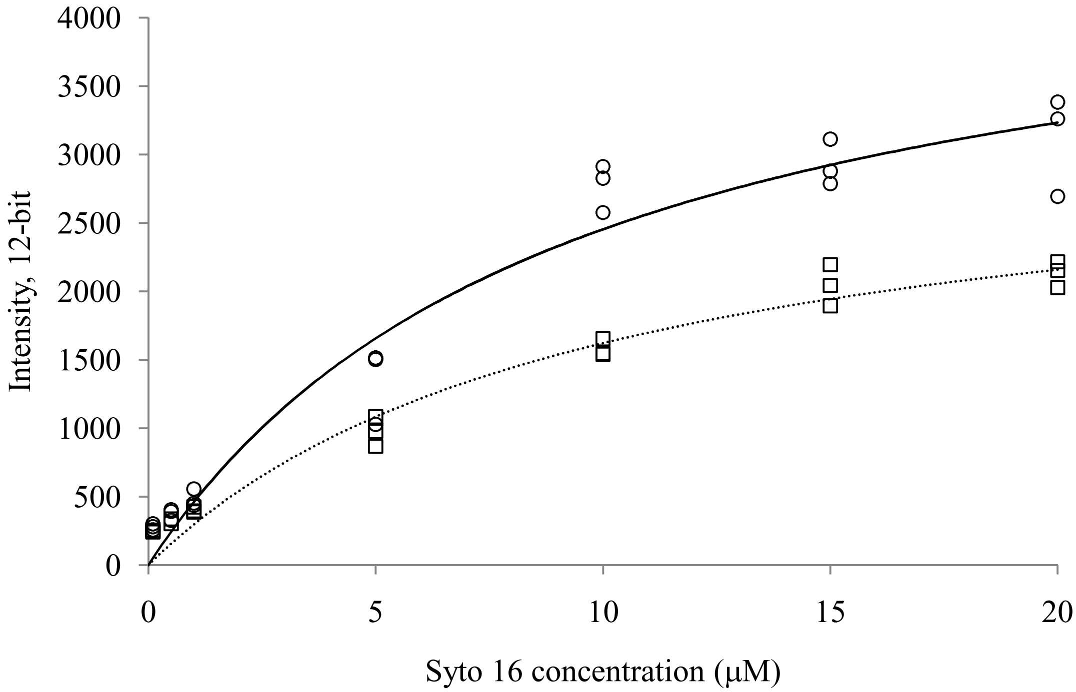

Figure 1.2. Mean- and maximum-average pixel intensity versus stain concentration in images of *A. tumefaciens* stained with Syto 16. Squares represent cell mean average pixel intensity values. Circles represent cell maximum average pixel intensity values. The dashed line is the fitted saturation model for the cell mean average pixel intensity data set. The solid line is the fitted saturation model for the cell maximum average pixel intensity data set.

1.3.4 Preliminary imaging of labeled Agrobacterium tumefaciens in leaf tissue

Lettuce leaf disks infiltrated with *A. tumefaciens* stained with 10 µM Syto 16 nucleic acid stain or water were sectioned and imaged two days post-infiltration. An exposure time of 5326 ms was used, as determined by an auto-exposure of the sample in confocal mode. In leaves infiltrated with *A. tumefaciens*, there were regions of the tissue that exhibited multiple distinct signals consistent with the size of the bacteria, which could be readily isolated from the background by defining signal and area thresholds (Figure 1.3). These signals could not be found in leaf tissue infiltrated with water alone (Figure 1.4). As a result, these signals are presumed to represent labeled bacteria.

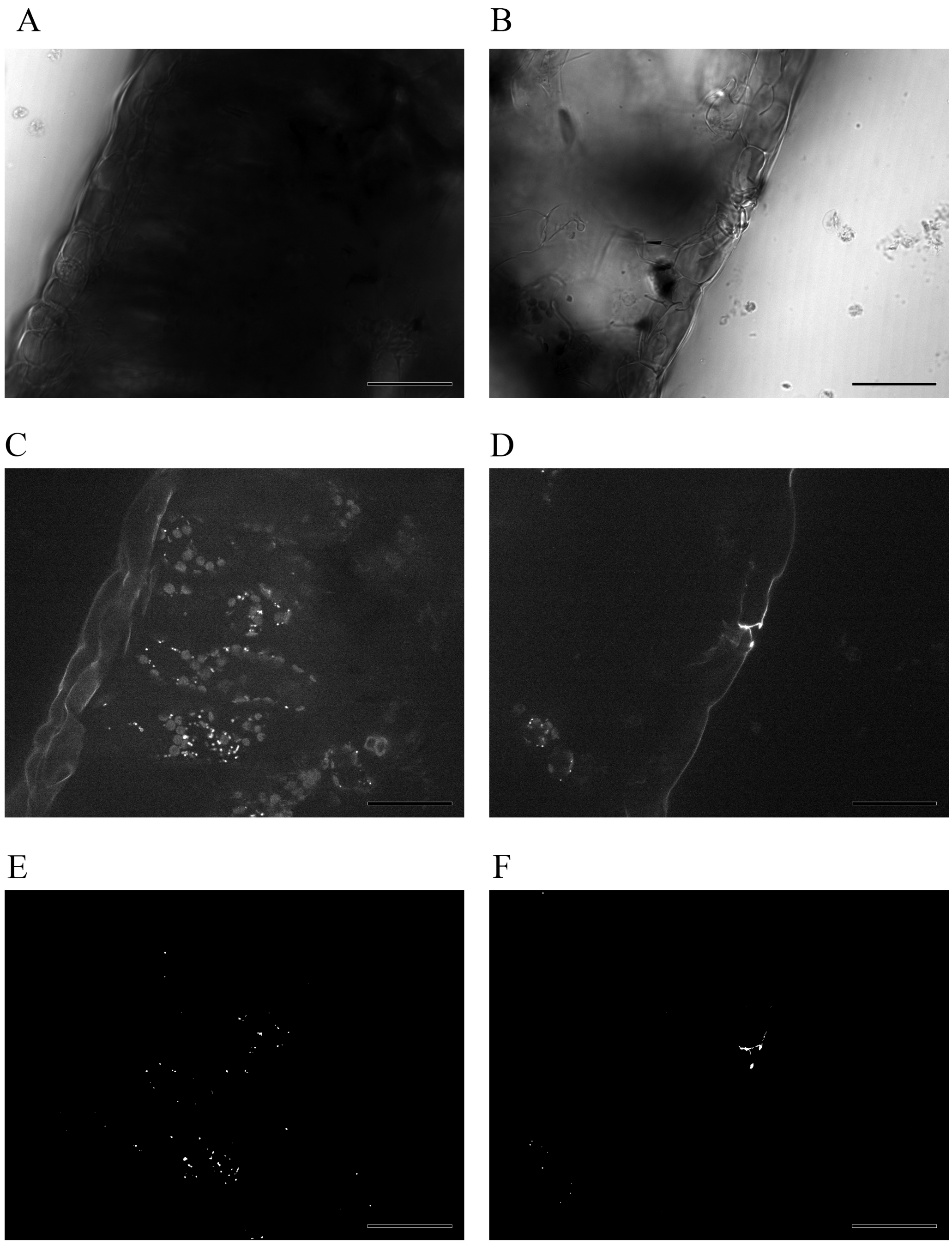

Figure 1.3. Images of leaf tissue following vacuum infiltration with *A. tumefaciens* labeled with Syto 16 nucleic acid stain. Brightfield microscopy was used to image the adaxial (A) and abaxial (B) sides of a 200 μm thick section of leaf tissue infiltrated with labeled *A. tumefaciens.* These same areas were also imaged using fluorescent confocal microscopy (C and D). Signals from the fluorescent micrographs were converted to binary by setting a minimum 12-bit signal intensity threshold of 240 (E and F). All scale bars represent 40 μm.

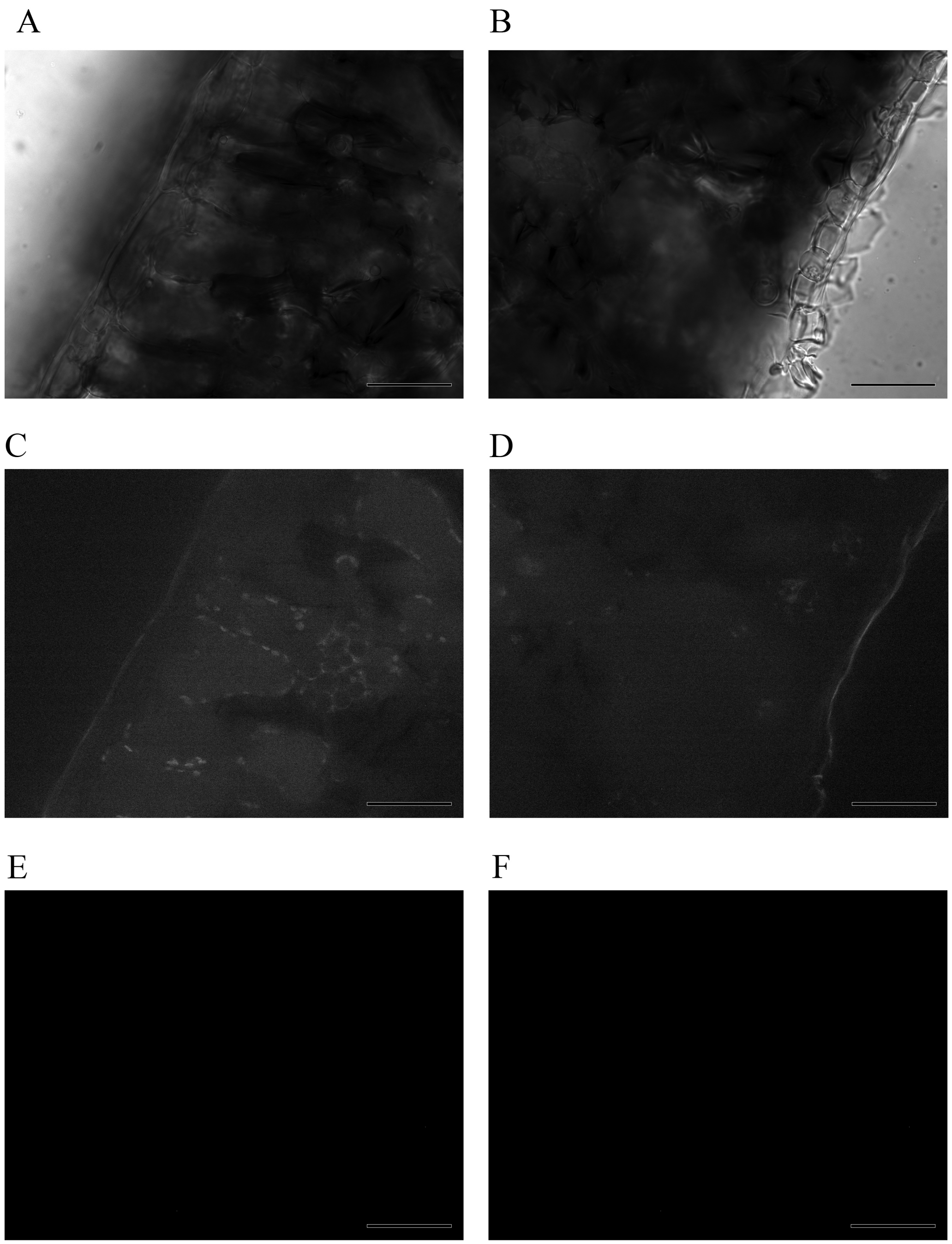

Figure 1.4. Images of leaf tissue following vacuum infiltration with water. Brightfield microscopy was used to image the adaxial (A) and abaxial (B) sides of a 200 μm thick section of leaf tissue infiltrated with water. These same areas were also imaged using fluorescent confocal microscopy (C and D). Signals from the fluorescent micrographs were converted to binary by setting a minimum 12-bit signal intensity threshold of 240 (E and F). All scale bars represent 40 μm.

1.3.5 Measurement of Syto 16 nucleic acid stain signal stability in labeled Agrobacterium tumefaciens

A. tumefaciens strain C58C1 was labeled by incubation with 10 μM Syto 16 nucleic acid stain and the mean average pixel intensity of bacteria were measured over time. Stained bacteria were suspended in dd water and incubated at room temperature in darkness. At each time point, 10 μl of bacterial suspension was mounted on a slide and imaged at 40x using confocal microscopy. Images were obtained using a 5 s exposure. Three images were taken for each time point, each at a different position on the slide. All images were analyzed with a minimum intensity threshold of 600 in order to remove ghost signals left from bacterial movement during the exposure period. As a further measure to isolate signals from cells that were relatively static during exposure, only signals with a shape factor between 0.8 and 1.0 were analyzed. For each image, the average pixel intensity for individual cells was measured (Figure 1.5, Appendix 1.5).

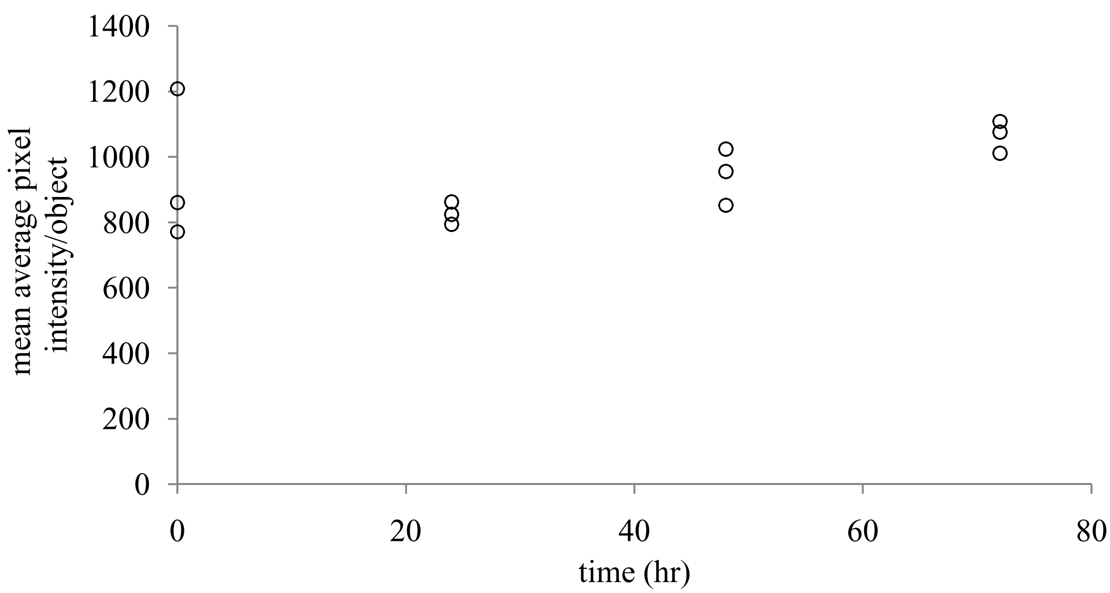

Figure 1.5. Mean average pixel intensity of Syto 16 nucleic acid stain-labeled *A. tumefaciens* over time.

The slope of cell mean average pixel intensity over time does not differ significantly from null ($\alpha = 0.05$), suggesting that signal intensity in labeled *A. tumefaciens* is stable over 72 hours.

1.3.6 Assessment of viability and virulence in labeled Agrobacterium tumefaciens

Bacteria stained with 10 μM Syto-16 nucleic acid stain were plated on solid YEP medium. Unstained bacteria were plated as a control. Colonies were counted on each plate for each treatment. Plates with stained bacteria exhibited 20 ± 3.7 colonies (corresponding to 400 ± 74 CFU/ml) (± 1 standard deviation, n=5) and plates with unstained bacteria had 19 ± 5.7 colonies (corresponding to 380 ± 114 CFU/ml) (± 1 standard deviation, n=5) (Appendix 1.6). There was no significant difference in colony count between the stained and unstained treatments ($\alpha = 0.05$).

Ten lettuce leaf disks were infiltrated with *A. tumefaciens* stained with 10 μM Syto-16 nucleic acid stain, unstained *A. tumefaciens*, or water. Pre- and post-vacuum leaf masses were measured. Leaves were histochemical stained 70 hours post-infiltration. The areas of leaf disks exhibiting GUS activity were measured (Table 1.4, Appendix 1.7).

Table 1.4. Virulence of stained and unstained *A. tumefaciens* as indicated by *in planta* expression of GUS following agroinfiltration.

Leaves infiltrated with	Mean leaf disk area exhibiting GUS activity/average volume of suspension infiltrated into leaf disk (mm^2/ml)*
Stained *A. tumefaciens*	4.204 (1.025)
Unstained *A. tumefaciens*	4.027 (1.261)
Water	0.000 (0.000)

*Expression values in parentheses represent the standard error of the mean. n = 10.

The data show that there is no statistically significant difference in the ability of stained *A. tumefaciens* to transfect leaf tissue relative to unstained bacteria.

1.3.7 Measurement of Agrobacterium tumefaciens proliferation in infiltrated leaf tissue

Diluted extracts of lettuce tissue infiltrated with Syto 16-labeled *A. tumefaciens* were plated to measure colony forming units present in the leaf tissue at various times post-infiltration. Bacterial concentrations in the leaf tissue increased approximately five-fold over the 72 hour incubation period following infiltration (Figure 1.6, Appendix 1.8).

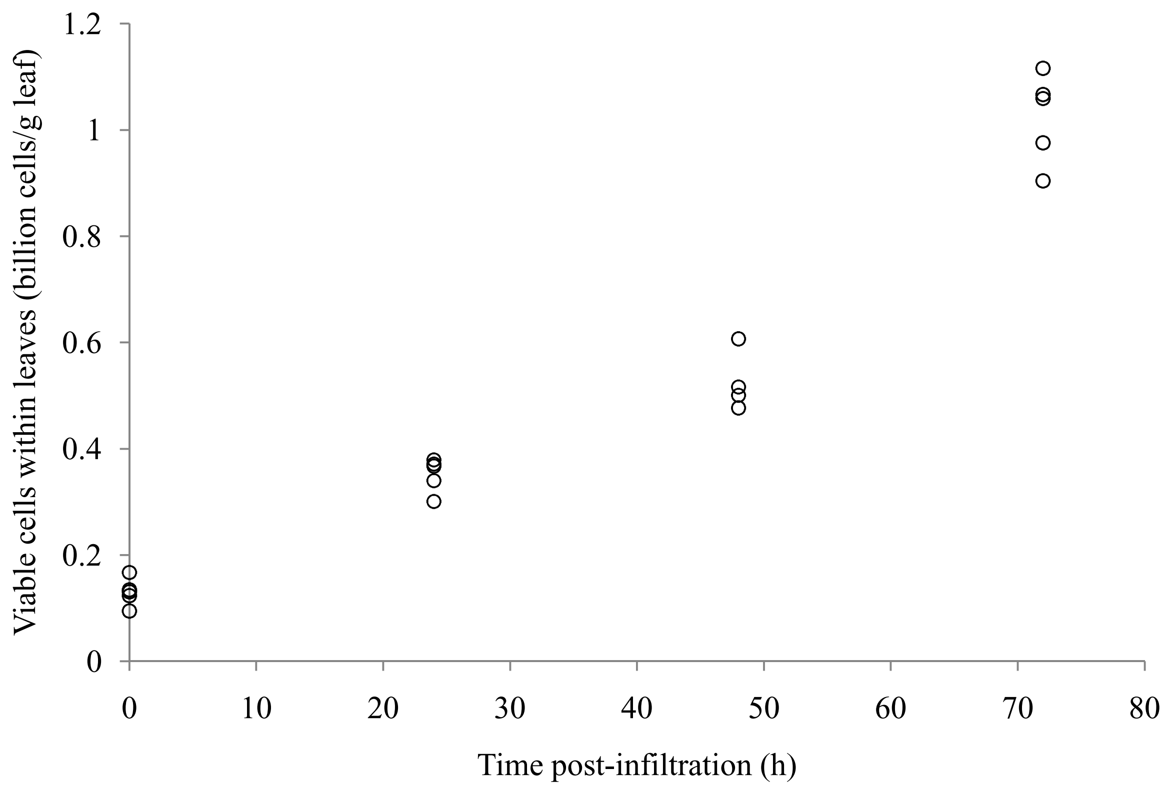

Figure 1.6. Viable *A. tumefaciens* in lettuce leaf tissue following infiltration.

1.4 Discussion

Labeling of *A. tumefaciens* with fluorescent dyes may be a rapid alternative to transforming the bacteria with genes encoding fluorescent or luminescent proteins. If dye labeling is to be an effective alternative to expression of recombinant proteins, the dye must yield a signal strong enough to detect the bacteria against a leaf background. Given that leaf tissue contains molecules with potent chromophores (e.g., chlorophyll) and may exhibit autofluorescence, careful selection of excitation wavelengths is needed to maximize the bacterial signal-to-background ratio. Sections of lettuce leaf tissue, an ideal model host for *A. tumefaciens* infection due its susceptibility to the bacteria (Joh et al., 2005), were excited with various wavelengths of light corresponding to common fluorophores: 355 nm, as would excite the common DNA stain 4',6-diamidino-2-phenylindole (DAPI); 488 nm, as would excite fluorescein isothiocyanate (FitC) and GFP; 550 nm, as would excite rhodamine; and 650 nm; as would excite cyanine 5. The resulting autofluorescence intensities were measured. Dyes with an excitation wavelength of 488 nm were chosen in order to minimize background due to leaf autofluorescence. Several types of dyes with an excitation wavelength of 488 nm were examined to determine which yielded the most intense signal in bacteria. Syto 16 nucleic acid stain yielded the greatest signal in bacteria compared to CFDA SE, a vital dye, and Alexa 488 CA SE, a dye that binds tyrosine residues on proteins displayed on the cell surface. As a result, Syto 16 nucleic acid stain was chosen as the ideal dye to use for *in situ* imaging of *A. tumefaciens* during agroinfiltration.

Varying the concentration of Syto 16 nucleic acid stain during labeling of *A. tumefaciens* revealed that the resultant signal intensity in stained cells follows a saturation trend. Based on these results, a concentration of 10 μM Syto 16 nucleic acid stain was chosen for use in all following experiments. Based on values of $S_{1/2}$, this concentration yields signal intensities in cells that are at least half of the theoretical maximum. Cell mean average pixel intensities at this level are nearly 10-fold higher than the average background pixel intensity stemming from plant autofluorescence.

Bacteria stained with 10 mM Syto 16 nucleic acid stain were vacuum infiltrated into lettuce leaf tissue. Leaves were infiltrated with water as a negative control. Leaves from both treatments were sectioned and imaged. Point-like signals were found in leaf tissue infiltrated with labeled bacteria but not in tissue infiltrated with water. These signals were detected only in areas where leaf cells were present (as determined from chloroplast autofluorescence in confocal micrographs), suggesting they are bacteria attached to plant cells and not bacteria simply trapped in the apoplast. Signals were sufficiently intense to be isolated from the leaf background, in agreement with the results predicted from the leaf autofluorescence and dye labeling concentration experiments. These preliminary results validate the use of fluorescent nucleic acid stain to image *A. tumefaciens* bound to leaf tissue *in situ*. However, in Figure 1.4 it can be seen that autofluorescence from a bisected stoma was intense enough to exceed the signal threshold used for isolating bacterial signals. This suggests that autofluorescence may contribute noise when measuring labeled *A. tumefaciens* in leaf tissue. Adding a signal shape factor filter to image analysis may minimize noise in future experiments.

Ideally, labeling nucleic acids with Syto 16 would allow for visualization of bacteria over at least 72 hours, the time to reach peak transient expression of agroinfiltrated transgenes in lettuce (Joh et al., 2005; Simmons and VanderGheynst, 2007), in order to accurately capture the distribution of bacteria within the plant over the duration of infection. The data show that signal intensity is stable in stained bacteria suspended in water over this time period. However, concentration measurements of stained bacteria in infiltrated leaf tissue over 72 hours show that bacteria continue to grow after infiltration into leaf tissue. Such growth may effectively dilute the amount of dye in each generation of cells and lower signal intensities. A decrease in signal intensity over 72 hours may not have been observed when bacteria were suspended in water due to a lack of nutrients preventing division. In light of this, it may not be possible to discern whether changes in bacterial signal levels over time in infiltrated leaves result from bacterial detachment or from the dilution effect. As a result, this method may be limited to observing only initial bacterial binding levels in infiltrated tissue.

It is vital that the act of staining does not affect the viability and virulence of bacteria relative to unstained cells. The data show that viability and virulence of Syto 16-stained *A. tumefaciens* is not significantly different from unstained bacteria on the basis of the ability to divide and *in planta* transient expression of GUS, indicating that observations of stained bacteria can be assumed to be representative of unstained bacteria. It is somewhat surprising that the presence of a nucleic acid stain does not interfere with *A. tumefaciens*' DNA replication or DNA secretion pathway. This may be due to the fact that Syto 16 nucleic acid stain is an intercalator. Previous studies have shown that Syto 16 nucleic acid stain is compatible with qPCR and exhibits no inhibition of the reaction (Gudnason et al., 2007). This confirms the reversible nature of Syto 16 binding to DNA and suggests that Syto 16 does not prevent polymerases from accessing DNA. While these data stem from observations made under the conditions of PCR, the results may extend to the physiological case. If true, this would explain how staining of bacterial DNA with Syto 16 nucleic acid stain does not inhibit transcription, DNA replication, and the variety of proteins that must interact with the T-strand, both in its double- and single-stranded forms, during agroinfiltration. Moreover, as T-strands are single stranded, they may be unaffected by the stain, which, as an intercalator, primarily binds double-stranded DNA. Alternately, under the staining protocol used in this research, *A. tumefaciens*' virulence is induced prior to staining, ensuring that bacteria are equipped with a full array of virulence proteins and semi-processed single-stranded T-strands before any stain is present. If Syto 16 nucleic acid stain does inhibit protein interactions with double-stranded DNA, the fact that these interactions are allowed to occur before staining may avoid any of the stain's deleterious effects.

1.5 Conclusions

A. tumefaciens labeled with Syto 16 nucleic acid stain exhibit stable fluorescence for up to 72 hours after staining for 2 hours in 10 μM dye. Stained bacteria can be readily visualized within leaf tissue following vacuum infiltration using fluorescence confocal microscopy. Furthermore, *A. tumefaciens* labeled with Syto 16 nucleic acid stain maintain similar virulence to unstained bacteria in terms of their ability to transform lettuce leaf tissue. These qualities suggest that fluorescent labeling of *A. tumefaciens* with Syto 16 nucleic acid stain is an excellent approach to visualizing bacteria bound to leaf tissue *in situ* while maintaining their native behavior. As a result, staining of *A. tumefaciens* with fluorescent dyes provides a rapid alternative to the cloning required to create bacteria expressing fluorescent proteins.

Chapter 2 – Factors affecting attachment of *Agrobacterium tumefaciens* to lettuce leaf tissue and the effect of attachment on *in planta* transient transgene expression

2.1 Introduction

Transient expression of recombinant proteins in plants, where transgenes are temporarily expressed at exceptionally high levels following insertion into the host, presents opportunities for furthering plant-based expression systems as a useful platform for large-scale recombinant protein production. Foremost, transient expression can lead to higher yields of product per unit plant tissue compared to stable expression (Lonsdale et al., 1988; Janssen and Gardner, 1989). Furthermore, transient expression may provide rapid product accumulation in leaf tissues due, in part, to the fact that inserted transgenes may undergo transient expression without integration into the host's genome. As a result, *in planta* transient expression of transgenes can be detected within hours to days following insertion (depending on the transformation method and plant tissue used), compared to the weeks or months needed to transform and regenerate plants with a stably inserted transgene. In fact, transient expression can occur so rapidly after transformation that it facilitates high-level expression of transgenes in harvested plant tissues (Kapila et al., 1997; Joh et al., 2005). This quality presents the interesting possibility of post-harvest plant expression systems that bypass regulations (7 C. F. R. § 3.340, 2008) and concerns related to growing transgenic plants in the field. However, transient expression of recombinant proteins in harvested plant tissues relies on high transformation efficiency to maximize yield, since only those plant cells that are transformed are able to produce the recombinant product. This is in contrast to stably transformed plants, where low transformation efficiencies are tolerated since only a single plant cell need be transformed from which an entire transgenic plant can be regenerated. As a result, research to improve transformation efficiency in plant tissues has important implications for plant biotechnology.

Agrobacterium-mediated transformation, or agroinfiltration, is a common method for transforming plant tissues and inducing *in planta* transient expression of transgenes. Agroinfiltration capitalizes on the bacterium's innate virulence pathway, which uses a type-IV DNA secretion system to export genetic material, the T-strand, to host plant cells for expression (reviewed by Zhu et al., 2000). Although agroinfiltration has proved incredibly useful for transforming a wide range of plant tissues spanning many species (reviewed by De Cleene and De Ley, 1976; Lacroix et al., 2006), many important crop plants cannot be readily agroinfiltrated (reviewed by van Wordragon and Dons, 1992). Even within plants that can be effectively agroinfiltrated there is great variability in transformation efficiency across various tissues (Sangwan et al., 1992; Kapila et al., 1997) and even within replicates (Janssen and Gardner, 1989; Collens et al., 2004). It is not well understood why these disparities exist. Certain elements of the *Agrobacterium* infection pathway have not been fully characterized, yet may be responsible, in part, for system-dependent agroinfiltration efficacy.

Attachment of *Agrobacterium* to host plant cells is an early and critical process in the infection pathway (Lippincott and Lippincott, 1969; Glogowski and Galsky, 1978). Although the bacteria may detect and respond to certain plant chemical signals (reviewed by Brencic and Winans, 2005), attachment is the first direct pathogen-host interaction. Broadly, attachment of *Agrobacterium* consists of two phases, reversible and irreversible, which proceed in that order. Reversible attachment is suspected to depend on receptorligand interactions. However, the specific identities of plant proteins that act as receptors or ligands are only partially resolved and some of the data is controversial (reviewed by Gelvin, 2010). Likewise, bacterial protein factors remain equally elusive, with bacterial motility playing an important yet not fully understood role and whole clusters of genes once thought vital to bacterial attachment now showing only a tenuous link to the process (reviewed by Tomlinson and Fuqua, 2009). Irreversible attachment is marked by bacterial production of cellulose fibrils that anchor bacteria to the plant cell surface. Cellulose fibril production provides enhanced persistence of bacteria on plant tissues but is not necessary for transformation to occur (Matthysse, 1983). Additionally, the biochemical cues that *Agrobacterium* uses to regulate the transition to irreversible binding remain unclear. Due to these knowledge gaps, attachment behavior cannot be completely predicted and, as a result, the fate of *Agrobacterium* once it enters a complex plant tissue, such as a leaf, is somewhat uncertain. Consequently, the possible contribution of attachment behavior to fluctuations in transformation efficiency during agroinfiltration presents an interesting topic for research. To this end, this work seeks to analyze the attachment behavior of *Agrobacterium tumefaciens* in leaf tissue.

Romaine lettuce served as a model plant host for attachment studies. Prior work has shown lettuce to be highly susceptible to agroinfiltration (Joh et al., 2005). Dicot plants, like lettuce, are most prominent in the established host range of *Agrobacterium* (De Cleene and De Ley, 1976). These properties, combined with its rapid and established cultivation procedures, make lettuce ideal for studying *Agrobacterium* attachment in a plant host compatible with the bacteria. Quantities of attached labeled bacteria, stained using the protocol developed in Chapter 1, were measured per volume leaf in infiltrated leaves as a novel *in situ* approach for gauging bacterial attachment. *A. tumefaciens* labeled with green fluorescent protein has previously been used in conjunction with fluorescent confocal microscopy to visualize bacteria attached to leaf tissue (Want et al., 2007). However, no effort was made to quantify attachment levels or discern attachment to specific plant cell types. In addition, bacterial attachment levels were studied in response to processes known to enhance agroinfiltration efficacy, such as applying vacuum or adding surfactant during infiltration of leaf tissues with suspended *Agrobacterium*, but whose modes of action are not entirely understood. Finally, *in planta* transient expression levels of an agroinfiltrated transgene were measured in response to varied attachment levels to investigate if a relationship exists and if modifying attachment levels is a viable strategy for improving transformation efficiency.

2.2 Materials and Methods

2.2.1 Bacterial strains, culture, and staining

A. tumefaciens strain C58C1 was cultivated as described in section 1.2.1. Suspensions of *A. tumefaciens* were stained with 10 μM Syto 16 green fluorescent nucleic acid stain using the procedure provided in section 1.2.4. Following staining and washing, bacterial suspensions were resuspended to 10^8, 10^9, or 10^{10} CFU/ml. A disarmed strain of *A. tumefaciens* strain C58, which lacks a T-strand (while retaining all virulence operons), was used as a negative control in experiments were *in planta* GUS expression was measured in response to bacterial attachment.

2.2.2 Preparation, infiltration, sectioning and histochemical staining of leaf tissue

Lactuca sativa valmaine was grown as described in section 1.2.2. Leaf explants were prepared as outlined in section 1.2.3. *A. tumefaciens* was vacuum infiltrated into leaf tissue as described in section 1.2.5. Agroinfiltrated leaf tissue was sectioned as live, unfixed tissue using a vibrating microtome as outlined in section 1.2.7. Sections were 200 μm thick. Histochemical staining of agroinfiltrated leaf tissue was performed as described in section 1.2.8 with staining time decreased to 6 hours.

2.2.3 Extraction of GUS from agroinfiltrated leaves

Agroinfiltrated leaf tissue was extracted by combining five leaf disks with 1 ml of extraction buffer (48 mM sodium phosphate, pH 7.5; 40 mM dithiothreitol) in a chilled mortar and then grinding until the mixture reached homogeneity. Crude lysates were transferred to tubes and centrifuged at 10,000×g for 10 minutes at 4 ˚C. Supernatants were aspirated to fresh tubes and stored at -80 ˚C.

2.2.4 Colorimetric GUS activity assay

GUS activity in leaf extracts was measured using a colorimetric GUS activity assay. The assay is based on the GUS-catalyzed cleavage of glucuronic acid from the substrate p-nitrophenyl glucuronide to yield p-nitrophenolate as a product. P-nitrophenylate absorbs light at 405 nm, permitting spectrophotometric measurement of product accumulation kinetics. For each reaction, 50 μl of extract was added to 500 μl of assay buffer (50 mM sodium phosphate, pH 7.5; 5 mM dithiothreitol; 0.1% (w/v) sodium lauryl sarcosine; 0.1% (v/v) Triton-X, 1 mM EDTA, and 6 mM p-nitrophenyl glucuronide (Sigma). Reactions were incubated at 37 ˚C and 100 μl samples were taken initially and every 15 minutes for one hour. Samples were combined with 800 μl of 200 mM sodium carbonate to halt the reaction. The absorbance at 405 nm of three 200 μl aliquots from each stopped sample were measured using a Vmax plate reader (Molecular Devices, Sunnyvale, CA). Absorbance readings were converted to product concentration values using Beer's Law with an extinction coefficient value of 18,700 $M^{-1}cm^{-1}$. Accounting for dilutions, GUS activity was calculated per unit mass leaf tissue as a measure of *in planta* GUS expression. GUS activity is described in activity units, U, per gram fresh weight leaf, where 1 U is equal to 1 nmol of product produced per minute.

2.2.5 Imaging of leaf tissue infiltrated with labeled Agrobacterium tumefaciens

The same equipment and software described in section 1.2.9 was used to perform spinning-disk confocal fluorescent microscopy. Excitation and emission wavelengths of 488 and 520 nm, respectively, were used to image *A. tumefaciens* labeled with Syto 16 nucleic acid stain. For each tissue section, the sample was first scanned visually at 40x in fluorescent widefield mode. A neutral density filter was used to decrease the intensity of the excitation beam by 50% in order to minimize photobleaching. During the preliminary scan, areas that represented localizations of attached bacteria relative to the rest of the sample were identified within tissue sections and designated as infection sites (Figure 2.1). Localizations proximal to the cut edge of a leaf explant were not selected as infection sites to avoid any confounding effects of leaf wounding.

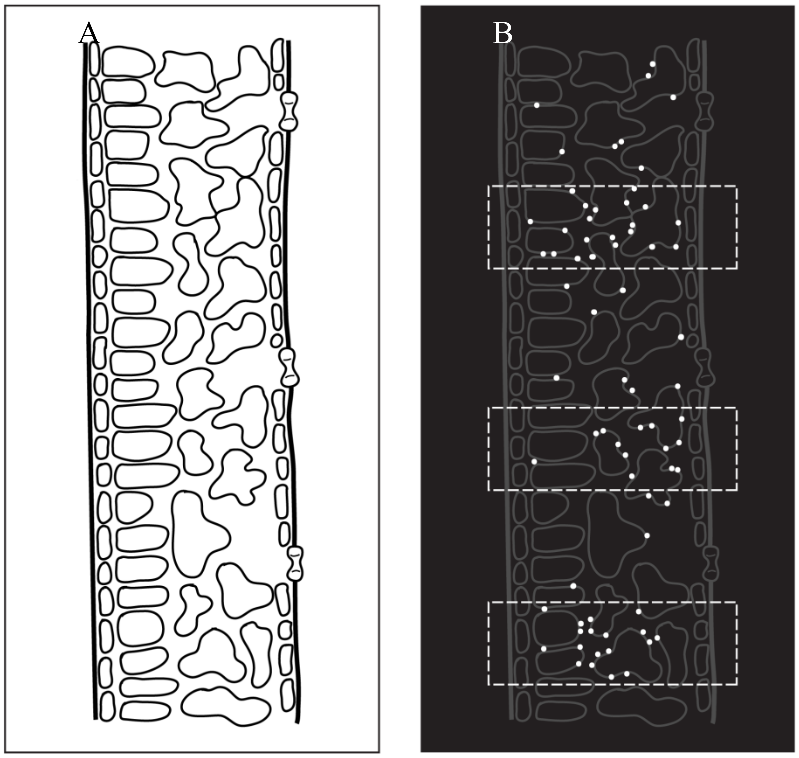

Figure 2.1. Identification of infection sites in sections of agroinfiltrated leaf tissue. The illustration shows a section from a hypothetical lettuce leaf infiltrated with labeled *A. tumefaciens* using A. brightfield and B. fluorescent microscopy. The white points in Figure 2.1B represent signals from stained bacteria. The areas bordered with dotted lines represent the three infection sites identified, based on their dense localizations of bacteria relative to the rest of the tissue. The height of the imaged infection site is equal to that of one viewing field at 40x. The length of the imaged site is one to two viewing fields, depending on what is required to capture the entire length of the section and, as a result, may require that two separate micrographs are joined and analyzed together.

Three infection sites were imaged at 40x in both brightfield and fluorescent confocal modes for each agroinfiltrated leaf explant. An exposure time of 5326 seconds was used for confocal fluorescent micrographs. At each infection site, three micrographs were taken spanning 20 μm into the tissue (Figure 2.2). Spacing micrographs 10 μm apart permitted sampling of a subset of attached bacteria throughout a volume of the infection site without risking confounding effects of individual bacteria being present across multiple micrographs.

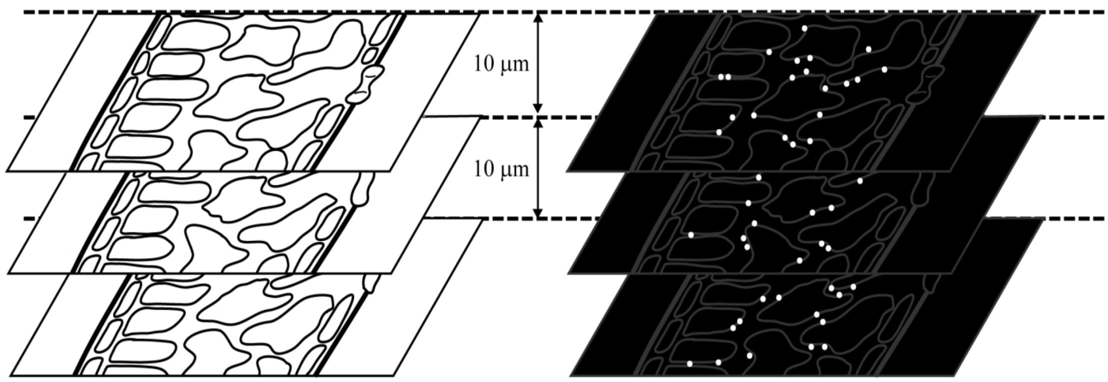

Figure 2.2. Imaging of infection sites at multiple depths. At each infection site, three images were obtained in both brightfield (left stack) and fluorescent confocal (right stack) modes, spanning a total of 20 μm of leaf tissue.

2.2.6 Analysis of micrographs

Brightfield infection site images were used to determine the area of leaf tissue visualized at each site. Area measurements were performed on a single layer of the three image depth stack, as changes in tissue area were assumed to be negligible over the 20 μm depth of the infection site. Photoshop CS3 version 10.0.1 software was used to measure the area of leaf tissue in images. Pixel areas were converted to μm^2 using a conversion factor of 0.026 μm/pixel. The area of the imaged section was multiplied by 20 μm^2 to calculate the volume of the infection site. Fluorescent confocal micrographs were analyzed using Methamorph Basic version 7.6.5.0 software. For each set of images comprising an experiment, signal intensity and signal area filters were used to isolate signal regions from the leaf background that had intensities greater than 230-300 (12-bit scale) and areas between 3 and 150 pixels (0.08 and 3.9 μm^2), which predominantly corresponded to stained bacteria. Signal regions were counted in each set of images comprising an infection site and this value was taken to represent the number of attached bacteria present. The total number of attached bacteria in a given site was divided by the infection site volume to calculate the density of bound bacteria per volume leaf tissue. The average density of attached bacteria was calculated for each leaf explant based on the three infection sites surveyed.

2.2.7 Statistical analysis

Statistical analyses and model fitting were performed with JMP version 8.0 and MATLAB R2009a as described in section 1.2.10.

2.2.8 Measurement of surfactant effects on vacuum-infiltrated liquid volume and leaf viability

The volume of infiltrated liquid and viability of lettuce leaf explants were measured in leaf disks infiltrated with varying levels of Break-Thru S240 surfactant (Goldschmidt Chemical, Hopewell, VA). Three groups of 10 explants each were infiltrated in 3 ml of water containing 1, 10, 100, or 1000 ppm (v/v) surfactant. Infiltration occurred at 25 kPa for 7.5 minutes. Each group of leaf explants was weighed prior to and following vacuum and the difference in the two weights was taken as the mass of infiltrated liquid. Explants were gently blotted dry with paper towels before each weight measurement. Following infiltration, explants were sealed in Petri dishes lined with gauze moistened with 3 ml of water. Infiltrated explants were incubated in darkness at 21-22 ˚C for 72 hours. Leaf explants were then examined for putrefaction. An explant was considered putrefied if any part of it was liquefied.

2.2.9 Measurement of bacterial attachment kinetics to leaf tissue

Bacterial adhesion to leaf tissue was measured over time in agroinfiltrated leaf tissue. Four groups containing three explants each were infiltrated with 10^9 CFU/ml Syto16-labeled *A. tumefaciens* at 25 kPa for 7.5 minutes. Infiltrated leaf explants were sealed in Petri dishes and incubated at 21-22 ˚C, as previously described. At 0, 24, 48, and 72 hours post-infiltration, one group was removed from incubation, sectioned, and infection sites were measured for attached bacteria using described methods. A signal intensity threshold of 259 (12-bit) was used for all images. As a negative control, the experiment was repeated with water replacing bacterial suspension.

2.2.10 Measurement of surfactant effects on initial bacterial attachment to leaf tissue

Attachment of bacteria to leaf tissue was measured in response to varied surfactant levels in bacterial suspensions. Groups of three leaf explants were infiltrated with suspensions of 10^9 CFU/ml Syto16-labeled *A. tumefaciens* containing 1, 10, 100, or 1000 ppm (v/v) Break-Thru S240 surfactant. Two groups leaf explants were assigned to each surfactant treatment. Explants were infiltrated with labeled bacteria in surfactant solution at 25 kPa for 7.5 minutes and then immediately processed to measure bacterial attachment at infection sites using previously described methods. A 12-bit signal intensity threshold of 250 was used in analyzing all images.

2.2.11 Measurement of vacuum infiltration effects on initial bacterial attachment to leaf tissue

The average density of attached bacteria at infection sites was measured in response to vacuum intensity applied during vacuum infiltration. Aliquots of three leaf explants were vacuum infiltrated with 10^9 CFU/ml Syto 16-labeled *A. tumefaciens* at 45, 25, and 5 kPa. Each explant was sectioned and a random sampling of sections was imaged as previously described to determine the average density of bound bacteria at infection sites using a 12-bit signal intensity threshold of 235.

2.2.12 Measurement of infiltrated bacterial density effects on initial bacterial attachment to leaf tissue

Bacterial attachment levels were measured in leaf explants infiltrated with varied concentrations of labeled *A. tumefaciens*. Bacteria were stained with Syto16 and then washed using described procedures. Following post-stain washing, bacteria were diluted in sterile water to 10^8, 10^9, and 10^{10} CFU/ml. Three groups of 10 leaf explants each were infiltrated in each bacterial suspension at 25 kPa for 7.5 minutes. Explants were then analyzed to measure levels of attached bacteria at infection sites. Signal intensity threshold values between 230 and 300 (12-bit scale) were used for analyzing images.

2.2.13 Measurement of recombinant GUS activity in agroinfiltrated leaf tissue versus time

Four groups of three leaf explants were agroinfiltrated with 10^9 CFU/ml *A. tumefaciens* st. C58C1 containing no surfactant at 25 kPa for 7.5 minutes. Leaf explants were weighed before and after infiltration to determine infiltrated liquid volume. Each group was incubated for 0, 24, 48, or 72 hours following infiltration. At each time point, a group of infiltrated leaves was stained using the histochemical staining method to visualize areas of leaf tissue with GUS activity. Stained leaves were photographed and the pixel area of stained regions was determined by setting an 8-bit intensity threshold of 128 in Photoshop CS3. Pixel area values were converted to mm^2 using a conversion factor of 92.08 px/mm^2. The area of each disk with GUS activity was normalized against the volume of bacterial suspension infiltrated into the disks of that treatment.

2.2.14 Correlation of initial bacterial attachment levels to transgene transient expression levels

GUS activity in agroinfiltrated leaf extracts was measured in response to varied concentrations of infiltrated *A. tumefaciens*. Three groups of 5 leaf explants each were infiltrated with *A. tumefaciens* at 10^8, 10^9, and 10^{10} CFU/ml at 25 kPa for 7.5 minutes. Infiltrated leaves were sealed in Petri dishes lined with moistened gauze and incubated at 21-22 ˚C for 72 hours in darkness. Following incubation, leaves were weighed and stored at -80 ˚C until extraction. Leaves were extracted and assayed for GUS activity using the colorimetric GUS assay as previously described. For measurement of GUS activity using histochemical staining, the experiment was repeated as described above with the addition of 10 ppm (v/v) Break-Thru S240 during infiltration. Leaves were stained using the described staining procedure for 6 hours immediately following the 72 hour incubation step.

2.3 Results

2.3.1 Measurement of bacterial attachment kinetics to leaf tissue

The maximum density of bacterial signals in lettuce leaves infiltrated with labeled bacteria was observed one hour following infiltration, the earliest time point possible given the time required to process leaf samples post-infiltration. The number of signals detected per volume leaf decreased significantly ($p = 0.004$) over 72 hours following infiltration (Figures 2.3 and 2.4, Appendices 2.1). The presence of one outlying data point at the 24 hour time point led to increased variability for that treatment compared to the rest of the data set. No significant signal trends were observed in leaf explants infiltrated with water alone (Appendix 2.2).

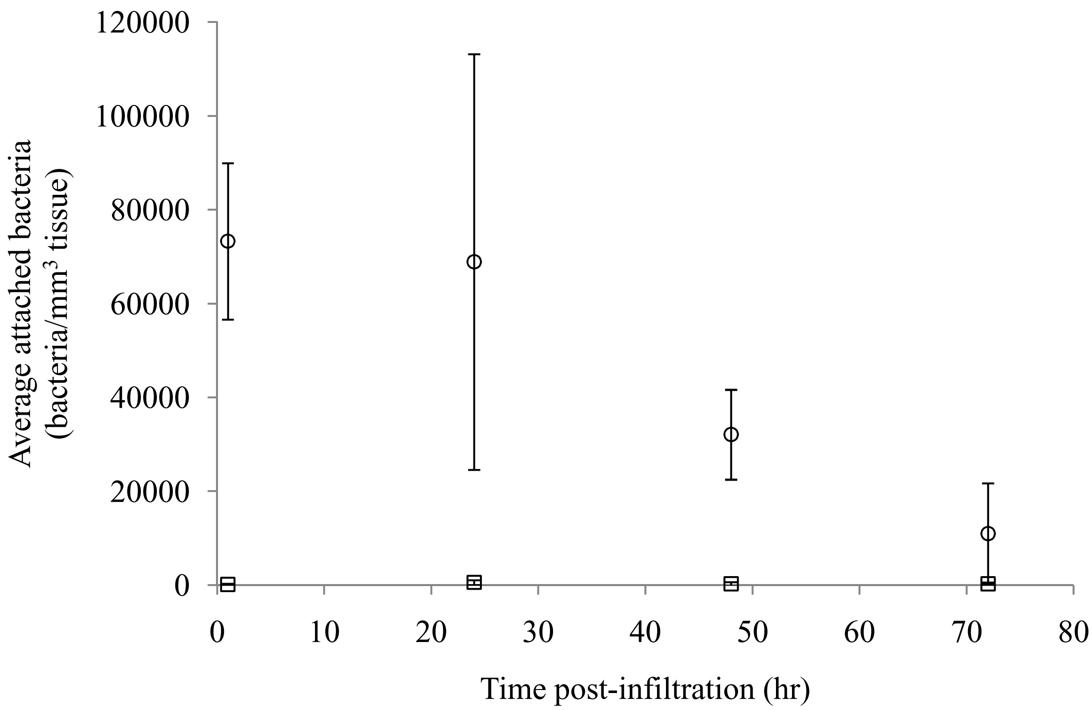

Figure 2.3. Density of attached bacteria at infection sites over time in agroinfiltrated lettuce leaf tissue. Circles and squares represent measurements from leaves infiltrated with labeled *A. tumefaciens* and water, respectively. Error bars represent one standard deviation.

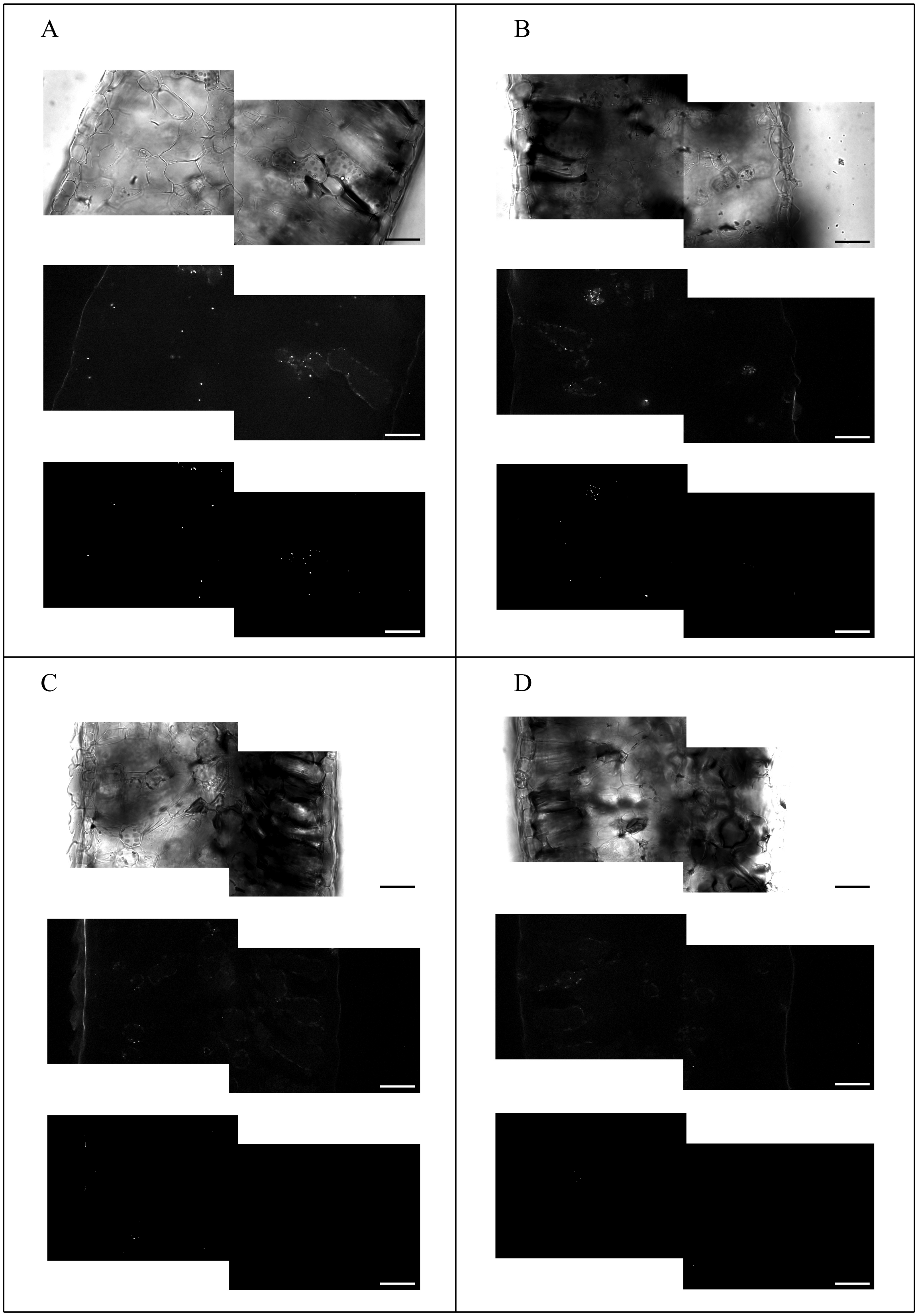
A
B
C
D

Figure 2.4. Representative micrographs of sectioned lettuce leaf explants at various times following infiltration with labeled *Agrobacterium tumefaciens*. Micrographs represent single focal planes from image stacks corresponding to sample infection sites at (A) 1 hour, (B) 24 hours, (C) 48 hours, and (D) 72 hours post-infiltration. For each treatment, brightfield, fluorescent confocal, and binary images (in descending order) are provided. Binary images show isolated signals (colored white) following signal intensity and signal area screening. Two separate images were required to capture the entire width of the leaf section at each infection site. The apparent disjointed nature of compiled infection site micrographs stems from the alignment of the two corresponding images. Scale bars represent 40 μm.

2.3.2 Measurement of recombinant GUS activity in agroinfiltrated leaf tissue versus time

Peak GUS activity was observed in agroinfiltrated leaf explants beginning 48 hours post-infiltration (Figure 2.5, Appendix 2.3). The activity observed at 48 hours remained constant thereafter ($p = 0.39$).

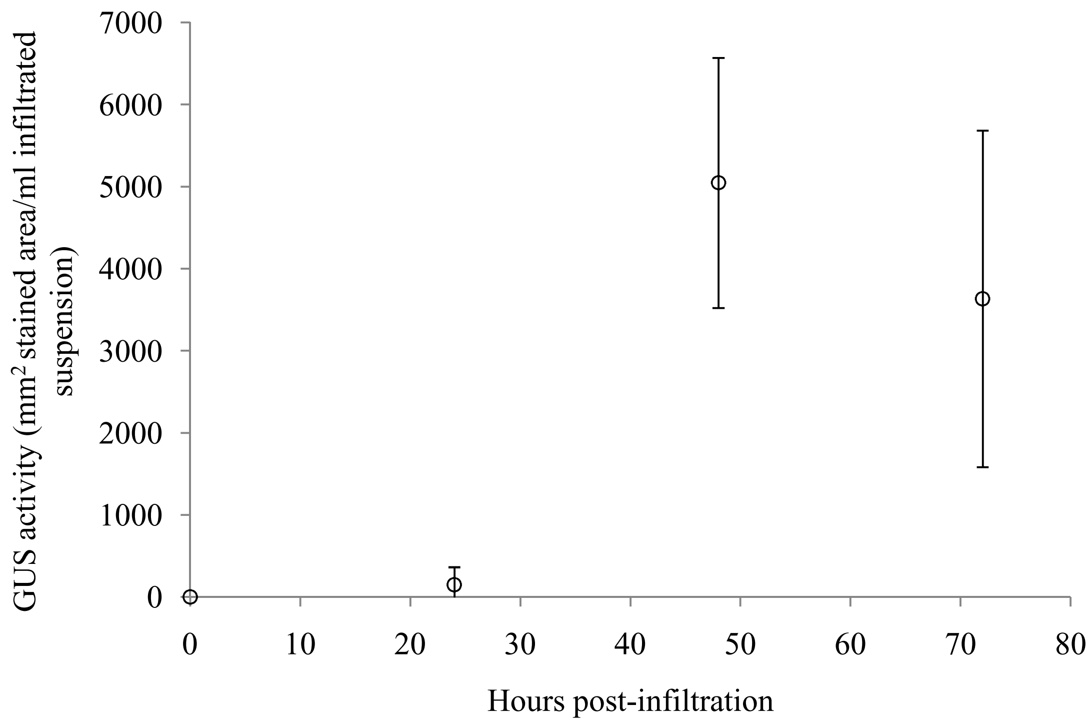

Figure 2.5. GUS activity in agroinfiltrated leaf tissue over time. Error bars represent one standard deviation.

2.3.3 Measurement of surfactant effects on vacuum-infiltrated liquid volume and leaf viability

The addition of surfactant had a significant positive effect on the volume of liquid vacuum-infiltrated into leaf tissue (p = 0.035) (Figure 2.6, Appendix 2.4). The effect was observed for surfactant concentrations up 100 ppm (v/v). Higher concentrations did not enhance the volume of infiltrated liquid. No putrefaction was observed in leaf explants for surfactant treatments up to 100 ppm. Treatment with 1000 ppm surfactant yielded detectable putrefaction in some leaf explants (Figure 2.7, Appendix 2.4).

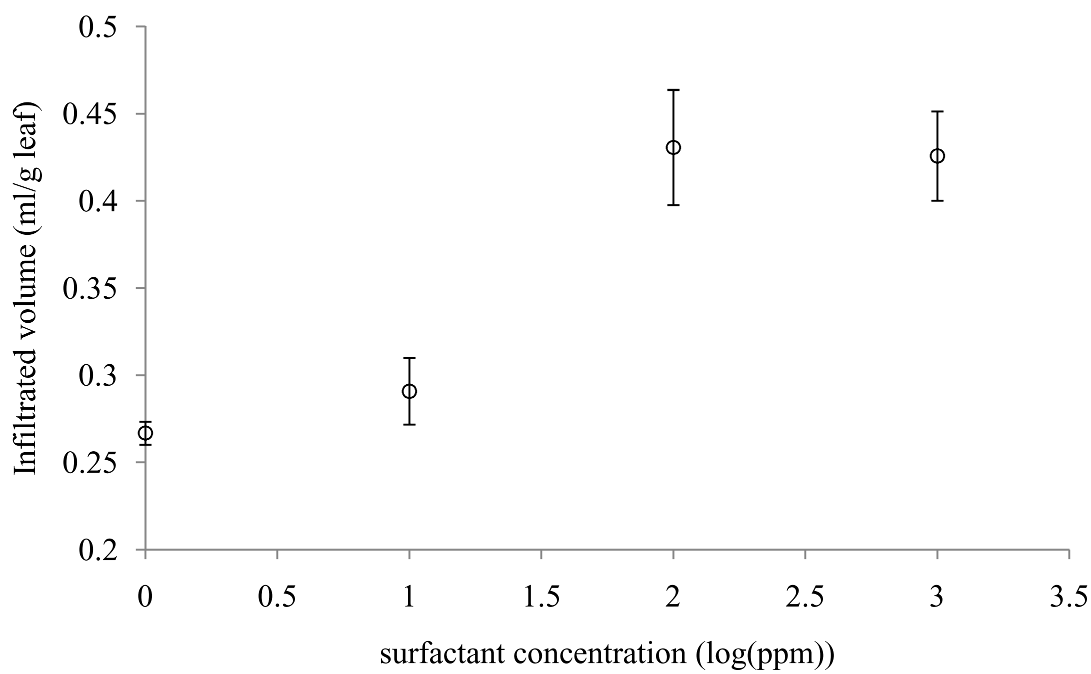

Figure 2.6. Volume of liquid infiltrated into leaf tissue per fresh weight of leaf versus surfactant concentration in the liquid phase. Error bars represent one standard deviation.

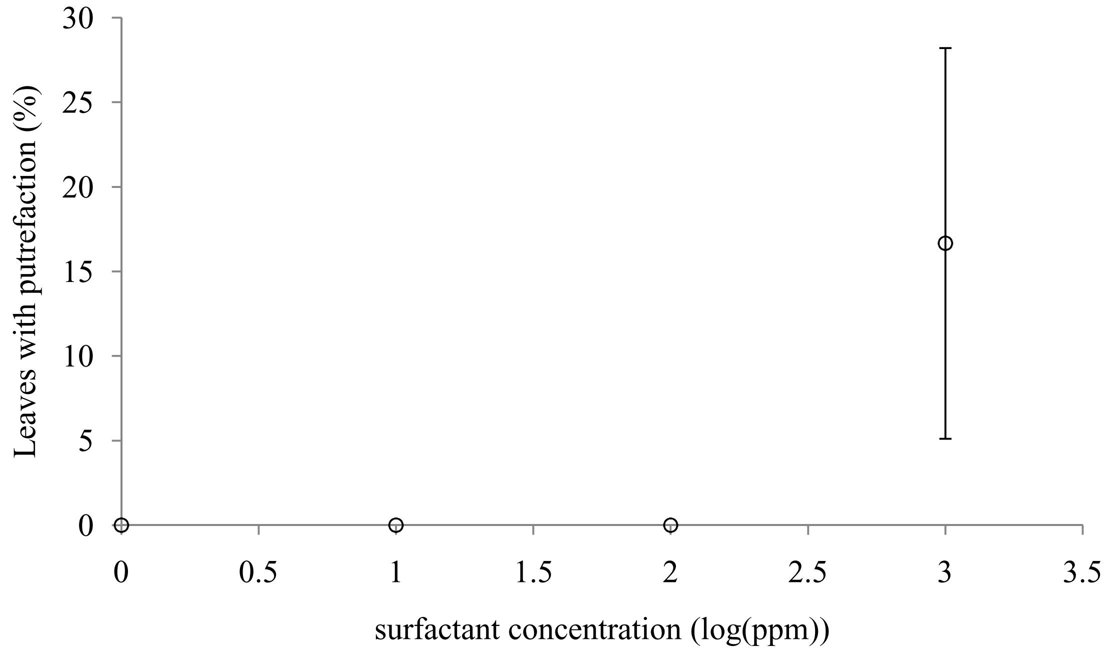

Figure 2.7. Percentage of leaf explants exhibiting putrefaction versus surfactant concentration in infiltrated liquid. Error bars represent one standard deviation.

2.3.4 Measurement of surfactant effects on initial bacterial attachment to leaf tissue

Surfactant was observed to have a significant positive effect on bacterial adhesion to leaf tissue at infection sites (p = 0.003) (Figure 2.8 and 2.9, Appendix 2.5). An outlying data point in the 1 ppm treatment led to increased error. If this point is omitted from analysis, the p-value of the linear trend decreases to <0.0001.

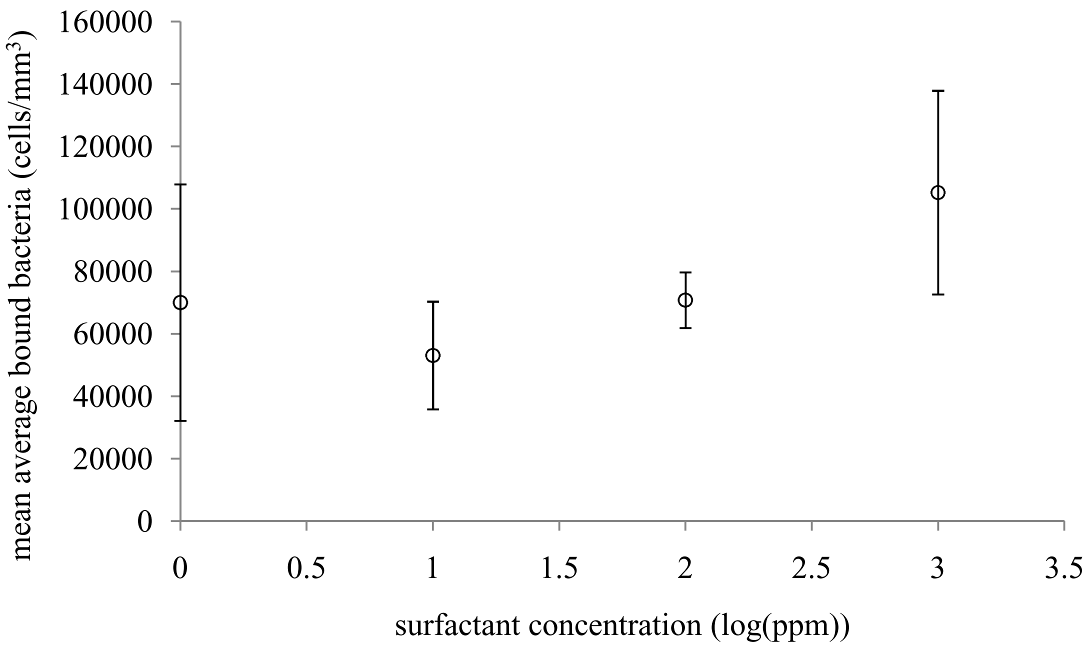

Figure 2.8. Average bacterial attachment to leaf tissue versus surfactant concentration in infiltrated bacterial suspension. Error bars represent one standard deviation.

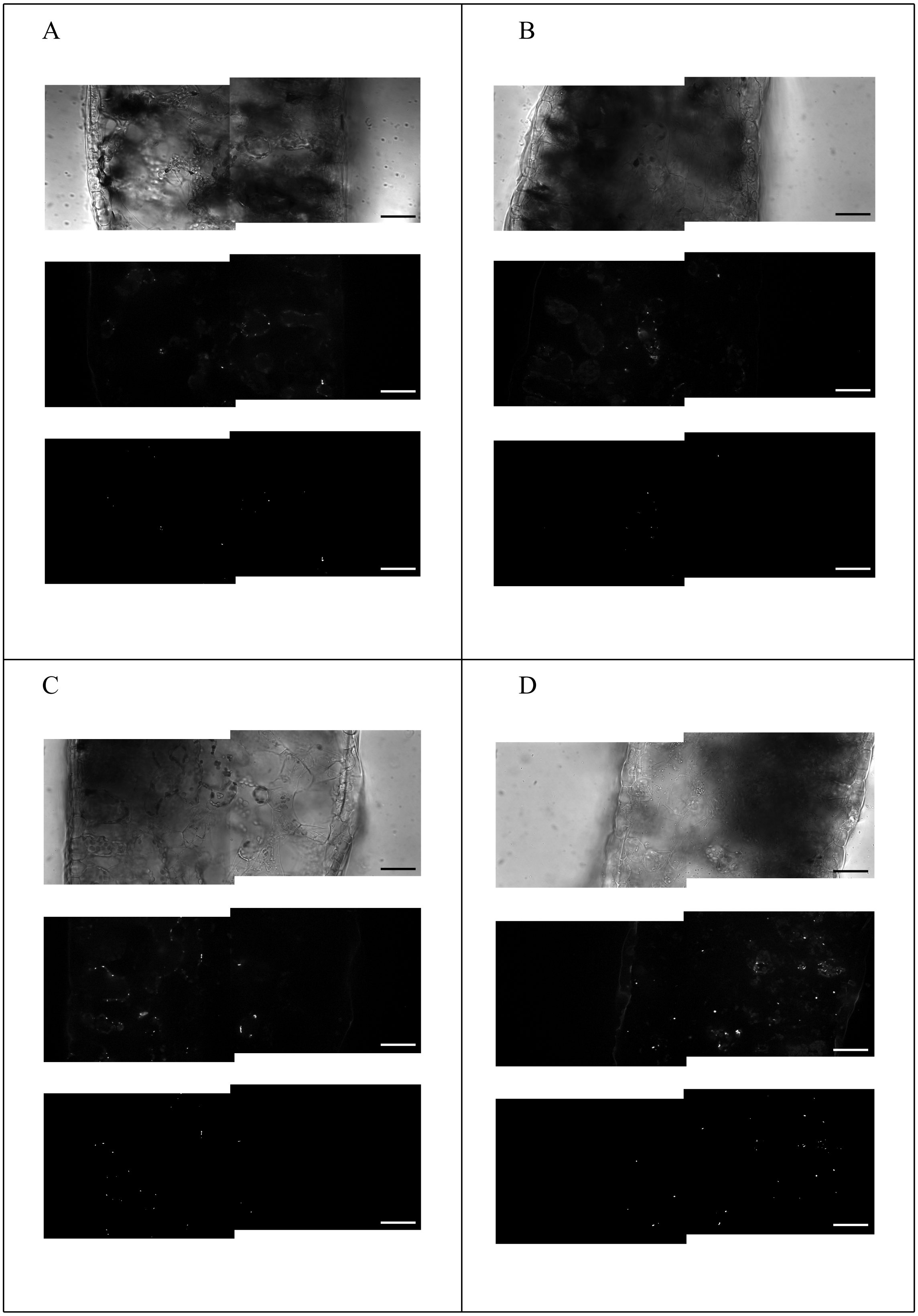

A
B
C
D

Figure 2.9. Representative micrographs of sectioned lettuce leaf explants infiltrated with labeled *Agrobacterium tumefaciens* and various surfactant concentrations. Micrographs represent single focal planes from image stacks corresponding to sample infection sites in leaf explants infiltrated with bacterial suspension containing (A) 1 ppm, (B) 10 ppm, (C) 100 ppm, and (D) 1000 ppm (v/v) surfactant. For each treatment, brightfield, fluorescent confocal, and binary images (in descending order) are provided. Binary images show isolated signals (colored white) following signal intensity and signal area screening. Two separate images were required to capture the entire width of the leaf section at each infection site. The apparent disjointed nature of compiled infection site micrographs stems from the alignment of the two corresponding images. Scale bars represent 40 μm.

2.3.5 Measurement of vacuum infiltration effects on initial bacterial attachment to leaf tissue

Bacterial attachment rates were measured in lettuce leaves vacuum-infiltrated with labeled *A. tumefaciens* at pressures of 5, 25, and 45 kPa. There was no significant difference ($p = 0.256$) between any of the pressures with regards to the amount of bound bacteria at infection sites (Figures 2.10 and 2.11, Appendix 2.6). The presence of an abnormally high outlier in the 5 kPa treatment led to large standard deviation. Removal of the outlier still yields no significant differences between the treatments.

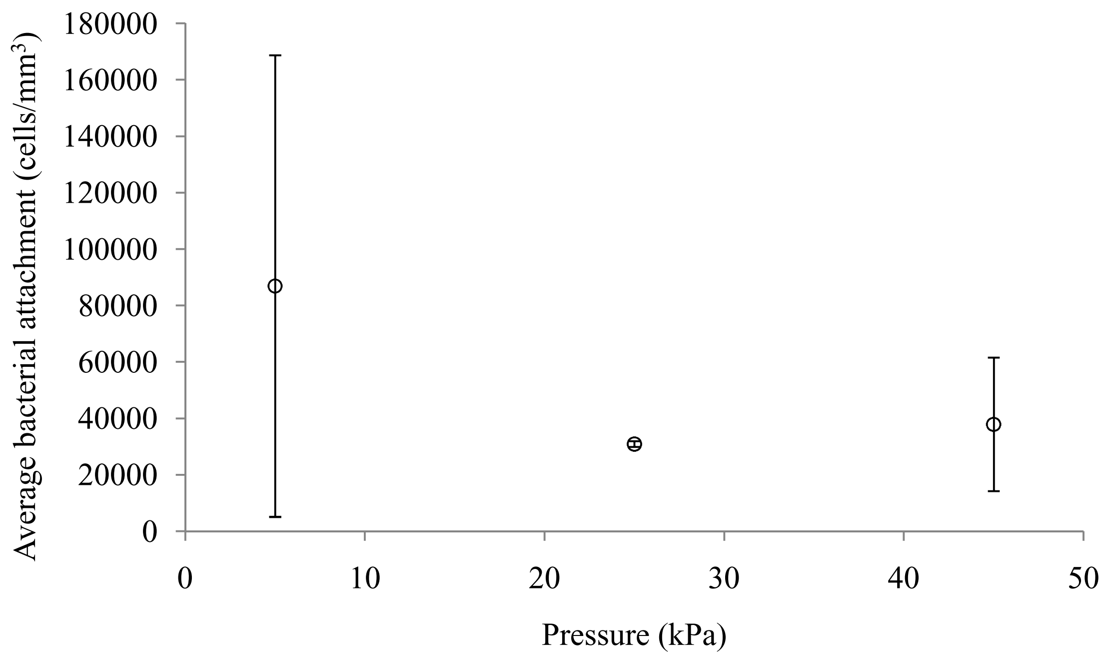

Figure 2.10. Density of attached bacteria sites versus pressure applied during vacuum infiltration of leaf tissue. Error bars represent one standard deviation.

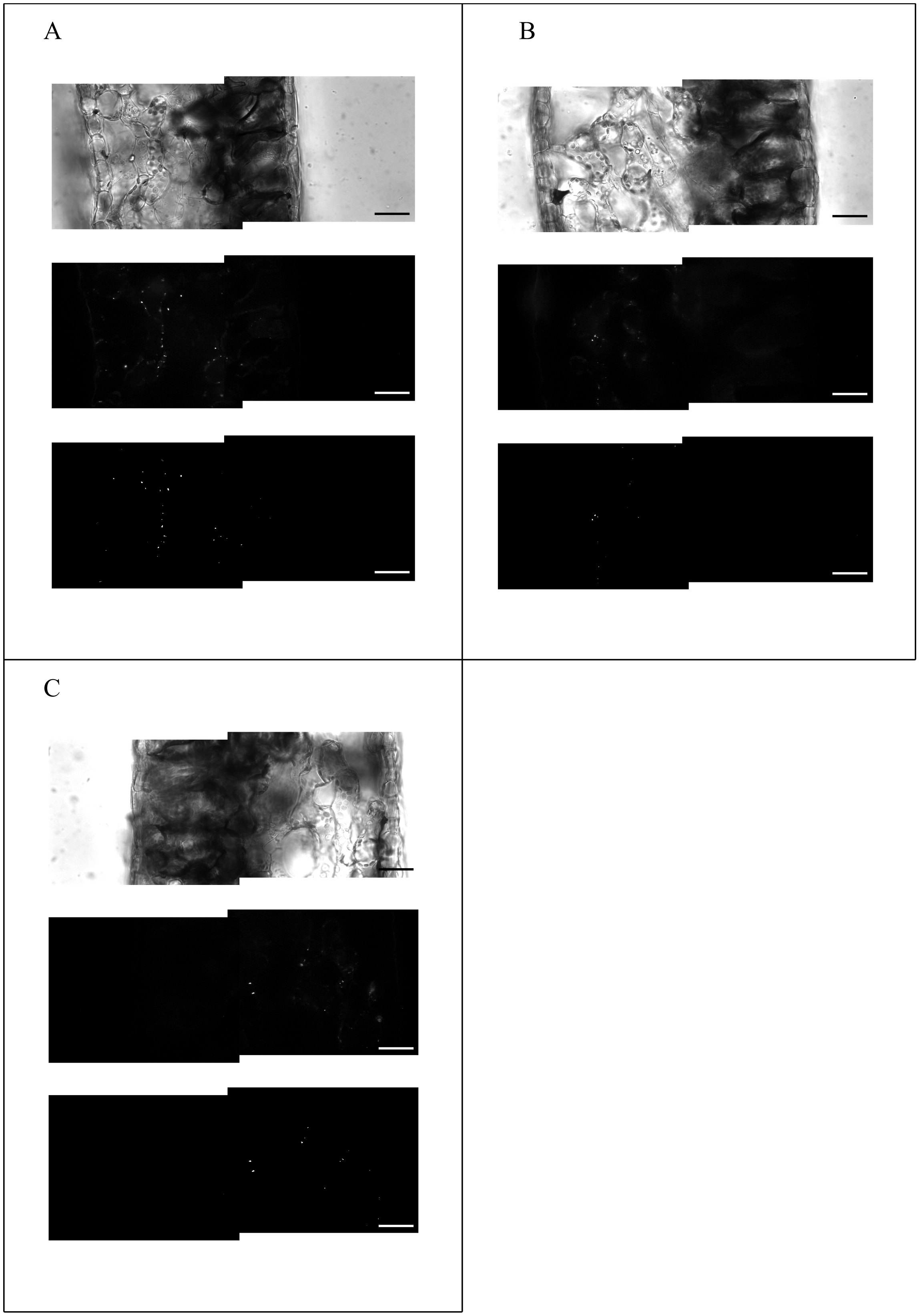
A
B
C

Figure 2.11. Representative micrographs of sectioned lettuce leaf explants infiltrated with labeled *Agrobacterium tumefaciens* at various vacuum levels. Micrographs represent single focal planes from image stacks corresponding to sample infection sites in leaf explants infiltrated with bacterial suspension at (A) 5 kPa, (B) 25 kPa, and (C) 45 kPa. For each treatment, brightfield, fluorescent confocal, and binary images (in descending order) are provided. Binary images show isolated signals (colored white) following signal intensity and signal area screening. Two separate images were required to capture the entire width of the leaf section at each infection site. The apparent disjointed nature of compiled infection site micrographs stems from the alignment of the two corresponding images. Scale bars represent 40 μm.

2.3.6 Measurement of infiltrated bacterial density effects on initial bacterial attachment to leaf tissue

Increased density of bacteria within the liquid infiltrated into lettuce leaf explants had a significant positive effect on the average density of attached bacteria at infection sites ($p = 0.001$) (Figure 2.12, Appendix 2.7). Attachment density shared a saturation relationship with infiltration density. The data were used to fit parameters in the following saturation model (Appendix 2.8):

$$d_A = \frac{d_{A,max}(d_I - d_{I,0})}{(\alpha - d_{I,0}) + (d_I - d_{I,0})} \qquad \text{(eq. 2.1)}$$

where d_A is the initial average density of *A. tumefaciens* attached at infection sites in units of cells per volume leaf tissue, $d_{A,max}$ is a constant describing the maximum possible initial average density of attached *A. tumefaciens* in units of cells per volume leaf tissue, d_I is the concentration of *A. tumefaciens* in the suspension infiltrated into leaf tissue in units of cells per volume suspension, $d_{I,0}$ is the highest density of infiltrated bacteria that does not yield detectable bacterial attachment in units of cells per volume suspension, and α is a constant describing the density of infiltrated bacteria needed to achieve half the value of $d_{A,max}$ in units of cells per volume suspension. The value of $d_{I,0}$ was estimated to be 10^8 CFU/ml based on the data. Fitted values for $d_{A,max}$ and α were 246,118 cells/mm^3 tissue and 2.2×10^9 CFU/ml, respectively.

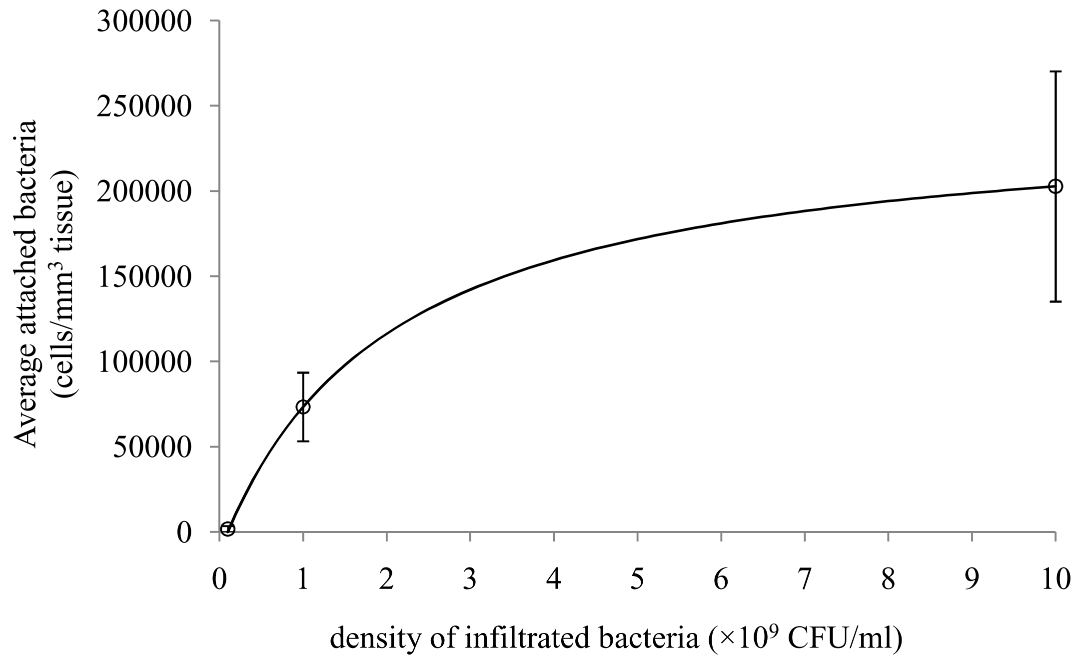

Figure 2.12. Average initial bacterial attachment versus density of infiltrated bacteria. Error bars represent one standard deviation. The solid line represents the fitted saturation model.

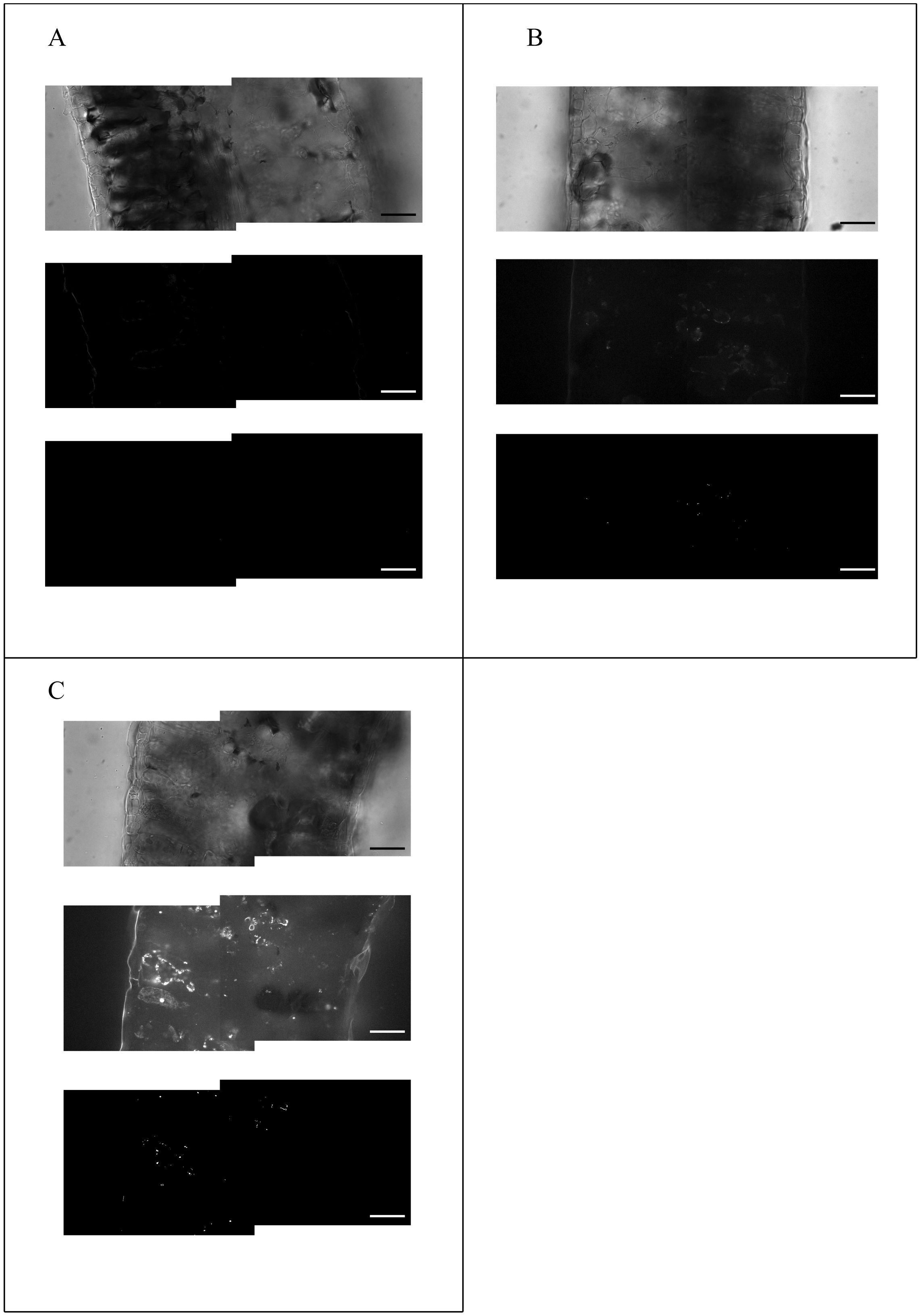
A
B
C

Figure 2.13. Representative micrographs of sectioned lettuce leaf explants infiltrated with various concentrations of labeled *Agrobacterium tumefaciens*. Micrographs represent single focal planes from image stacks corresponding to sample infection sites in leaf explants infiltrated with bacterial suspension containing (A) 10^8, (B) 10^9, and (C) 10^{10} CFU/ml. For each treatment, brightfield, fluorescent confocal, and binary images (in descending order) are provided. Binary images show isolated signals (colored white) following signal intensity and signal area screening. Two separate images were required to capture the entire width of the leaf section at each infection site. The apparent disjointed nature of compiled infection site micrographs stems from the alignment of the two corresponding images. Scale bars represent 40 μm.

2.3.7 Correlation of initial bacterial attachment levels to transgene transient expression levels

There was no significant difference in GUS expression levels between leaves infiltrated with *A. tumefaciens* at 10^8 CFU/ml and those infiltrated with 10^9 CFU/ml ($p = 0.45$). However, GUS expression fell significantly in leaves infiltrated with 10^{10} CFU/ml bacteria ($p = 0.016$) (Figure 2.14, Appendix 2.9). This trend was also observed in agroinfiltrated leaves that underwent histochemical staining to visualize GUS activity (Figure 2.15). Explants exhibiting GUS activity typically had intense expression along the cut edge, with lower, regionalized areas of GUS activity within the interior of the leaf disk. GUS expression at both the cut edge and central area of leaf disks decreased in leaves infiltrated with 10^{10} CFU/ml. Negative control leaves infiltrated with disarmed *A. tumefaciens* strain C58 exhibited no stain. No putrefaction was observed in leaves from any treatment following the 72 hour incubation step to facilitate *in planta* GUS expression.

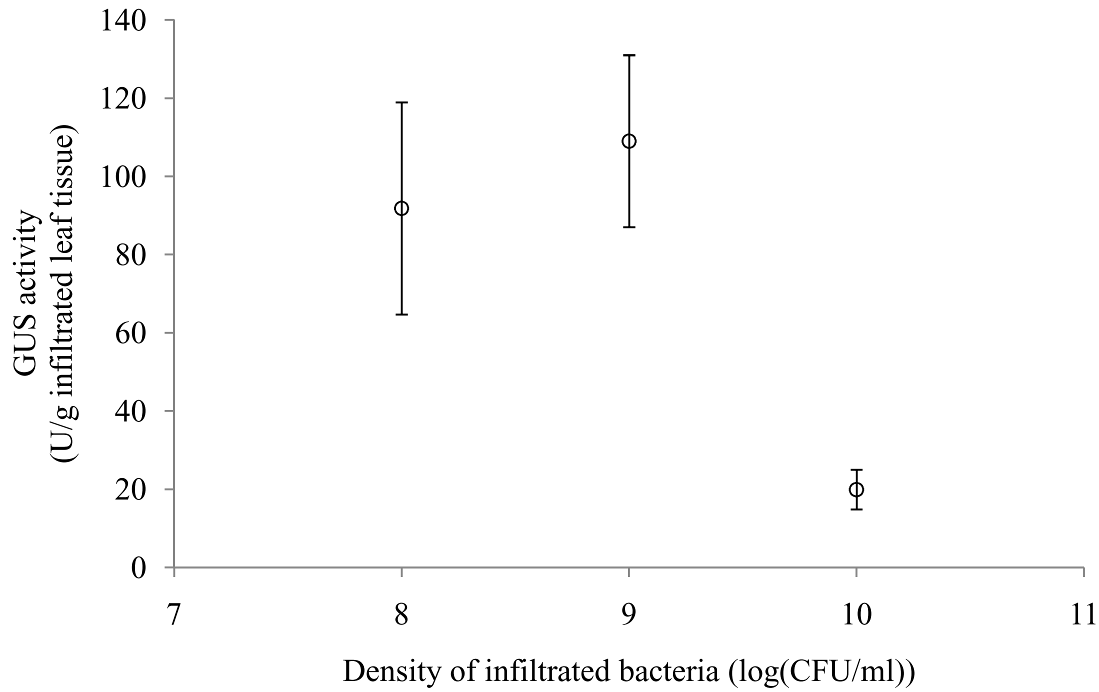

Figure 2.14. GUS activity in lettuce leaf tissue infiltrated with varying concentrations of *A. tumefaciens*. Error bars represent one standard deviation.

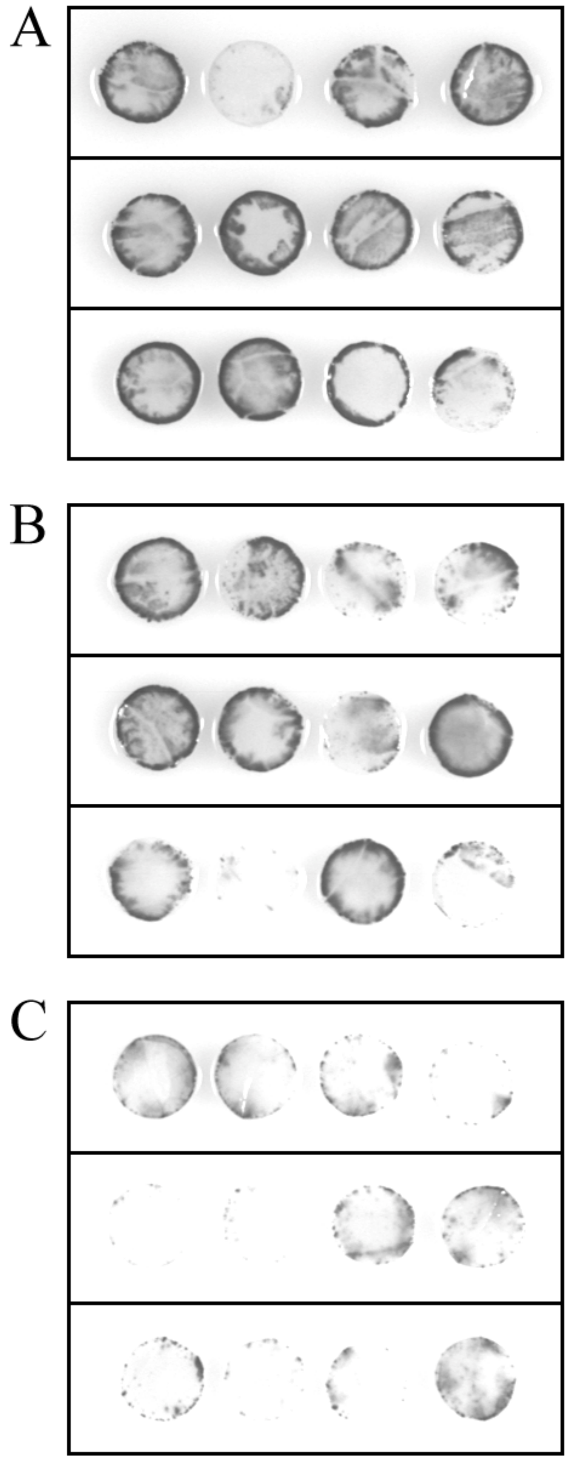

Figure 2.15. Agroinfiltrated lettuce leaf explants with histochemical stain to show regions of GUS activity. Leaves were agroinfiltrated with (A) 10^8, (B) 10^9, and (C) 10^{10} CFU/ml.

2.4 Discussion

2.4.1 Measurement of bacterial attachment to leaf tissue and in planta transgene expression kinetics

The observed decrease in bacterial signal density over time in agroinfiltrated leaf tissue following infiltration must be interpreted in conjunction with results observed in Chapter 1. Specifically, the observation that *A. tumefaciens* proliferates within leaf tissue after infiltration must be considered along with the nature of Syto 16 nucleic acid stain's mode of action when contemplating the cause of the observed signal density kinetics. It is possible that decreased signal densities indicate lower levels of *A. tumefaciens* attached to leaf cells over time. However, given that the finite amount of nucleic acid stain present in the initial population of infiltrated bacteria is effectively diluted as the bacteria divide, such decreases in signal densities may also be explained by the concentration of stain in bacteria falling below the detection limit. The experiment does not allow one to determine which scenario is correct and reflects a weakness in using nucleic acid stain to label cells that actively grow during the period of observation. Using transgenic bacteria that express a fluorescent protein or another system where the concentration of fluorophore is maintained in each cell regardless of division would eliminate this uncertainty.

Despite the technique's shortcoming for measuring attachment kinetics over periods longer than the doubling time of *A. tumefaciens*, the data demonstrate that high-level attachment to plant cells can be detected almost immediately after infiltration, as indicated by data at the first time point of one hour. These data are in agreement with observations made on *A. tumefaciens* binding to potato tuber disks (Kluepfel and

Pueppke, 1986), which show that binding of the plant tissue is saturated within one hour of exposure to *A. tumefaciens*. These initial measurements are likely minimally affected by growth-associated dilution of the nucleic acid stain since the time that passes between infiltration and imaging is less than the approximately 3 hour doubling time of *A. tumefaciens* in liquid culture.

In addition to the stain dilution issue, actively growing bacteria present another challenge for selecting a response to characterize attachment of *A. tumefaciens* to leaf tissue. For an adsorption process, the Langmuir adsorption constant is often used to quantify the affinity of a particle attaching to a surface. Calculation of the Langmuir constant requires measurements of bound and free particles at steady-state. However, such readings may be difficult to acquire in agroinfiltrated leaf tissue since the bacteria continue to divide within it, potentially preventing steady-state from being reached. In light of these issues and the fact that high-level binding is observed rapidly after infiltration, the measured attachment levels of labeled *A. tumefaciens* immediately after infiltration of leaf tissue, which equates to approximately one hour of co-incubation time due to sample processing, was defined as the initial attachment level and used as the response to gauge bacterial avidity to leaf tissue in following experiments.

2.4.2 Measurement of vacuum infiltration effects on initial bacterial attachment to leaf tissue

The pressure applied to lettuce leaf tissue submerged in *A. tumefaciens* suspension did not have a significant effect on the density of bacteria bound to leaf cells at infection sites. This result suggests that applied vacuum does not alter the plant tissue or bacteria in such a way as to promote or inhibit bacterial attachment. Previous research has shown that vacuum infiltration can cause wounding in tomato fruit as indicated by increased ethylene production (Gross, 1985). However, vacuum application to lettuce leaves, which occurs commonly (and at greater magnitudes than those used in this study) during vacuum cooling of commercially-grown lettuce, does not lead to a loss in quality (Martinez and Artes, 1999), suggesting that minimal wounding occurs during vacuum. The data agree with this suggestion, showing no evidence that vacuum compromises plant cell walls to release phenolics or alter the avidity of *A. tumefaciens* to plant cells.

The volume of liquid infiltrated into leaf tissue depends on vacuum intensity during infiltration (Simmons et al., 2009). Likewise, GUS expression levels have been shown to increase when higher vacuum levels are applied during vacuum infiltration (Simmons et al., 2009). These observations, along with the bacterial attachment data, provide a better understanding of the mechanism behind the positive relationship between vacuum intensity and transient transgene expression. Specifically, that the elevation in transient expression is most likely solely due to an increased number of plant cells being exposed to bacteria by way of more suspension entering leaf tissue when subjected to higher vacuum levels. Stated otherwise, higher vacuum levels lead to a wider distribution of bacteria within leaf tissue, likely creating more infection sites but not altering the way that bacteria attach to leaf cells at those infection sites. The greater number of infection sites may promote more of the leaf tissue being transformed and ultimately expressing the transgene. Given that vacuum application does not affect bacterial attachment, it follows that alteration of vacuum levels may only improve transgene expression levels in plants that are already compatible with agroinfiltration and not those to which *A. tumefaciens* cannot attach to.

2.4.3 Measurement of surfactant level effects on infiltrated liquid volume, leaf viability, and initial bacterial attachment to leaf tissue

Although it is well documented that the addition of surfactant to the infiltration medium boosts transgene transient expression in dicots (Clough and Bent, 1998; Kim et al., 2009), little work has been done to understand why this is so. The data show that addition of surfactant to bacterial suspensions improved both the volume of infiltrated liquid and the amount of bacteria attached to leaf tissue. Both phenomena may contribute to the positive effect of surfactant on transformation efficiency. Previous work has shown that gases within leaf tissues expand and evacuate the tissue during vacuum application. Upon repressurization, liquid enters the leaf to replace the volume of escaped gas (Simmons et al., 2009). Evacuation of gases from leaf tissue depends on gases first leaving the leaf interior, resulting in bubbles on the leaf surface, and then the detachment of those bubbles from the surface. Incomplete detachment of surface-bound bubbles may lead to those gases reentering the leaf interior as vacuum is released, negating the infiltration of bacterial suspension. A decrease in surface tension through the addition of surfactant promotes bubble detachment by decreasing the force necessary to separate a bubble adhered to a solid surface (Janczuk, 1983). In this way, higher surfactant levels may increase transformation rates across a leaf explant by working in conjunction with vacuum infiltration to maximize the volume of bacterial suspension that enters the leaf after being subjected to a given vacuum pressure, effectively increasing the number of plant cells brought into contact with bacteria. However, unlike vacuum application alone, there is evidence that surfactant also has an effect on attachment of individual bacteria to plant cells.

The mechanism by which surfactant enhances penetration of compounds through the leaf cuticle is relatively well understood due to its relevance to sprayed application of chemicals to leaves. By comparison, surfactant effects on the plant cell wall remain unknown. As a result, the mode of action responsible for surfactant-dependent enhancement of bacterial attachment to leaf cells is largely a matter of speculation. Prior studies have shown that treatment with the surfactant UBI-1126 can accelerate abscission in the leaf abscission zone of *Coleus blumei*, a dicot plant (Morrison-Baird et al., 1978). Accelerated abscission correlated with increased degradation of the middle lamella and disruption of the cell wall. As a result, cells in the abscission zone were more loosely bound to one another, with separation cavities present in the shared middle lamella of neighboring cells and some cells completely detached from adjacent cells. As the surfactant was observed to disrupt membranes, it was submitted that surfactant could possibly facilitate release of hydrolytic enzymes either through directly breaching the plasma membrane or activating pathways that result in enzyme release. Further research supported this hypothesis by showing that *Coleus* plants treated with UBI-1126 surfactant exhibited increased cellulase activity in the abscission zone compare to untreated control plants (Baird and Reid, 1992). Surfactant treatment may be causing a similar effect in lettuce leaf tissue and the resultant changes to the plant cell wall could promote bacterial attachment. Dissolution of the middle lamella and resultant detachment of neighboring plant cells may expose more of the cell surface for *Agrobacterium* attachment.

Furthermore, it has been shown that at least one factor influencing *Agrobacterium* attachment to plant cells is housed within the pectin fraction of plant cell walls (Rao et al., 1982; Neff et al., 1987). As surfactant can alter the integrity of the middle lamella, which contains pectin as a major component (Albersheim et al., 1960), these attachment factors may be made more accessible to *Agrobacterium*, resulting in increased avidity to plant cells.

In addition to possibly altering the structure and composition of the plant cell wall, surfactant may also affect the motility of *Agrobacterium*. Research has indicated that *Agrobacterium vitis* exhibits swarming behavior, or the ability to move over solid surfaces. While most species of *Agrobacterium* employ swimming motility to move through liquids, *A. vitis* uniquely possesses surface motility. The ability of *A. vitis* to migrate across surfaces correlates with production of a biosurfactant by the bacteria (Süle et al., 2009). Unlike *A. vitis*, *A. tumefaciens* does not produce biosurfactant. The addition of exogenous surfactant may alter the colonization of plant tissue by *A. tumefaciens* in a way similar to that utilized natively by *A. vitis*.

While the highest surfactant concentration tested, 1000 ppm, yielded the greatest levels of initially attached bacteria, this treatment ultimately proved toxic to the leaf tissue 72 hours post-infiltration, as indicated by necrosis of the leaf tissue. This result suggests that the addition of surfactant induces wounding of the plant tissue. Such wounding may also contribute to attachment of *A. tumefaciens*, as the bacteria are known to be opportunistic pathogens, and highlights the need to balance surfactant level with plant viability when seeking to alter bacterial attachment levels. The unknown aspects of both plant wounding and plant-microbe interactions highlight the need for further research to reveal the exact nature of surfactant's effect on plant cell walls and *A. tumefaciens*.

2.4.4 Measurement of infiltrated bacterial density effects on initial bacterial attachment to leaf tissue and in planta GUS expression

The concentration of bacteria in infiltrated suspension had the most influence over initial attachment rates. The relationship between the level of bound bacteria and density of bacteria in the infiltrated solution exhibited a saturation trend. This trend is similar to a Langmuir isotherm adsorption curve, with the notable exception that it is based off initial readings of attached bacteria instead of steady-state measurements needed to calculate a true Langmuir isotherm. Fitting a saturation model similar in form to the Lagmuir isotherm to the data allowed for the maximum theoretical density of attached bacteria to be estimated (given by the value of $d_{A,max}$). This value may be indicative of the total number of *A. tumefaciens* binding sites present on the surface of plant cells per unit leaf volume. Moreover, unlike a traditional Langmuir isotherm, the x-intercept of the plotted data does not lie at the origin, necessitating the introduction of the constant $d_{I,0}$ in the modified saturation model to correct for the offset. The fact that the attachment curve does not run through the origin suggests that other phenomena are influencing attachment, causing the attachment behavior to deviate from that predicted by standard adsorption alone. In typical adsorption processes, if adsorbate is present in the liquid phase then some fraction will also be adhered to the adsorbant at equilibrium. Given that relatively high concentrations of *A. tumefaciens* in infiltrated liquid, up to 10^8 CFU/ml, yield barely detectable adhesion to plant cells and more typical adsorption behavior only begins after crossing that threshold of bacterial density in the liquid phase indicates that a synergistic mechanism between bacteria may influence attachment to the plant host.

Quorum sensing, in which organisms use a signal to determine the population density of the colony they reside in, is used in many different species of bacteria for triggering various pathways. Often, virulence pathways in bacteria are only activated once bacterial density has achieved a level sufficient for resisting the host's immune response. In *A. tumefaciens*, horizontal transfer of the Ti-plasmid is regulated by quorum sensing (Zhang and Kerr, 1991). In response to opines, a product of *in planta* expression of genes encoded on wild-type T-strands, bacteria produce a compound that promotes the expression of genes related to conjugal gene transfer (Piper et al., 1993; Zhang et al., 1993). One of the genes that is regulated by this form of quorum sensing is *attM*, a member of the attachment (*att*) gene family known to play a role in binding to plant cells (Zhang et al., 2002). Moreover, certain *A. tumefaciens att* mutants that are unable to attach to plant cells can regain the ability to attach following incubation with media obtained from nonmutants incubated with wounded plant tissue (Matthyse, 1987). These prior observations, coupled with the data reported here, provide compelling circumstantial evidence that quorum sensing may be linked to bacterial attachment to plant tissues and warrant further research to elucidate whether a direct linkage exists.

As the concentration of infiltrated bacteria was found to have the most influence on bacterial attachment rates of the infiltration factors studied, bacterial density was varied to investigate the relationship between bacterial attachment levels and transient expression of an agroinfiltrated transgene. The data showed a dramatic decrease in expression levels when high concentrations of bacteria are infiltrated into leaf tissue, although leaf viability appeared unaffected. In *Arabidopsis,* agroinfiltration with levels of *A. tumefaciens* st. C58C1 ranging from OD_{600} 0.3 to 1.2 (estimated to be approximately 1×10^9 to 5×10^9 CFU/ml using the empirical equation provided in the methods section of chapter 2 to relate optical density to bacterial density) yielded consistent expression levels. However, leaf viability decreased when high bacterial densities were infiltrated (Kim et al., 2009). In lettuce, previous work has shown that infiltrated bacterial densities beyond a critical threshold resulted in decreased transgene transient expression (Simmons et al., 2009). The attachment data from this work show that these high densities of infiltrated bacteria result in increased bacterial adhesion to plant cells. In turn, these higher populations of attached bacteria may result in elevated levels of T-strands inserted into host plant cells. It is possible that higher *in planta* T-strand levels trigger plant defenses against foreign genetic material, resulting in attenuated expression. Prior work has shown that *Arabidopsis* seedlings homozygous for a particular transgene showed higher post-transcriptional gene silencing (PTGS) of transgenes compared to plants that were hemizygous (Dehio and Schell, 1994). A previous study showed that coexpression of viral post-transcriptional gene silencing suppressors in lettuce did not improve recombinant GUS expression following agroinfiltration (Simmons and VanderGheynst, 2007). However, that work was performed using *A. tumefaciens* infiltrated at a density of 10^9 CFU/ml, a concentration shown to not lead to decreased transgene transient expression. It is possible that coexpression of PTGS suppressors may prove effective at preventing lowered transgene expression when higher bacterial densities are infiltrated, although it is unclear whether such measures would increase the maximum level of expression or simply maintain expression levels seen at lower infiltrated bacterial densities.

Overall, there appears to be a second order relationship between the density of *A. tumefaciens* attached to plant cells at infection sites and the level of *in planta* transgene expression. In turn, increasing transgene expression levels is not simply a matter of promoting as much bacterial attachment to plant cells as possible. This research related attachment trends at specific infection sites to transgene expression levels across the entire leaf explant. Future research could better resolve the connection between bacterial attachment and *in planta* transgene expression by correlating infection site attachment levels to transgene expression levels at those infection sites. Such measurements were not possible in this study because the protocols for measuring attached bacteria and GUS activity do not permit both metrics to be measured on the same leaf explant. Moreover, the data motivate future investigation into the relationship between the density of attached bacteria and *in planta* T-strand levels. Studies that track T-strand migration from bacteria to host plant cells would be especially useful for determining how a population of bacteria attached to a given plant cell relates to the number of transgenes that ultimately enter the plant cell nucleus.

2.5 Conclusions

The attachment of *A. tumefaciens* to plant cells is a critical but incompletely understood step in agroinfiltration. Lettuce was used as a model host to study *A. tumefaciens* attachment due to its known susceptibility to transformation by the bacteria. Bacterial attachment was detected almost immediately following infiltration of lettuce leaf tissue. Given that maximum recombinant GUS expression levels in leaves weren't achieved until 48 hour post-infiltration, attachment of *A. tumefaciens* to leaf tissue does not appear to be the rate-limiting step in T-strand transfer to plant cells. Further research is needed to elucidate the kinetics of T-pilus construction as well as T-strand transfer through the T-pilus, plant cell cytoplasm, and into the nucleus in order to determine what the rate-limiting transfer step is.

Several infiltration factors were studied with respect to any effect they may have on bacterial attachment to leaf tissue. Vacuum intensity did not have a significant effect on attachment rates. Surfactant level and the concentration of infiltrated bacteria both exhibited a significant positive effect on binding. However, bacterial concentration had a much larger impact on attachment levels compared to surfactant level. High levels of surfactant were toxic to leaf tissue but yielded greatest bacterial attachment rates. While an infiltrated bacterial density of 10^{10} CFU/ml did not appear to affect leaf viability, it did lead to decreased *in planta* transgene expression levels compared to lower bacterial concentrations of 10^{8} and 10^{9} CFU/ml. The data show that bacterial attachment rates affect transgene expression and that there is a specific range of bacterial attachment that leads to optimal transient expression of transgenes. However, to better understand how bacterial attachment levels translate to transformation rates and more research is needed to measure T-strand transfer to plant cells following bacterial attachment.

Chapter 3 - Factors affecting attachment of *Agrobacterium tumefaciens* to switchgrass leaf tissue and the effect of attachment on *in planta* transient transgene expression

3.1 Introduction

While many dicots are readily transformed with *Agrobacterium*, monocots are typically far more recalcitrant to agroinfiltration (reviewed by Sood et al., 2011). Agroinfiltration is often used to transform monocot calli and generate plants with stable transformation. However, generally low transformation efficiencies stymie high-level transient expression in monocot plants. The reason for the drastic disparity in agroinfiltration competency between dicots and monocots is unknown. *Agrobacterium* virulence and chemotaxis is induced by monocot-produced compounds (Ashby et al., 1988), suggesting that inhibition of agroinfiltration lies downstream of these steps. Bacterial attachment is the subsequent step in the infection pathway and has not yet been investigated in relation to attenuated transformation efficiency. Prior work has demonstrated that at least one protein that acts as an *Agrobacterium* attachment factor lies within the pectin fraction of the plant cell wall (Rao et al., 1982; Neff et al., 1987). Generally, monocot cell walls contain significantly lower levels of pectin compared to dicots (Jarvis et al., 1988), raising the possibility that monocots exhibit decreased levels or altogether lack certain *Agrobacterium* attachment factors. Furthermore, additional structural and compositional differences exist between monocot and dicot cell walls that may influence attachment behavior. For these reasons, bacterial attachment may be a rate limiting step in agroinfiltration of monocots and a potential contributor to low transformation efficiency.

In this study, attachment of *Agrobacterium* to *Panicum virgatum*, a monocot plant, was measured in a similar manner to the work performed with lettuce in Chapter 2. *P. virgatum* (switchgrass) was chosen as a model plant for its ease of cultivation and blossoming commercial relevance. As a hearty, perennial plant that produces high yields of lignocelluloses, switchgrass has garnered interest as a potential feedstock for the emerging lignocellulosic biofuel industry (reviewed by Keshwani and Cheng, 2009). As part of the processing scheme for lignocellulosic feedstocks, the highly ordered cell wall must be deconstructed to free constituent sugars for fermentation to biofuels. Enzymes that catalyze cell wall deconstruction are often used to this end. High-level transient expression of various cell wall degrading enzymes in switchgrass, if possible, would be useful for testing novel enzymes and enzyme mixes or for exploring the possibility of post-harvest self-deconstruction via feedstock-expressed enzymes. In light of this, bacterial attachment was studied in response to infiltration variables, as described in Chapter 2, to determine if switchgrass recalcitrance to agroinfiltration lies at the level of *Agrobacterium* attachment and if transformation efficiency can be improved through alteration of attachment levels.

3.2 Materials and Methods

3.2.1 Bacterial strains, culture, and staining

A. tumefaciens was cultured and stained with Syto 16 green fluorescent nucleic acid stain as described in Chapter 1.

3.2.2 Plant materials and preparation

Panicum virgatum var. alamo was grown in a greenhouse using methods described for lettuce in Chapter 1. Leaves were harvested for use from 8 to 16 week old plants. Harvested leaves were chosen to have a maximum blade width between 0.75 and 1 cm. Leaves were washed in distilled deionized water and stored at 4 ˚C and 100% humidity following harvest. Leaves were not stored longer than two hours before processing for experimentation. Prior to infiltration, explants were cut from the middle section of the leaf blade using a razor blade at 1 cm intervals.

3.2.3 Infiltration of Agrobacterium tumefaciens into leaf tissue, sectioning, and histochemical staining of agroinfiltrated leaf tissue

Switchgrass leaf explants were infiltrated with suspensions of *A. tumefaciens* using the protocol described in Chapter 1. Switchgrass leaf explants were sectioned using the protocol described for lettuce in Chapter 1. Switchgrass leaves were sectioned parallel to leaf venation, as this orientation was found to best preserve leaf structure. Leaf explants were stained for GUS activity using the method described in Chapter 1. Leaves were incubated in staining solution for 6 hours.

3.2.4 Extraction of GUS from agroinfiltrated leaves

Agroinfiltrated leaves frozen at -80 ˚C were combined with frozen aliquots of -80 ˚C extraction buffer (as defined in the extraction protocol of Chapter 2) on a 2:1 buffer volume to leaf mass ratio in 10 ml stainless steel grinding jars with two 1 cm stainless steel grinding balls. Leaves were lysed within grinding jars using a Tissuelyser II

(Qiagen) by shaking at 30 Hz for 60 seconds. Frozen lysates were removed from grinding jars, placed in 1.5 ml tubes, and centrifuged at 10,000×g for 10 minutes at 4 ˚C. Supernatants were aspirated into fresh tubes and then stored at -80 ˚C.

3.2.5 Colorimetric GUS activity assay

Leaf extracts were assayed for GUS activity using the enzyme activity-based spectrophotometric assay described in Chapter 2, except the assay was run over 24 hours instead of 60 minutes. Initial and final time point readings were used to calculate activity levels.

3.2.6 Imaging of leaf tissue infiltrated with labeled Agrobacterium tumefaciens

Infiltrated leaf tissue sections were imaged using brightfield and fluorescent confocal microscopy as described in Chapter 2.

3.2.7 Analysis of micrographs

Brightfield and fluorescent confocal micrographs of agroinfiltrated leaf tissue were analyzed for bacterial attachment using the techniques described in Chapter 2.

3.2.8 Statistical analysis

Parameter fitting and hypothesis testing were performed using JMP version 8.0.

3.2.9 Measurement of surfactant effects on vacuum-infiltrated liquid volume and leaf viability

Switchgrass leaf explants were infiltrated at 25 kPa with varying levels of Break-Thru S240 surfactant as described in Chapter 2. The volume of infiltrated liquid and the viability of leaf tissue 72 hours post-infiltration were measured.

3.2.10 Measurement of surfactant effects on initial bacterial attachment to leaf tissue

Switchgrass leaf explants were infiltrated with 10^9 CFU/ml Syto 16-labeled *A. tumefaciens* containing 1, 10, 100, and 1000 ppm (v/v) Break-Thru S240 surfactant as described in Chapter 2. Microscopy and image analyses were performed as outlined in Chapter 2. A 12-bit signal intensity threshold of 230 was used to isolate bacterial signals.

3.2.11 Measurement of vacuum infiltration effects in infiltrated liquid volume in leaf tissue

Groups of ten leaf explants were infiltrated with water containing no surfactant at varying pressures. Three replicate groups were each infiltrated at 5, 25, and 45 kPa. Groups of explants were gently blotted dry and weighed prior to and following vacuum infiltration to determine the volume of liquid infiltrated.

3.2.12 Measurement of vacuum infiltration effects on initial bacterial attachment to leaf tissue

Switchgrass leaf explants were infiltrated with 10^9 CFU/ml Syto 16-labeled *A. tumefaciens* at 5, 25, and 45 kPa and resultant bacterial attachment was measured as described in Chapter 2. A 12-bit signal intensity threshold of 235 was used to isolate bacterial signals.

3.2.13 Measurement of infiltrated bacterial density effects on initial bacterial attachment to leaf tissue

Switchgrass leaf explants were infiltrated with 10^8, 10^9, and 10^{10} CFU/ml Syto 16-labeled *A. tumefaciens* and resultant bacterial attachment levels were measured as described in Chapter 2. A 12-bit signal intensity threshold of 235 was used to isolate bacterial signals.

3.2.14 Correlation of initial bacterial attachment levels to transgene transient expression levels

Groups of 10 leaf explants were infiltrated with 10^8, 10^9, or 10^{10} CFU/ml *A. tumefaciens* as described in Chapter 2. Leaves were infiltrated with *A. tumefaciens* strain C58 and water as negative controls. Three groups of leaves were infiltrated with each concentration treatment containing 100 ppm Break-Thru S240 at 25 kPa for 7.5 minutes. Following post-infiltration incubation, five explants from each group of leaves underwent histochemical staining. The remaining five explants from each group were weighed, extracted, and assayed for GUS activity using the colorimetric assay, as previously described.

3.3 Results

3.3.1 Measurement of surfactant effects on vacuum-infiltrated liquid volume and leaf viability

There was not a significant difference in infiltrated liquid volume as function of surfactant concentration in infiltrated liquid (p = 0.62) (Figure 3.1, Appendix 3.1). Regardless of surfactant concentration, the amount of infiltrated liquid following vacuum infiltration held constant at approximately 0.05 ml/g leaf tissue. No yellowing or putrefaction of leaf explants were observed following 72 hours of incubation post-infiltration.

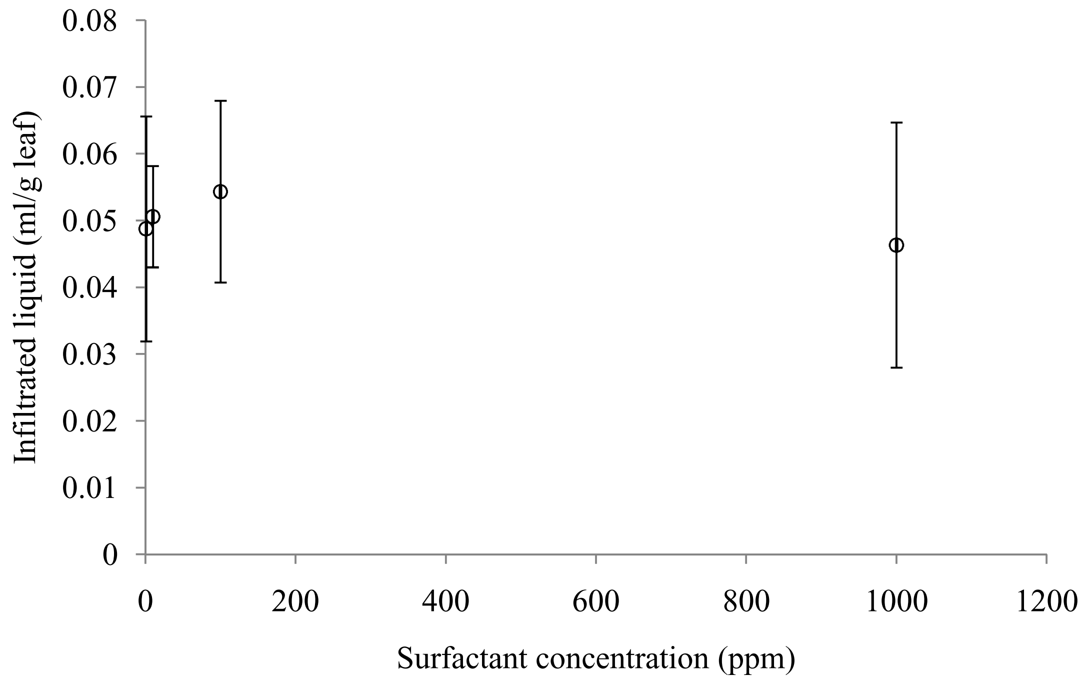

Figure 3.1. Volume of infiltrated liquid following vacuum infiltration versus surfactant concentration in the infiltrated liquid. Error bars represent one standard deviation.

3.3.2 Measurement of surfactant effects on initial bacterial attachment to leaf tissue

The addition of surfactant did not significantly affect the attachment of *A. tumefaciens* to switchgrass leaf tissue (p = 0.22) (Figures 3.2 and 3.3, Appendix 3.2). At higher surfactant levels (100 and 1000 ppm), some samples exhibited large attachment levels that were orders of magnitude greater than any values seen using 1 or 10 ppm surfactant. These values were not consistently observed within their respective treatments, leading to great variability at higher surfactant treatments. However, the phenomenon is apparent when the maximum attachment rate in each surfactant treatment is regressed against surfactant concentration, yielding a positive relationship that approaches significance (p = 0.08) (Figure 3.4).

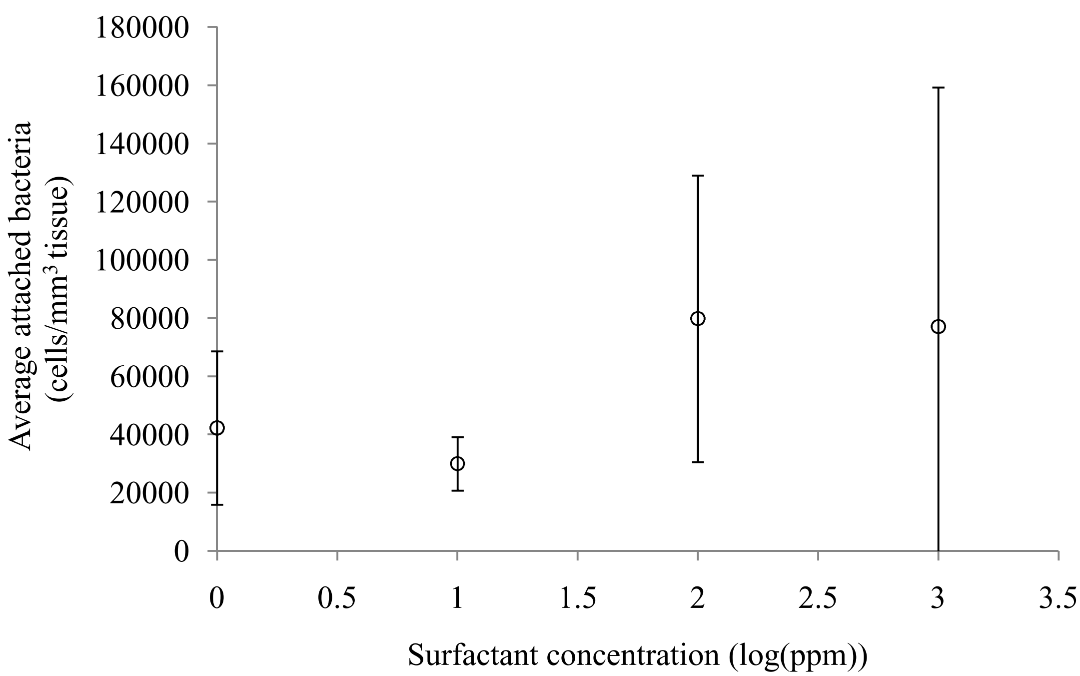

Figure 3.2. Average density of bacteria attached to infection sites in response to surfactant level within infiltrated bacterial suspensions. Error bars represent one standard deviation.

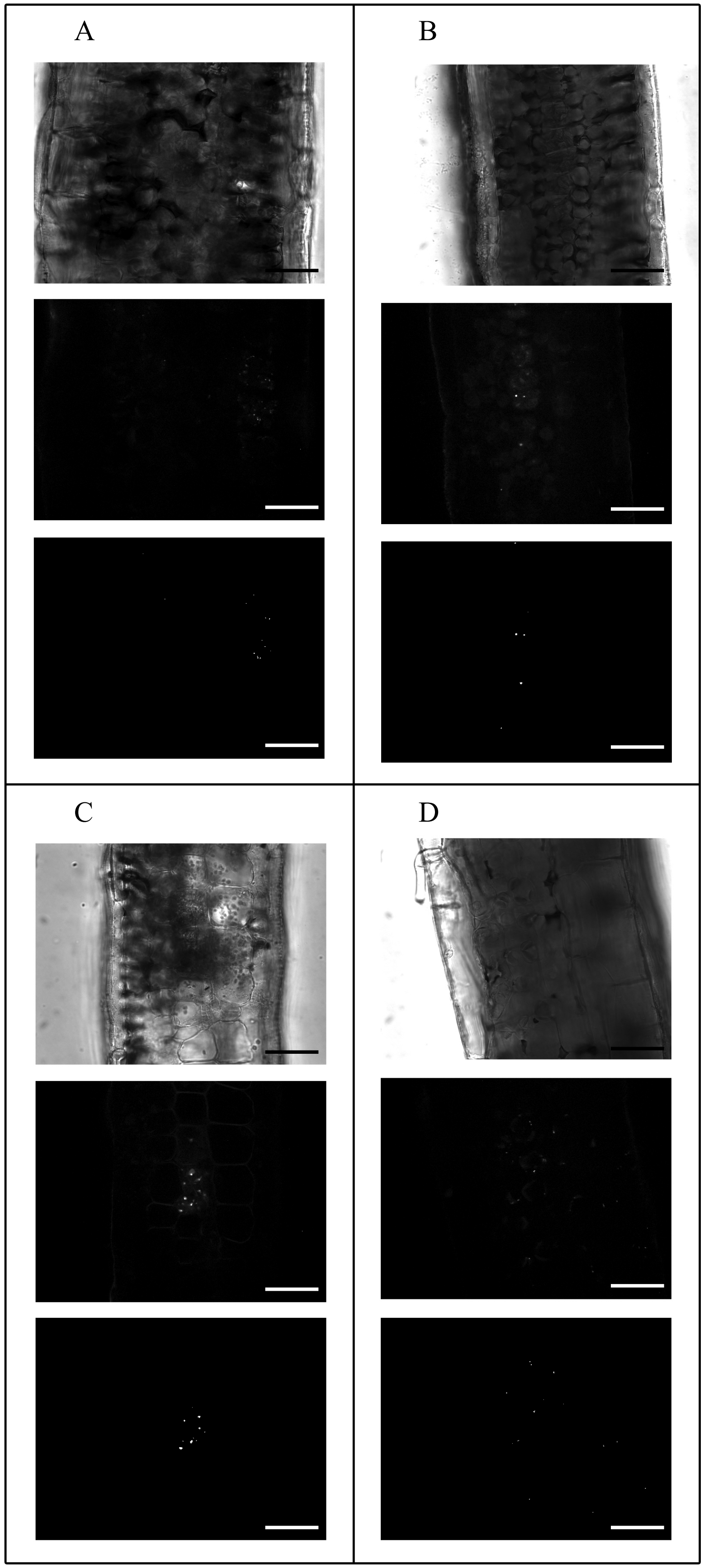

Figure 3.3. Representative micrographs of sectioned switchgrass leaf explants infiltrated with labeled *Agrobacterium tumefaciens* and various surfactant concentrations. Micrographs represent single focal planes from image stacks corresponding to sample infection sites in leaf explants infiltrated with bacterial suspension containing (A) 1 ppm, (B) 10 ppm, (C) 100 ppm, and (D) 1000 ppm (v/v) surfactant. For each treatment, brightfield, fluorescent confocal, and binary images (in descending order) are provided. Binary images show isolated signals (colored white) following signal intensity and signal area screening. Scale bars represent 40 μm.

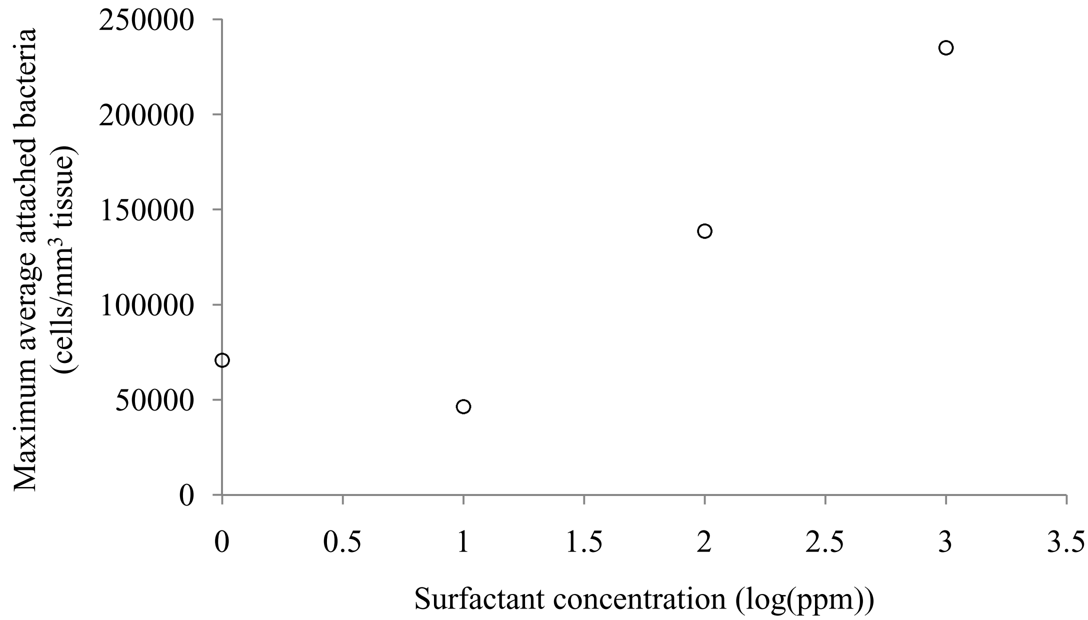

Figure 3.4. Maximum observed average density of attached bacteria versus surfactant concentration in infiltrated bacterial suspension.

3.3.3 Measurement of vacuum infiltration effects on infiltrated liquid volume in leaf tissue

There was a significant negative effect of pressure applied during vacuum infiltration and the volume of liquid infiltrated into leaf tissue ($p = 0.008$) (Figure 3.5, Appendix 3.3). Greater vacuum intensities (i.e., lower pressures) resulted in larger volumes of infiltrated liquid.

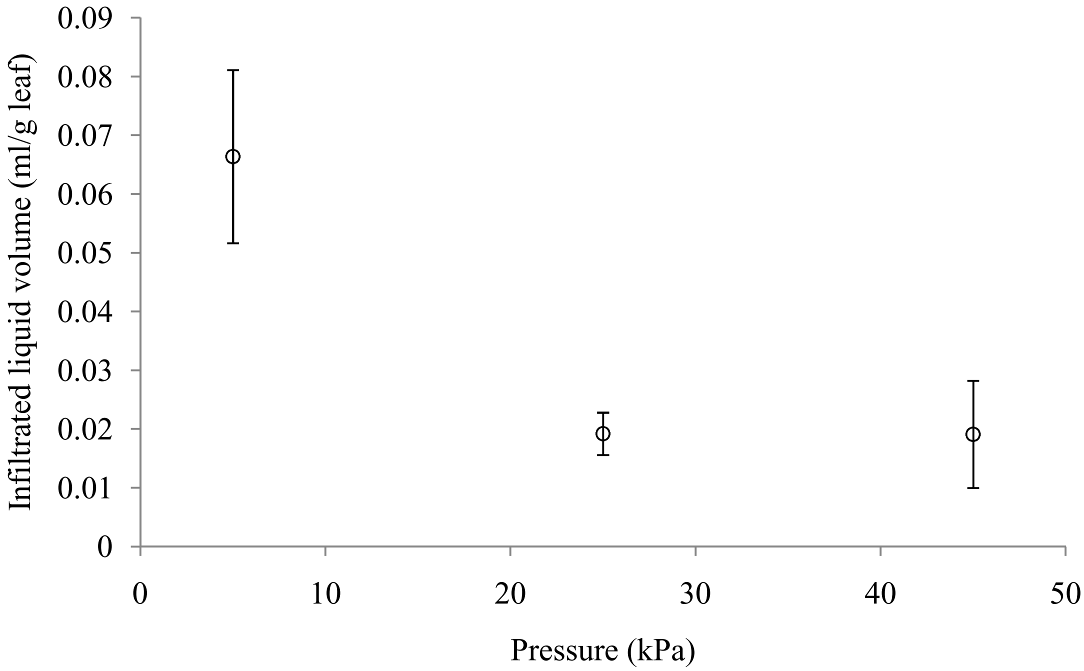

Figure 3.5. Volume of infiltrated liquid following vacuum infiltration versus pressure applied during infiltration. Error bars represent one standard deviation.

3.3.4 Measurement of vacuum infiltration effects on initial bacterial attachment to leaf tissue

There was not a significant relationship between the intensity of vacuum applied during infiltration and subsequent bacterial attachment rates (p = 0.86) (Figures 3.6 and 3.7, Appendix 3.4).

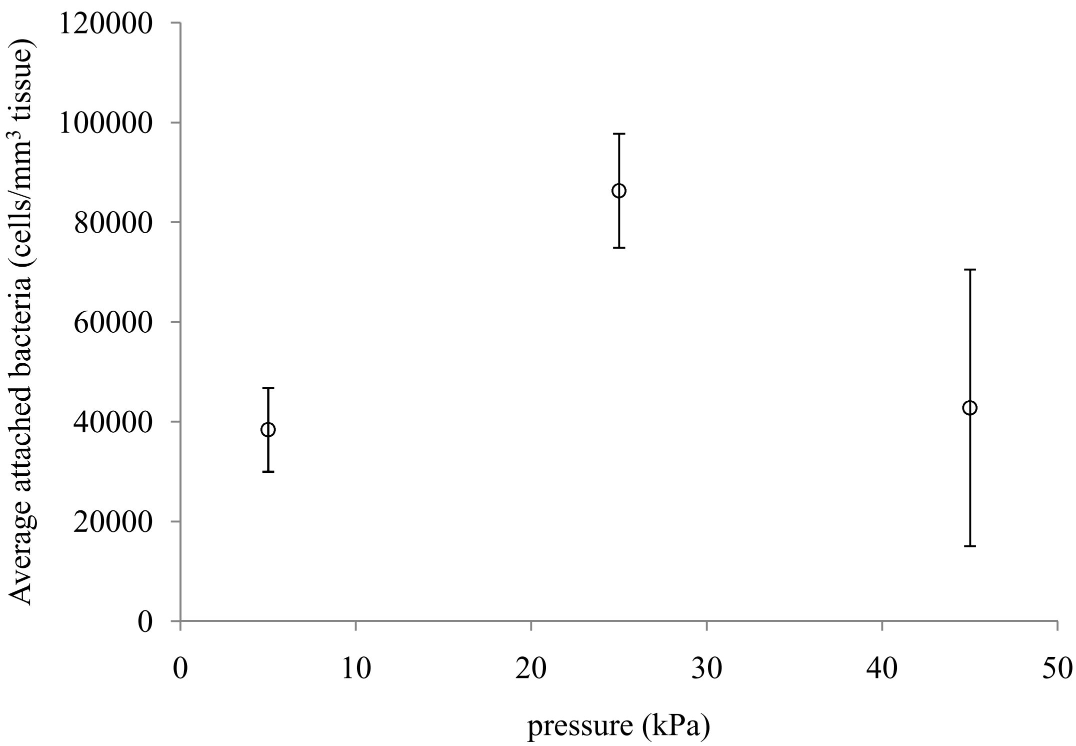

Figure 3.6. Average density of attached bacteria at infection sites versus pressure applied during vacuum infiltration of bacterial suspensions into leaf explants. Error bars represent one standard deviation.

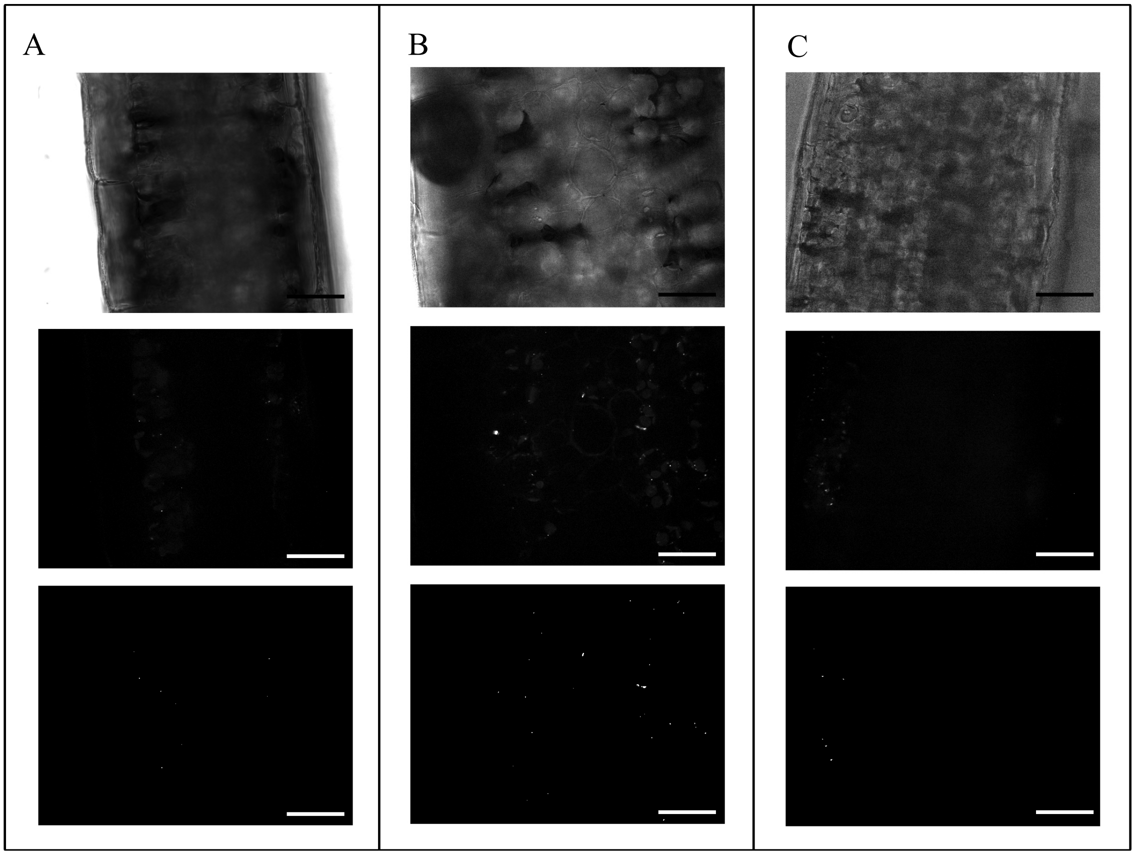

Figure 3.7. Representative micrographs of sectioned switchgrass leaf explants infiltrated with labeled *Agrobacterium tumefaciens* at various vacuum levels. Micrographs represent single focal planes from image stacks corresponding to sample infection sites in leaf explants infiltrated with bacterial suspension at (A) 5 kPa, (B) 25 kPa, (C) and 45 kPa. For each treatment, brightfield, fluorescent confocal, and binary images (in descending order) are provided. Binary images show isolated signals (colored white) following signal intensity and signal area screening. Scale bars represent 40 μm.

3.3.5 Measurement of infiltrated bacterial density effects on initial bacterial attachment to leaf tissue

The density of bacteria infiltrated into switchgrass leaf tissue had a significant positive linear effect on bacterial attachment rates ($p < 0.0001$) (Figures 3.8 and 3.9, Appendix 3.5). The equation for the line of best fit describing the data is

$$d_A = (3.762 \times 10^{-5}\ cells \cdot ml/mm^3 \cdot CFU)d_I - 6717\ cells/mm^3 \qquad \text{(eq. 3.1)}$$

where d_A is the average density of attached bacteria at infection sites in units of cells per volume leaf tissue and d_I is the density of bacteria in the infiltrated suspension in units of colony forming units per volume.

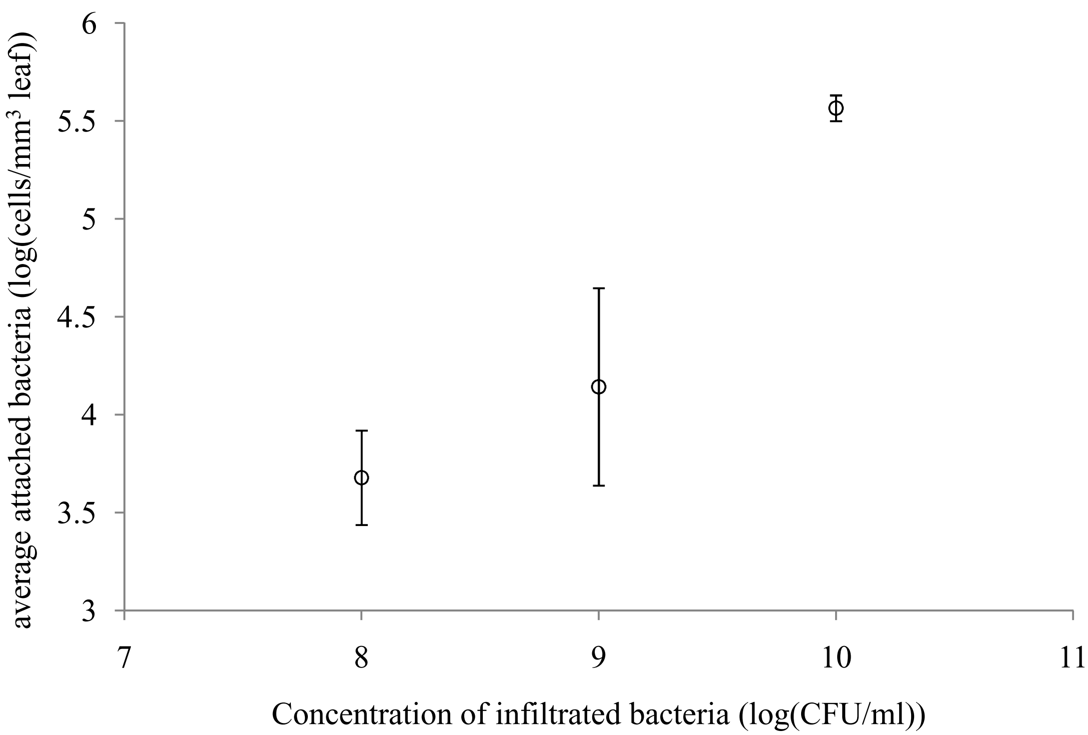

Figure 3.8. Average density of attached bacteria at infection sites versus the concentration of bacteria in infiltrated suspensions. Error bars represent one standard deviation.

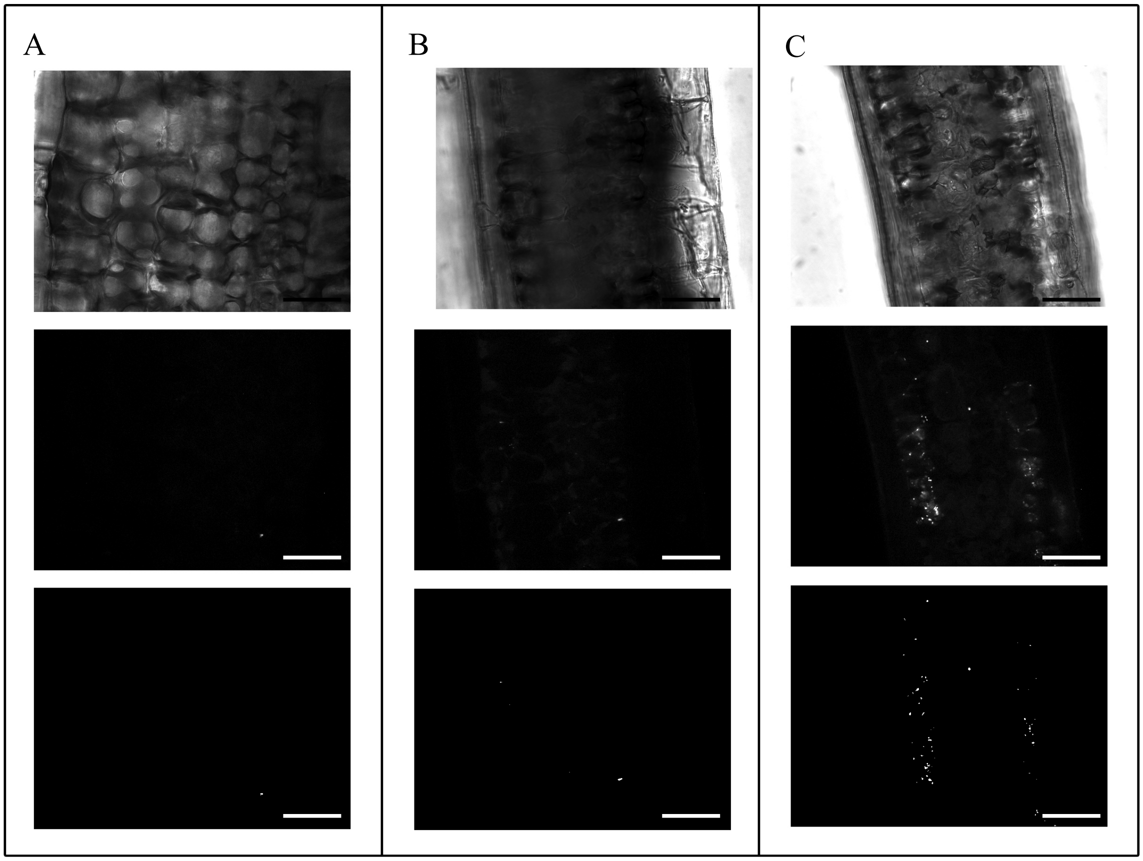

Figure 3.9. Representative micrographs of sectioned switchgrass leaf explants infiltrated with various concentrations of labeled *Agrobacterium tumefaciens*. Micrographs represent single focal planes from image stacks corresponding to sample infection sites in leaf explants infiltrated with bacterial suspension containing (A) 10^8, (B) 10^9, and (C) 10^{10} CFU/ml. For each treatment, brightfield, fluorescent confocal, and binary images (in descending order) are provided. Binary images show isolated signals (colored white) following signal intensity and signal area screening. Scale bars represent 40 μm.

3.3.6 Correlation of initial bacterial attachment levels to transgene transient expression levels

GUS activity levels in extracts from switchgrass leaves agroinfiltrated with strain C58C1 were not significantly different from negative controls infiltrated with water or strain C58 (Figure 3.10, Appendix 3.6). Overall activity values were low and any activity stemming from transient expression of GUS could not be distinguished from native GUS-like activity.

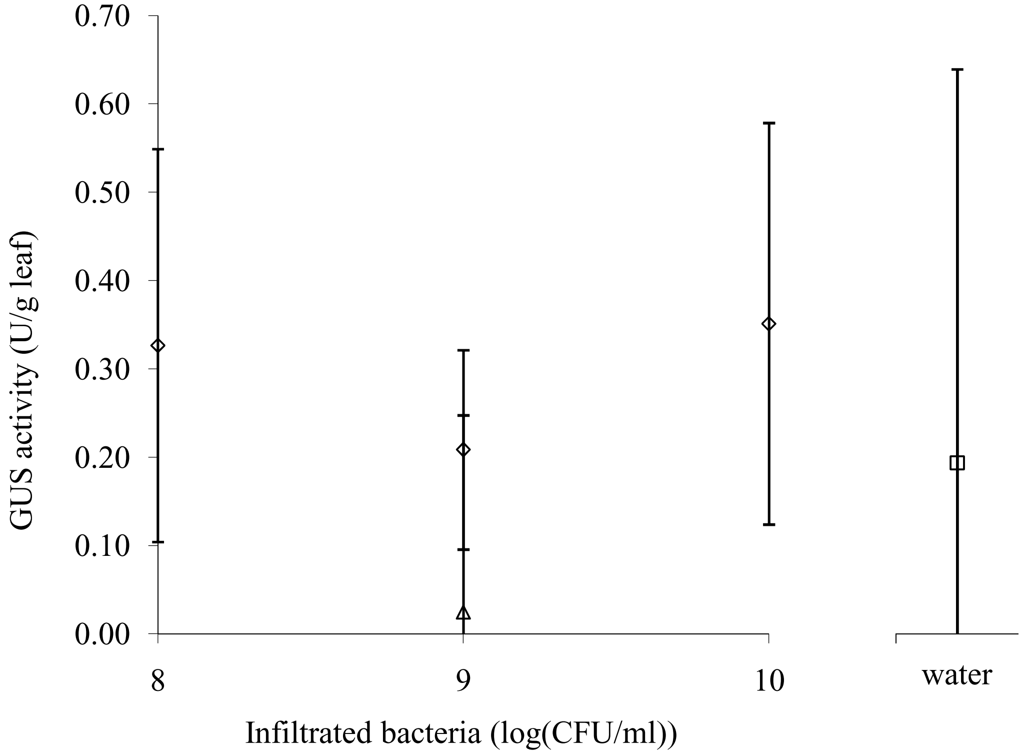

Figure 3.10. GUS activity in switchgrass leaf tissue infiltrated with various concentrations of *Agrobacterium tumefaciens*. Diamonds represent measurements from leaves infiltrated with strain C58C1. Negative controls infiltrated with strain C58 or water are represented by triangles and squares, respectively. Error bars represent one standard deviation.

Histochemical staining of switchgrass explants infiltrated with various levels of *A. tumefaciens* yielded no stained areas visible to the unaided eye. However, when viewed at 10x in brightfield mode under a microscope, small regions of indigo precipitate could be observed. These regions appeared as either compact spherical particles or more diffuse clouds of indigo coloring. Areas of the leaf explant containing localizations of stained regions were termed expression sites. Three expression sites were imaged for each explant. For each micrograph of an expression site, regions of indigo stain were counted and normalized against the total leaf area captured in the image. A conversion factor of 0.625 μm/pixel was used to determine leaf area from micrographs. The density of stained regions increased significantly with infiltrated bacterial density ($p = 0.02$) (Figure 3.11, Appendix 3.7) following a semi-logarithmic relationship. Significantly more stained regions were observed in explants infiltrated with strain C58C1 at 10^9 CFU/ml compared to explants infiltrated with disarmed strain C58 at the same concentration ($p = 0.015$).

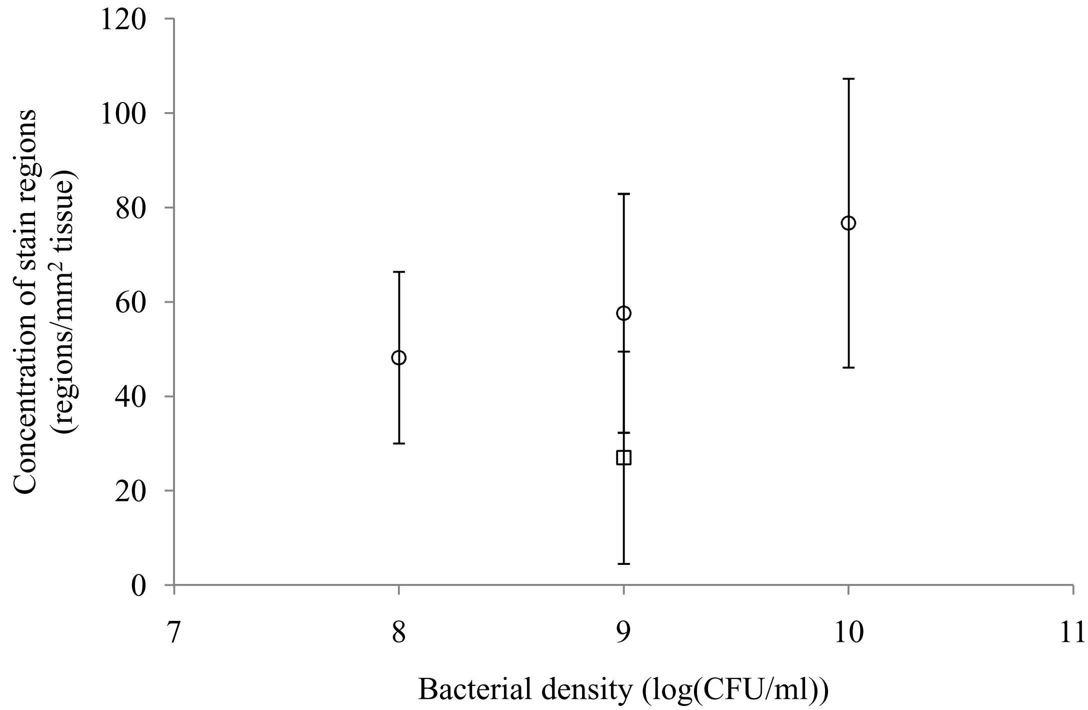

Figure 3.11. Number of indigo stain regions per unit area leaf tissue at expression sites versus density of infiltrated bacteria. Circles represent samples infiltrated with strain C58C1. The square represents samples infiltrated with disarmed strain C58. Error bars represent one standard deviation.

3.4 Discussion

3.4.1 Measurement of surfactant effects on infiltrated liquid volume, leaf viability, and initial bacterial attachment to leaf tissue

The addition of surfactant to the infiltrated liquid phase did not enhance infiltration of liquid or bacterial attachment rates for the domain of surfactant concentrations examined. This is in contrast to lettuce, where surfactant had a significant positive effect on both responses. The lack of enhanced infiltration volume in response to added surfactant cannot be attributed to switchgrass leaves having a thicker hydrophobic cuticle compared to lettuce. The cuticle of both plants comprises approximately 0.5% dry weight of the leaf (Tulloch and Hoffman, 1980; Bakker et al., 1998). However, these prior studies also show that the cuticles of each plant differ greatly in their composition. Switchgrass leaf cuticles contain primarily diketones while lettuce leaf cuticles are mainly comprised of linear alcohols. Cuticle composition influences both cuticle morphology and chemistry (reviewed by Koch and Ensikat, 2008). Perhaps the composition of the switchgrass cuticle leads to a less stable water-cuticle interface compared to lettuce and the range of surfactant concentrations tested was not sufficient to provide the interface stability needed for effective contact between the liquid phase and leaf explants during vacuum infiltration. Such a scenario may promote the adherence of bubbles from evacuated intra-leaf gases to the leaf surface in order to minimize contact of the surface with the aqueous phase. If surface-bound bubbles are not removed from the leaf surface, the gases within may collapse back into the leaf interior upon repressurization, negating infiltration of liquid. Alternately, stomatal size, behavior, and density may affect evacuation of gases and subsequent infiltration of liquids. Differences in stomatal characteristics between switchgrass and lettuce may account for their dissimilar infiltration responses. Future work may benefit from investigating how differences in stomatal properties relate to vacuum infiltration of liquids into leaves.

While surfactant elicited a moderate but significant positive effect on bacterial attachment in lettuce, the data show only tenuous evidence of a similar effect in switchgrass. Plotting the maximum observed attachment density in a treatment against that treatment's surfactant concentration yielded a relationship that was close to significant ($p = 0.08$). This result presents the possibility that surfactant can raise the maximum number of bacteria attached at an infection site, but not consistently enough to significantly raise the average attachment rate. Possibly, a repeat experiment with more replicates could better elucidate if a weak, but significant relationship exists between surfactant level and bacterial attachment.

The inefficacy of surfactant for altering attachment levels may stem from inherent differences in monocot plant cell walls compared to those of dicots. One explanation stems from the possibility that monocot cell walls lack certain attachment factors that are present in dicot cell walls that somehow interact with surfactant. Such factors could be inhibitory agents that are solubilized and removed by surfactant. Alternately, they could be promotive agents that become more accessible to *Agrobacterium* after surfactant treatment. Regardless, if monocots lack these factors, then surfactant would have no effect on bacterial attachment levels. Nevertheless, it has been documented that surfactant enhances transformation rates in immature embryos and embryogenic calli of wheat, another monocot (Cheng et al., 1997). It may be that surfactant enhances transformation through some mechanism other than alteration of bacterial attachment or, alternately, the effects observed in embryos and calli simply do not translate to more mature tissues, such as the leaves used in this study. As with lettuce, further research is needed to better understand the specific components of *Agrobacterium* attachment to plant cells and the effects of surfactants on plant cell walls in order to determine the mechanism behind the influence of surfactant on bacterial attachment.

3.4.2 Measurement of vacuum infiltration effects on infiltrated liquid volume and initial bacterial attachment to leaf tissue

Increasing vacuum intensity during infiltration resulted in greater volumes of infiltrated liquid. This result is similar to that previously observed for lettuce (Simmons et al., 2009). Unlike lettuce, the relationship between infiltrated liquid volume and applied pressure during infiltration does not appear to be linear in switchgrass. However, the model describing vacuum infiltration of liquids into the leaf interior predicts a linear relationship between the two variables (Simmons et al., 2009). It should be noted, though, that the model assumes complete removal of evacuated gases from leaf tissue. Prior work has shown that incomplete removal of gases from the leaf, signified by the presence of bubbles adhered to the leaf surface, can result in volumes of infiltrated liquid that are lower than those predicted by the model (unpublished data). Only at higher vacuum intensities are sufficient gas volumes evacuated such that bubbles adhered to the leaf surface grow large enough to be removed by the buoyant force. This phenomenon may explain the apparent nonlinear relationship observed in switchgrass. The issue of incomplete gas removal from leaves during vacuum infiltration was also raised during investigation of surfactant effects on infiltrated liquid volume, where it was proposed that some property of the switchgrass cuticle may cause bubbles from evacuated gases to adhere more strongly to the leaf surface compared to lettuce leaves. Future studies that examine vacuum infiltration of liquids into switchgrass leaves that have had their cuticles digested or mechanically removed may help determine if the cuticle acts as a barrier to infiltration.

Infiltrated liquid volumes observed following exposure to high vacuum intensities can be used to estimate the total airspace volume in leaf tissue accessible to infiltrated bacteria, as described previously (Simmons et al., 2009). Based on the data, the estimated total airspace volume is approximately 0.07 ml/g fresh leaf. In lettuce, total airspace volume was estimated to be approximately 0.5 ml/g fresh leaf (Simmons et al., 2009). Assuming that lettuce and switchgrass leaves have similar densities, switchgrass leaves contain much less air space compared to lettuce leaves. Further research is required to determine if, as a result, fewer plant cells within switchgrass leaves are exposed to *Agrobacterium* compared to lettuce leaves.

Like lettuce, vacuum intensity did not have a significant effect on *Agrobacterium* attachment levels in switchgrass. As with lettuce, any effect of vacuum intensity on switchgrass leaf transformation efficiency following agroinfiltration is likely a result of changes in the distribution of infiltrated bacteria within the leaf due to altered infiltration volumes rather than changes in the way individual bacteria attach to plant cells.

3.4.3 Infiltrated bacterial density effects on initial bacterial attachment to leaf tissue and transient transgene expression

Like lettuce, the density of *A. tumefaciens* in liquid suspension was the most influential infiltration factor with regards to bacterial attachment to switchgrass leaves. Moreover, bacterial attachment to leaf cells when 10^8 CFU/ml bacteria were infiltrated was barely detectable, a result also observed in lettuce leaves. However, unlike lettuce, a saturation trend was not observed for bacterial attachment in the domain of infiltration concentrations tested. Instead, attachment levels versus infiltrated bacterial density exhibited a constant slope up to 10^{10} CFU/ml, a density at which saturation of attachment levels started to become apparent in lettuce. It is possible that a saturation trend may be observed in switchgrass if higher levels of infiltrated bacterial density are tested. The data show that at when 10^9 CFU/ml bacteria were infiltrated into switchgrass leaf tissue, average bacterial attachment at infection sites was significantly less ($p = 0.05$) than that observed when the same concentration was infiltrated into lettuce leaf tissue. This result suggests that *A. tumefaciens* has decreased avidity for switchgrass tissue compared to lettuce. Interestingly, when 10^{10} CFU/ml bacteria were infiltrated, switchgrass showed significantly higher attachment rates than lettuce ($p = 0.03$). Moreover, the value of attached bacteria measured for switchgrass when 10^{10} CFU/ml bacteria are infiltrated is higher than the maximum estimated number of bacteria that can bind to lettuce at infection sites (embodied by the estimated value of $d_{A,max}$ for lettuce). Further experimentation is needed to elucidate the saturation behavior of bacterial attachment to switchgrass and determine values for $d_{A,max}$ and α (as defined in equation 2.1). Comparison of the parameter values between switchgrass and lettuce will permit a more quantitative, definitive analysis of differences between *A. tumefaciens* avidity and attachment site density in these tissues. However, based on this work, the data show that switchgrass leaf tissue potentially contains a greater number of bacterial attachment sites per unit volume compared to lettuce. This could be an indication that switchgrass leaf cells contain a higher density of *A. tumefaciens* binding sites compared to lettuce leaf cells. This possibility is particularly interesting considering prior research has suggested that plant-produced attachment factors are present in the pectin fraction of the plant cell wall (Rao et al., 1982; Neff et al., 1987) and that monocots generally contain less pectin than dicots (Jarvis et al., 1988). Within the plant cell wall, pectin is mostly present in the primary cell wall and middle lamella (Willats et al., 2001). The middle lamella lies at the outer surface of the cell wall and *A. tumefaciens* likely directly interacts with it during attachment. Monocots cell walls may generally contain lower pectin levels compared to dicots due to their having a less substantial primary cell wall (Jarvis et al., 1988). As switchgrass, a monocot, may contain a greater density of *A. tumefaciens* attachment sites compared to lettuce, a dicot, despite containing less primary cell wall pectin, the data suggest that it is the pectin constituting the middle lamella that houses *A. tumefaciens* attachment factors. Alternately, lettuce and switchgrass leaf cells may have similar densities of attachment sites on the cell surface, but switchgrass leaves may contain more cells per unit volume. This scenario could be validated with further research to define the ultrastructures of switchgrass and lettuce leaf interiors. The protocol used in this research makes identification of individual plant cells difficult, prohibiting attachment analysis on a per plant cell basis. Nevertheless, the observed differences in *A. tumefaciens* attachment trends between switchgrass and lettuce are compelling and warrant further research to determine if these trends hold true for monocots versus dicots in general.

Similar to lettuce, transient expression of GUS was measured via GUS activity in switchgrass leaves in response to varied densities of attached bacteria. Infiltrated concentration of *Agrobacterium* suspensions was varied to control attachment rates, as this parameter was found to most influence attachment levels. The GUS spectrophotometric activity assay revealed no significant trend in activity levels related to varying bacterial attachment levels. Furthermore, GUS activity levels in explants infiltrated with strain C58C1 were not significantly different from those observed in explants infiltrated with disarmed strain C58 or water, suggesting that no recombinant GUS expression occurred and the measured activity stemmed from either native GUS-like activity in the plant extracts or a shift in the absorbance properties of the extracts over the course of the assay. Alternately, a significant positive relationship was observed between GUS activity and infiltrated bacterial density when microscopic measurements of indigo precipitate were made in leaf explants that were histochemically stained. Activity levels were significantly higher than negative controls infiltrated with disarmed strain C58. However, negative control samples did exhibit stained regions, suggesting that a fraction of GUS activity measured in explants infiltrated with strain C58C1 can be attributed to background GUS-like activity in agroinfiltrated leaves. Prior work has shown that non-infiltrated switchgrass leaves do not exhibit stained regions following histochemical staining (VanderGheynst et al., 2008). This observation indicates that staining in leaves infiltrated with disarmed strain C58 possibly results from a plant response to bacterial exposure that produces areas with GUS-like activity. Taken together, data from the spectrophotometric and histochemical staining assays are inconclusive for proving transient expression of recombinant GUS in agroinfiltrated switchgrass. If any transient expression is occurring, the fact that it is barely detectable indicates that expression levels are extremely low. These results are in contrast to those observed in lettuce. In lettuce, even relatively low attachment levels, such as those resulting from infiltration with 10^8 CFU/ml bacteria, led to readily detectable GUS expression. Since extremely low-level expression was detected in agroinfiltrated switchgrass leaves over the range of attachment levels tested, it appears transformation of switchgrass with *Agrobacterium* is not inhibited at the level of bacterial attachment but at some following step. Additional research is needed to investigate T-pilus formation and the progression of T-strands through the pilus, plant cytoplasm, and plant nucleus to further resolve the inhibitory stage of T-strand transfer in switchgrass and other monocot plants.

3.5 Conclusions

Lettuce and switchgrass leaf tissue are similar in that the density of infiltrated *Agrobacterium* is the most influential infiltration factor affecting the attachment of the bacteria to leaf cells. Additionally, bacterial attachment levels in both plants are not affected by the intensity of vacuum applied during infiltration. However, bacterial attachment trends in switchgrass differed from those observed in lettuce in several aspects. The data suggest that *Agrobacterium* may have lower avidity for switchgrass leaf tissue compared to that of lettuce, but switchgrass leaves may contain more attachment sites than lettuce leaves. Moreover, the addition of surfactant to bacterial suspensions did not enhance attachment levels in switchgrass, unlike lettuce. Furthermore, alteration of attachment levels via control of infiltrated bacterial density yielded only extremely low levels of *in planta* transient transgene expression, suggesting that the recalcitrance of switchgrass to agroinfiltration lies downstream of the bacterial attachment step. These results warrant future investigation into T-strand transfer kinetics through steps in the secretion pathway in order to better determine the rate-limiting step in agroinfiltration of switchgrass and other monocots.

References

Albersheim, P., K. Mühlethaler, and A. Frey-Wyssling (1960). "Stained pectin as seen in the electron microscope." The Journal of Cell Biology **8**(2): 501-506.

Ashby, A. M., M. D. Watson, G. J. Loake, and C. H. Shaw (1988). "Ti plasmid-specified chemotaxis of *Agrobacterium tumefaciens* C58C1 toward vir-inducing phenolic compounds and soluble factors from monocotyledonous and dicotyledonous plants." Journal of Bacteriology **170**(9): 4181-4187.

Baird, L. M., and P. D. Reid (1992). "Cellulase activity and localization during induced abscission of *Coleus blumei*." Journal of Plant Growth Regulation **11**: 129-134.

Bakker, M. I., W. J. Baas, D. T. H. M. Sijm, and C. Kollöfel (1998). "Leaf wax of *Lactuca sativa* and *Plantago major*." Phytochemistry **47**(8): 1489-1493.

Brencic, A., and S. C. Winans (2005). "Detection of and response to signals involved in host-microbe interactions by plant-associated bacteria." Microbiology and Molecular Biology Reviews **69**(1): 155-194.

Cheng, M., J. E. Fry, S. Pang, H. Zhou, C. M. Hironaka, D. R. Duncan, T. W. Conner, and Y. Wan (1997). "Genetic transformation of wheat mediated by *Agrobacterium tumefaciens*." Plant Physiology **115**: 971-980.

Clauce-Couple, H., S. Chateau, C. Ducrocq, V. Niot, S. Kaveri, F. Dubois, B. Sangwan-Norreel, R. S. Sangwan (2008). "Role of vitronectin-like protein in *Agrobacterium* attachment and transformation of *Arabidopsis* cells." Protoplasma **234**(1-4): 65-75.

Clough, S. J. and A. F. Bent (1998). "Floral dip: a simplified method for *Agrobacterium*-mediated transformation of *Arabidopsis thaliana*." The Plant Journal **16**(6): 735-743.

Collens, J. I., D. R. Lee, A. M. Seeman, and W. R. Curtis (2004). "Development of auxotrophic *Agrobacterium tumefaciens* for gene transfer in plant tissue culture." Biotechnology Progress **20**(3): 890-896.

De Cleene, M., and J. De Ley (1976). "The host range of crown gall." The Botanical Review **42**(4): 389-466.

Dehio, C., and J. Schell (1994). "Identification of plant genetic loci involved in a posttranscriptional mechanism for meiotically reversible transgene silencing." Proceedings of the National Academy of Sciences of the United States of America **91**: 5538-5542.

Douglas, C. J., W. Halperin, and E. W. Nester (1982). "*Agrobacterium tumefaciens* mutants affected in attachment to plant cells." Journal of Bacteriology **152**(3): 1265-1275.

Finer, K. R., and J. J. Finer (2000). "Use of *Agrobacterium* expressing green fluorescent protein to evaluate colonization of sonication-assisted *Agrobacterium*-mediated transformation-treated soybean cotyledons." Letters in Applied Microbiology **30**: 406-410.

Gelvin, S. B. (2010). "Plant proteins involved with *Agrobacterium*-mediated genetic transformation." Annual Reviews in Phytopathology **48**: 45-68.

Glowgowski, W., and A. G. Galsky (1978). "*Agrobacterium tumefaciens* site attachment as a necessary prerequisite for crown gall tumor formation on potato discs." Plant Physiology **61**: 1031-1033.

Graves, A. E., S. L. Goldman, S. W. Banks, and A. C. F. Graves (1988). "Scanning electron microscope studies of *Agrobacterium tumefaciens* attachment to *Zea mays, Gladiolus* sp., and *Triticum aestivum*." Journal of Bacteriology **170**(5): 2395-2400.

Gross, K. C. (1985). "Promotion of ethylene evolution and ripening of tomato fruit by galactose." Plant Physiology **79**: 306-307.

Gudnason, H., M. Dufva, D. D. Bang, and A. Wolff (2007). "Comparison of multiple DNA dyes for real-time PCR: effects of dye concentration and sequence composition on DNA amplification and melting temperature." Nucleic Acids Research **35**(19): e127.

Hamilton, C. M. (1997). “A binary BAC-system for plant transformation with high molecular-weight-DNA.” Gene **200**(1-2): 107-116.

Introduction of organisms and products altered or produced through genetic engineering which are plant pests or which there is reason to believe are plant pests (2008). Code of Federal Regulations Title 7, Section 3.340.

Janczuk, B. (1983). “Detachment force of air bubble from the solid surface (sulfur or graphite) in water.” Journal of Colloid and Interface Science **93**(2): 411-418.

Janssen, B. -J. and R. C. Gardner (1989). “Localized transient expression of GUS in leaf disks following cocultivation with *Agrobacterium*.” Plant Molecular Biology **14**: 61-72.

Jarvis, M. C., W. Forsyth, and H. J. Duncan (1988). “A survey of the pectic content of nonlignified monocot cells walls.” Plant Physiology **88**: 309-314.

Jefferson, R. A. (1987). “Assaying chimeric genes in plants: the GUS gene fusion system.” Plant Molecular Biology Reporter **5**(1): 387-405.

Joh, L. D., T. Wroblewski, N. N. Ewing, and J. S. VanderGheynst (2005). “High-level transient expression of recombinant protein in lettuce.” Biotechnology and Bioengineering **91**(7): 861-871.

Jones, J. D., L. Shlumukov, F. Carland, J. English, S. R. Scofield, G. J. Bishop, and K. Harrison (1992). "Effective vectors for transformation, expression of heterologous genes and assay in transposon excision in transgenic plants." Transgenic Research **1**(6): 285-297.

Kapila, J., R. De Rycke, M. Van Montagu, and G. Angenon (1997). "An *Agrobacterium*-mediated transient gene expression system for intact leaves." Plant Science **122**: 101-108.

Keshwani, D. R., and J. J. Cheng (2009). "Switchgrass for bioethanol and other value-added applications: A review." Bioresource Technology **100**(4): 1515-1523.

Kim, M. J., K. Baek, C.-M. Park (2009). "Optimization of conditions for transient *Agrobacterium*-mediated gene expression assays in *Arabidopsis*." Plant Cell Reports **28**: 1159-1167.

Kluepfel, D. A. and S. G. Pueppke (1986). "Adsorption of *Agrobacterium tumefaciens* to susceptible potato tissues: a physisorption process." Applied and Environmental Microbiology **51**(5): 1130-1132.

Koch, K., and H.-J. Ensikat (2008). "The hydrophobic coatings of plant surfaces: Epicuticular wax crystals and their morphologies, crystallinity and molecular self-assembly." Micron **39**(7): 759-772.

Lacroix, B., T. Tzfira, A. Vainstein, and V. Citovsky (2006). “A case of promiscuity: *Agrobacterium*’s endless hunt for new partners.” Trends in Genetics **22**(1): 29-37.

Lippincott, B. B., and J. A. Lippincott (1969). “Bacterial attachment to a specific wound site as an essential stage in tumor initiation by *Agrobacterium tumefaciens*.” Journal of Bacteriology **97**(2): 620-628.

Lonsdale, D. M., S. Lindup, L. J. Moisan, and A. J. Harvey (1988). “Using firefly luciferase to identify the transition from transient to stable expression in bombarded wheat scutellar tissue.” Physiologia Plantarum **102**: 447-453.

Martinez, J. A. and F. Artes (1999). “Effect of packaging treatments and vacuum-cooling on quality of winter harvested iceberg lettuce.” Food Research International **32**(9): 621-627.

Matthysse, A. G. (1983). “Role bacterial cellulose fibrils in *Agrobacterium tumefaciens* infection.” Journal of Bacteriology **154**(2): 906-915.

Matthysse, A. G. (1986). “Initial interactions of *Agrobacterium tumefaciens* with plant host cells.” Critical Reviews in Microbiology **13**(3): 281-307.

Matthysse, A. G. (1987). "Characterization of non-attaching mutants of *Agrobacterium tumefaciens*." Journal of Bacteriology **169**(1): 313-323.

Matthysse, A. G., M. Marry, L. Krall, M. Kaye, B. E. Ramey, C. Fuqua, and A. R. White (2005). "The effect of cellulose overproduction on binding and biofilm formation on roots by *Agrobacterium tumefaciens*." Molecular Plant-Microbe Interactions **18**(9): 1002-1010.

Matthysse, A. G., P. M. Wyman, and K. V. Holmes (1978). "Plasmid-dependant attachment of *Agrobacterium tumefaciens* to plant tissue culture cells." Infection and Immunity **22**(2): 516-522.

Merritt, P. M., T. Danhorn, and C. Fuqua (2007). "Motility and chemotaxis in *Agrobacterium tumefaciens* surface attachment and biofilm formation." Journal of Bacteriology **189**(22): 8005-8014.

Morrison-Baird, L. A., P. D. Reid, and B. D. Webster (1978). "Ultrastructural modification associated with the induction of abscission in Coleus." Botannical Gazette **139**(2): 165-170.

Neff, N. T., A. N. Binns, and C. Brandt (1987). "Inhibitory effects of a pectin-enriched tomato cell wall fraction on *Agrobacterium tumefaciens* binding and tumor formation." Plant Physiology **83**: 525-528.

Piper, K. R., S. B. Von Bodman, and S. K. Farrand (1993). "Conjugation factor of *Agrobacterium tumefaciens* regulates Ti plasmid transfer by autoinduction." Nature **362**: 448-450.

Ramey, B. E., M. Koutsoudis, S. B. von Bodman, and C. Fuqua (2004). "Biofilm formation in plant-microbe associations." Current Opinion in Microbiology 7(6): 602-609.

Rao, S. S., B. B. Lippincott, and J. A. Lippincott (1982). "*Agrobacterium* adherence involves the pectic portion of the host cell wall and is sensitive to the degree of pectin methylation." Physiologia Plantarum **56**(3): 374-380.

Reuhs, B. L., J. S. Kim, and A. G. Matthysse (1997). "Attachment of *Agrobacterium tumefaciens* to carrot cells and *Arabidopsis* wound sites is correlated with the presence of a cell-associated, acidic polysaccharide." Journal of Bacteriology **179**(17): 5372-5379.

Sangwan, R. S., Y. Bourgeois, S. Brown, G. Vasseur, and B. Sangwan-Norreel (1992). "Characterization of competent cells and early events of *Agrobacterium*-mediated genetic transformation in *Arabidopsis thaliana*." Planta **188**: 439-456.

Simmons, C. W. and J. S. VanderGheynst (2007). "Transient co-expression of post-transcriptional gene silencing suppressors and β-glucuronidase in harvested lettuce leaf tissue does not improve recombinant protein accumulation in planta." Biotechnology Letters **29**: 641-645.

Simmons, C. W., J. S. VanderGheynst, and S. K. Upadhyaya (2009). "A model of *Agrobacterium tumefaciens* vacuum infiltration into harvested leaf tissue and subsequent in planta transgene transient expression." Biotechnology and Bioengineering **102**(3): 965-970.

Sood, P., A. Bhattacharya, and A. Sood (2011). "Problems and possibilities of monocot transformation." Biologia Plantarum **55**(1): 1-15.

Süle, S., L. Cursino, D. Zheng, H. C. Hoch, and T. J. Burr (2009). "Surface motility and associated surfactant production in *Agrobacterium vitis*." Letters in Applied Microbiology **49**(5): 596-601.

Tonlinson, A. D., and C. Fuqua (2009). "Mechanisms and regulation of polar surface attachment in *Agrobacterium tumefaciens*." Current Opinion in Microbiology **12**: 708-714.

Tulloch, A. P., and L. L. Hoffman (1980). "Epicuticular wax of *Panicum virgatum*." Phytochemistry **19**(5): 837-839.

van Wordragon, M. F., and H. J. M. Dons (1992). "*Agrobacterium tumefaciens*-mediated transformation of recalcitrant crops." Plant Molecular Biology Reporter **10**(1): 12-36.

Verma, A., V. Nain, C. Kumari, S. K. Singh, M. L. Narasu, and P. A. Kumar (2008). "Tissue specific response of *Agrobacterium tumefaciens* attachment to *Sorghum bicolor* (L) Moench." Physiology and Molecular Biology of Plants **14**(4): 307-313.

Wallats, W. G. T., L. McCartney, W. Mackie, and J. P. Knox (2001). "Pectin: Cell biology and prospects for functional analysis." Plant Molecular Biology **47**: 9-27.

Wang, K., L. Kang, A. Anand, G. Lazarovits, and K. S. Mysore (2007). "Monitoring *in planta* bacterial infection at both cellular and whole-plant levels using the green fluorescent protein variant GFPuv." New Phytologist **174**(1): 212-223.

Wroblewski, T., A. Tomczak, and R. Michelmore (2005). "Optimization of *Agrobacterium*-mediated transient assays of gene expression in lettuce, tomato and *Arabidopsis*." Plant Biotechnology Journal **3**(2): 259-273.

Zhang, L. H. and A. Kerr (1991). "A diffusible compound can enhance conjugal transfer of the Ti plasmid in *Agrobacterium tumefaciens*." Journal of Bacteriology **173**(6): 1867-1872.

Zhang, L., P. J. Murphy, A. Kerr, and M. E. Tate (1993). "*Agrobacterium* conjugation and gene regulation by *N*-acyl-L-homoserine lactones." Nature **362**: 446-448.

Zhang, H.-B., L.-H. Wang, and L.-H. Zhang (2002). "Genetic control of quorum-sensing signal turnover in *Agrobacterium tumefaciens*." Proceedings of the National Academy of Sciences of the United States of America **99**(7): 4638-4643.

Zhu, J., P. M. Oger, B. Schrammeijer, P. J. J. Hooykaas, S. K. Farrand, and S. C. Winans (2000). "The bases of crown gall tumorigenesis." Journal of Bacteriology **182**(14): 3885-3895.

Appendices

Appendix 1.1 – Leaf autofluorescence data

Excitation wavelength (nm)	Emission wavelength (nm)	Treatment designation
355	460	DAPI wavelengths
488	520	FitC wavelengths
550	576	TritC wavelengths
650	666	Cy5 wavelengths

Treatment	Image number	Average 12-bit pixel intensity across image
Cy5 wavelengths	1	1575.76
DAPI wavelengths	1	411.81
FitC wavelengths	1	264.80
TritC wavelengths	1	299.30
Cy5 wavelengths	2	2291.83
DAPI wavelengths	2	474.04
FitC wavelengths	2	271.77
TritC wavelengths	2	290.35
Cy5 wavelengths	3	2421.13
DAPI wavelengths	3	471.08
FitC wavelengths	3	274.50
TritC wavelengths	3	305.68

Average pixel intensity ratio of	To	Image	Average pixel intensity ratio
Cy5 wavelengths	Cy5 wavelengths	1	1.00
Cy5 wavelengths	DAPI wavelengths	1	3.83
Cy5 wavelengths	FitC wavelengths	1	5.95
Cy5 wavelengths	TritC wavelengths	1	5.26
Cy5 wavelengths	Cy5 wavelengths	2	1.00
Cy5 wavelengths	DAPI wavelengths	2	4.83
Cy5 wavelengths	FitC wavelengths	2	8.43
Cy5 wavelengths	TritC wavelengths	2	7.89
Cy5 wavelengths	Cy5 wavelengths	3	1.00
Cy5 wavelengths	DAPI wavelengths	3	5.14
Cy5 wavelengths	FitC wavelengths	3	8.82
Cy5 wavelengths	TritC wavelengths	3	7.92

Appendix 1.1 continued

Average pixel intensity ratio of	To	Image	Average pixel intensity ratio
DAPI wavelengths	Cy5 wavelengths	1	0.26
DAPI wavelengths	DAPI wavelengths	1	1.00
DAPI wavelengths	FitC wavelengths	1	1.56
DAPI wavelengths	TritC wavelengths	1	1.38
DAPI wavelengths	Cy5 wavelengths	2	0.21
DAPI wavelengths	DAPI wavelengths	2	1.00
DAPI wavelengths	FitC wavelengths	2	1.74
DAPI wavelengths	TritC wavelengths	2	1.63
DAPI wavelengths	Cy5 wavelengths	3	0.19
DAPI wavelengths	DAPI wavelengths	3	1.00
DAPI wavelengths	FitC wavelengths	3	1.72
DAPI wavelengths	TritC wavelengths	3	1.54
FitC wavelengths	Cy5 wavelengths	1	0.17
FitC wavelengths	DAPI wavelengths	1	0.64
FitC wavelengths	FitC wavelengths	1	1.00
FitC wavelengths	TritC wavelengths	1	0.88
FitC wavelengths	Cy5 wavelengths	2	0.12
FitC wavelengths	DAPI wavelengths	2	0.57
FitC wavelengths	FitC wavelengths	2	1.00
FitC wavelengths	TritC wavelengths	2	0.94
FitC wavelengths	Cy5 wavelengths	3	0.11
FitC wavelengths	DAPI wavelengths	3	0.58
FitC wavelengths	FitC wavelengths	3	1.00
FitC wavelengths	TritC wavelengths	3	0.90
TritC wavelengths	Cy5 wavelengths	1	0.19
TritC wavelengths	DAPI wavelengths	1	0.73
TritC wavelengths	FitC wavelengths	1	1.13
TritC wavelengths	TritC wavelengths	1	1.00
TritC wavelengths	Cy5 wavelengths	2	0.13
TritC wavelengths	DAPI wavelengths	2	0.61
TritC wavelengths	FitC wavelengths	2	1.07
TritC wavelengths	TritC wavelengths	2	1.00
TritC wavelengths	Cy5 wavelengths	3	0.13
TritC wavelengths	DAPI wavelengths	3	0.65
TritC wavelengths	FitC wavelengths	3	1.11
TritC wavelengths	TritC wavelengths	3	1.00

Appendix 1.2 – *Agrobacterium tumefaciens* stain screening data

Stain	Average 12-bit pixel intensity across image
Syto 16 nucleic acid stain	227.75
Syto 16 nucleic acid stain	228.54
Syto 16 nucleic acid stain	228.27
CFDA SE	213.18
CFDA SE	213.39
CFDA SE	213.28
Alexa 488 CA SE	213.64
Alexa 488 CA SE	211.90
Alexa 488 CA SE	212.22
none	214.05
none	215.73
none	215.07

Appendix 1.3 – *Agrobacterium tumefaciens* stain concentration optimization data

Concentration of Syto 16 nucleic acid stain (uM)	12-bit signal intensity threshold used to isolate cells	Object count in image	Object mean average pixel intensity	Object maximum average pixel intensity
0	No detectable signals	N/A	N/A	N/A
0	No detectable signals	N/A	N/A	N/A
0	No detectable signals	N/A	N/A	N/A
0.1	234	103	241.60	301.55
0.1	234	22	253.54	279.59
0.1	234	8	244.03	257.18
0.5	285	15	337.37	403.08
0.5	285	14	337.38	390.70
0.5	285	9	303.40	327.18
1	345	14	424.87	555.68
1	345	26	395.88	451.33
1	345	14	387.28	435.19
5	752	12	1083.05	1502.86
5	752	19	976.56	1514.49
5	752	9	867.30	1028.17
10	925	49	1653.56	2827.48
10	925	49	1547.86	2912.82
10	925	46	1539.65	2576.12
15	1108	23	2194.86	3112.66
15	1108	26	2042.93	2878.51
15	1108	17	1894.93	2787.23
20	1260	35	2027.64	3383.48
20	1260	30	2216.10	3260.69
20	1260	15	2152.70	2693.80

Appendix 1.4 - MATLAB script for estimating parameters in saturation model describing mean and maximum average signal intensity per cell versus staining concentration

Script:

```
% Script for fitting saturation function to signal intensity versus
stain concentration data
% Written by Christopher Simmons
% May 17, 2010

% Stain concentration values used in experiment (uM)
s=[0.1 0.1 0.1 0.5 0.5 0.5 1 1 1 5 5 5 10 10 10 15 15 15 20 20 20];

% Mean average pixel intensity per object values observed in experiment
i=[241.6 253.54 244.03 337.37 337.38 303.4 424.87 395.88 387.28 1083.05
976.56 867.3 1653.56 1547.86 1539.65 2194.86 2042.93 1894.93 2027.64
2216.1 2152.7];

% Maximum average pixel intensity values observed in experiment
mi=[301.55 279.59 257.18 403.08 390.7 327.18 555.68 451.33 435.19
1502.86 1514.49 1028.17 2827.48 2912.82 2576.12 3112.66 2878.51 2787.23
3383.48 3260.69 2693.8];

% Initial estimates for parameters a and b in model y = ax/(b+x)
beta=[1 1];

% Call nlinfit function to estimate parameter values for mean average
pixel intensity per object vs stain concentration
[betahat1,f1,J1]=nlinfit(s,i,'nlinfit_i_vs_s',beta);

% Call nlinfit function to estimate parameter values for maximum
average pixel intensity per object vs stain concentration
[betahat2,f2,J2]=nlinfit(s,mi,'nlinfit_mi_vs_s',beta);

% Display parameter estimates for mean average pixel intensity per
object vs stain concentration
a_est1=betahat1(1);
b_est1=betahat1(2);
fprintf('For mean average pixel intensity per object vs stain
concentration data, the parameters in the model I = aS/(b + S) are
estimated as a = %3.1f\n and b = %3.1f\n uM', a_est1, b_est1)

% Call nlparci function to determine 95% confidence intervals for
maximum average pixel intensity per object vs stain concentration
parameter estimates
beta1ci=nlparci(betahat1,f1,J1);
fprintf('The 95 percent confidence intervals for parameter estimates
are %3.2f\n <= a <= %3.2f\n, %3.2f\n <= b <= %3.2f\n uM', beta1ci(1,1),
beta1ci(1,2), beta1ci(2,1), beta1ci(2,2))

% Display parameter estimates for mean average pixel intensity per
object vs stain concentration
a_est2=betahat2(1);
b_est2=betahat2(2);
```

Appendix 1.4 continued

```
fprintf('For maximum average pixel intensity per object vs stain
concentration data, the parameters in the model I = aS/(b + S) are
estimated as a = %3.1f\n and b = %3.1f\n uM', a_est2, b_est2)

% Call nlparci function to determine 95% confidence intervals for mean
average pixel intensity per object vs stain concentration parameter
estimates
beta2ci=nlparci(betahat2,f2,J2);
fprintf('The 95 percent confidence intervals for parameter estimates
are %3.2f\n <= a <= %3.2f\n, %3.2f\n <= b <= %3.2f\n uM', beta2ci(1,1),
beta2ci(1,2), beta2ci(2,1), beta2ci(2,2))
```

Function files:

```
function ihat=nlinfit_i_vs_s(beta,s)

a_est1=beta(1);
b_est1=beta(2);

ihat=a_est1*s./(b_est1+s);

function mihat=nlinfit_mi_vs_s(beta,s)

a_est2=beta(1);
b_est2=beta(2);

mihat=a_est2*s./(b_est2+s);
```

Output:

```
For mean average pixel intensity per object vs stain concentration
data, the parameters in the model I = aS/(b + S) are estimated as a =
3227.1 and b = 9.9 uM

The 95 percent confidence intervals for parameter estimates are 2573.33
<= a <= 3880.88, 5.30 <= b <= 14.43 uM

For maximum average pixel intensity per object vs stain concentration
data, the parameters in the model I = aS/(b + S) are estimated as a =
4736.0 and b = 9.3 uM

The 95 percent confidence intervals for parameter estimates are 3620.23
<= a <= 5851.78, 4.19 <= b <= 14.50 uM
```

Appendix 1.5 – Stained *A. tumefaciens* signal stability over time data

Incubation time (hr)	Object count in image	Mean average 12-bit pixel intensity/object
0	29	771.09
0	44	860.76
0	33	1208.17
24	144	794.03
24	138	824.11
24	127	862.31
48	54	852.17
48	54	955.24
48	43	1023.51
72	87	1075.65
72	91	1010.81
72	81	1108.31

Appendix 1.6 – Colony counts for plated labeled and unlabeled *A. tumefaciens*

Treatment	Number of colonies on plate
unstained bacteria	13
unstained bacteria	21
unstained bacteria	20
unstained bacteria	27
unstained bacteria	14
stained bacteria	24
stained bacteria	18
stained bacteria	23
stained bacteria	20
stained bacteria	15

Appendix 1.7 – GUS expression data for leaf disks infiltrated with Syto 16-stained and unstained *A. tumefaciens*

Histochemical stained leaf disks agroinfiltrated with stained *A. tumefaciens* (left) and a binary conversion of the image obtained by setting an 8-bit threshold level of 100 (right).

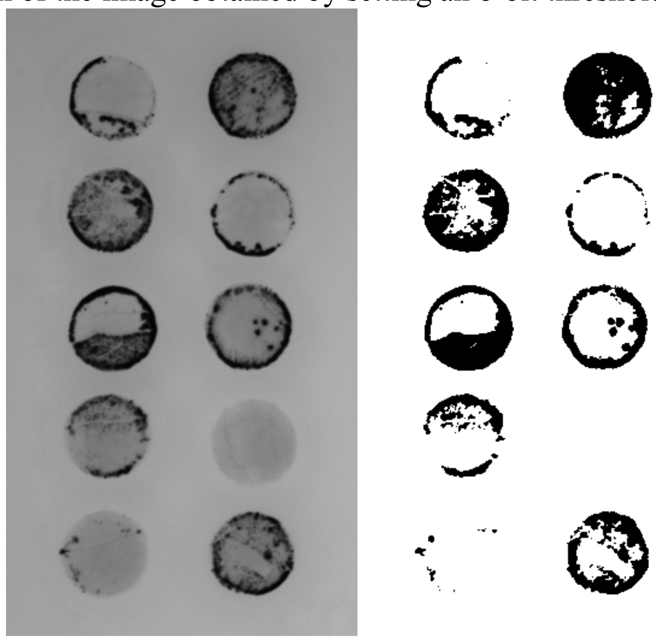

Histochemical stained leaf disks agroinfiltrated with unstained *A. tumefaciens* (left) and a binary conversion of the image obtained by setting an 8-bit threshold level of 100 (right).

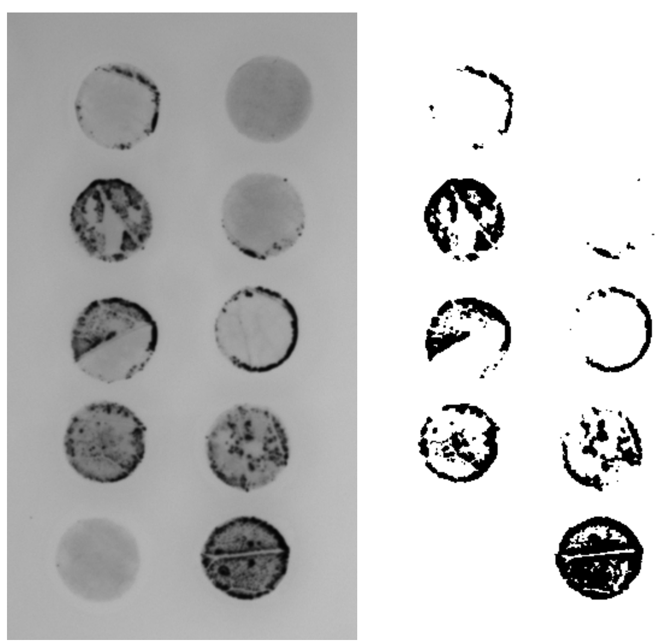

Appendix 1.7 continued

Histochemical stained leaf disks agroinfiltrated with water (left) and a binary conversion of the image obtained by setting an 8-bit threshold level of 100 (right). No leaves exhibited a signal greater than the threshold.

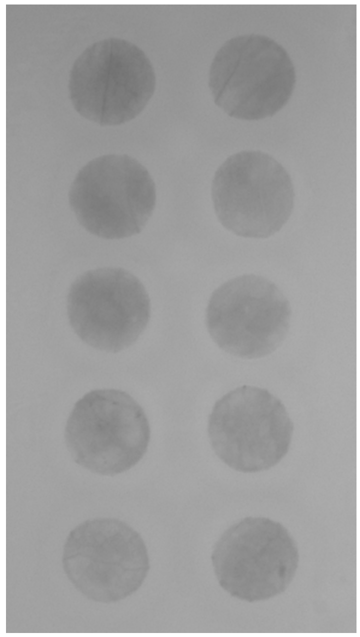

Leaves infiltrated with	Total mass of suspension vacuum-infiltrated into all leaves (g)	Average volume of vacuum-infiltrated suspension per leaf disk (ml)
Stained *A. tumefaciens*	0.0701	0.00701
Unstained *A. tumefaciens*	0.0488	0.00488
Water	0.0447	0.00447

Appendix 1.7 continued

Leaf disk infiltrated with	Leaf disk area exhibiting GUS activity (px)	Leaf disk area exhibiting GUS activity (mm^2)	Leaf disk area exhibiting GUS activity/average volume infiltrated suspension per leaf disk ($mm^2/\mu l$)
Stained *A. tumefaciens*	852	16.5	2.35
Stained *A. tumefaciens*	3615	69.9	9.97
Stained *A. tumefaciens*	2643	51.1	7.29
Stained *A. tumefaciens*	656	12.7	1.81
Stained *A. tumefaciens*	2466	47.7	6.80
Stained *A. tumefaciens*	1626	31.4	4.48
Stained *A. tumefaciens*	1187	23.0	3.27
Stained *A. tumefaciens*	0	0	0
Stained *A. tumefaciens*	120	2.32	0.331
Stained *A. tumefaciens*	2077	40.2	5.73
Unstained *A. tumefaciens*	368	7.12	1.46
Unstained *A. tumefaciens*	0	0	0
Unstained *A. tumefaciens*	2023	39.1	8.02
Unstained *A. tumefaciens*	126	2.44	0.499
Unstained *A. tumefaciens*	1250	24.2	4.95
Unstained *A. tumefaciens*	607	11.7	2.40
Unstained *A. tumefaciens*	1441	27.9	5.71
Unstained *A. tumefaciens*	1242	24.0	4.92
Unstained *A. tumefaciens*	0	0	0
Unstained *A. tumefaciens*	3106	60.1	12.3
Water	0	0	0
Water	0	0	0
Water	0	0	0
Water	0	0	0
Water	0	0	0
Water	0	0	0
Water	0	0	0
Water	0	0	0
Water	0	0	0
Water	0	0	0

Note: a conversion factor of 0.01933 px/mm^2 was used to convert pixel area values to mm^2. Bacterial suspensions were assumed to have a density of 1 g/ml.

Appendix 1.8 – Bacterial proliferation versus time post-infiltration data

Hours post-infiltration	Leaf weight pre-infiltration (g)	Leaf weight post-infiltration (g)	Infiltrated suspension (g)
0	0.0655	0.0839	0.0184
24	0.065	0.078	0.013
48	0.0638	0.0773	0.0135
72	0.0637	0.0806	0.0169

Hours post-infiltration	Colonies on plate	Estimated cells/g leaf at time point
0	46	1.67E+08
0	36	1.31E+08
0	37	1.35E+08
0	26	9.45E+07
0	34	1.24E+08
24	94	3.67E+08
24	77	3.01E+08
24	97	3.79E+08
24	95	3.71E+08
24	87	3.40E+08
48	127	5.01E+08
48	127	5.01E+08
48	154	6.07E+08
48	121	4.77E+08
48	131	5.16E+08
72	239	9.04E+08
72	295	1.12E+09
72	258	9.76E+08
72	282	1.07E+09
72	280	1.06E+09

Appendix 2.1 – Signal density versus incubation time data for lettuce leaves infiltrated with labeled *A. tumefaciens*

<table>
<tr><th>Incubation time (hr)</th><th>Leaf</th><th>Infection site</th><th>Relative depth (μm)</th><th>Number of signals (bacteria)</th><th>Tissue area (μm^2)</th><th>Average bacteria per mm^3 tissue</th><th>Mean average bacteria per mm^3 tissue</th><th>Standard deviation of average bacteria per mm^3 tissue</th></tr>
<tr><td rowspan="27">1</td><td rowspan="9">1</td><td rowspan="3">1</td><td>0</td><td>30</td><td rowspan="3">63237</td><td rowspan="9">57151</td><td rowspan="27">73299</td><td rowspan="27">16656</td></tr>
<tr><td>10</td><td>30</td></tr>
<tr><td>20</td><td>36</td></tr>
<tr><td rowspan="3">2</td><td>0</td><td>34</td><td rowspan="3">59761</td></tr>
<tr><td>10</td><td>19</td></tr>
<tr><td>20</td><td>13</td></tr>
<tr><td rowspan="3">3</td><td>0</td><td>14</td><td rowspan="3">58273</td></tr>
<tr><td>10</td><td>20</td></tr>
<tr><td>20</td><td>13</td></tr>
<tr><td rowspan="9">2</td><td rowspan="3">1</td><td>0</td><td>38</td><td rowspan="3">53868</td><td rowspan="9">90419</td></tr>
<tr><td>10</td><td>20</td></tr>
<tr><td>20</td><td>24</td></tr>
<tr><td rowspan="3">2</td><td>0</td><td>23</td><td rowspan="3">51478</td></tr>
<tr><td>10</td><td>24</td></tr>
<tr><td>20</td><td>16</td></tr>
<tr><td rowspan="3">3</td><td>0</td><td>60</td><td rowspan="3">58975</td></tr>
<tr><td>10</td><td>63</td></tr>
<tr><td>20</td><td>35</td></tr>
<tr><td rowspan="9">3</td><td rowspan="3">1</td><td>0</td><td>87</td><td rowspan="3">67825</td><td rowspan="9">72327</td></tr>
<tr><td>10</td><td>42</td></tr>
<tr><td>20</td><td>38</td></tr>
<tr><td rowspan="3">2</td><td>0</td><td>38</td><td rowspan="3">64577</td></tr>
<tr><td>10</td><td>25</td></tr>
<tr><td>20</td><td>4</td></tr>
<tr><td rowspan="3">3</td><td>0</td><td>19</td><td rowspan="3">58343</td></tr>
<tr><td>10</td><td>17</td></tr>
<tr><td>20</td><td>13</td></tr>
</table>

Appendix 2.1 continued

Incubation time (hr)	Leaf	Infection site	Relative depth (µm)	Number of signals (bacteria)	Tissue area (µm^2)	Average bacteria per mm^3 tissue	Mean average bacteria per mm^3 tissue	Standard deviation of average bacteria per mm^3 tissue
24	1	1	0	9	55922	17994	68883	44311
			10	8				
			20	4				
		2	0	10	52292			
			10	2				
			20	6				
		3	0	n/a	n/a			
			10	n/a				
			20	n/a				
	2	1	0	41	59108	89733		
			10	34				
			20	30				
		2	0	33	56805			
			10	16				
			20	15				
		3	0	56	51190			
			10	41				
			20	30				
	3	1	0	20	53714	98923		
			10	30				
			20	20				
		2	0	48	52771			
			10	18				
			20	14				
		3	0	79	47815			
			10	40				
			20	30				

Note: only two infection sites could be located in the first leaf explants.

Appendix 2.1 continued

Incubation time (hr)	Leaf	Infection site	Relative depth (µm)	Number of signals (bacteria)	Tissue area (μm^2)	Average bacteria per mm^3 tissue	Mean average bacteria per mm^3 tissue	Standard deviation of average bacteria per mm^3 tissue
48	1	1	0	2	52453	22804	32089	9578
			10	8				
			20	13				
		2	0	2	57745			
			10	0				
			20	2				
		3	0	20	47649			
			10	16				
			20	5				
	2	1	0	2	52286	41935		
			10	4				
			20	0				
		2	0	48	63444			
			10	27				
			20	18				
		3	0	30	58794			
			10	21				
			20	4				
	3	1	0	19	51682	31528		
			10	17				
			20	3				
		2	0	8	51517			
			10	6				
			20	3				
		3	0	18	56997			
			10	9				
			20	19				

Appendix 2.1 continued

Incubation time (hr)	Leaf	Infection site	Relative depth (μm)	Number of signals (bacteria)	Tissue area (μm^2)	Average bacteria per mm^3 tissue	Mean average bacteria per mm^3 tissue	Standard deviation of average bacteria per mm^3 tissue
72	1	1	0	0	52772.6	1245	10952	10791
			10	0				
			20	0				
		2	0	2	53531.2			
			10	0				
			20	2				
		3	0	0	54168.9			
			10	0				
			20	0				
	2	1	0	9	56130.6	22571		
			10	7				
			20	3				
		2	0	23	61703.2			
			10	14				
			20	4				
		3	0	12	56930.2			
			10	5				
			20	3				
	3	1	0	7	41869.8	9040		
			10	5				
			20	4				
		2	0	1	51335.5			
			10	2				
			20	4				
		3	0	0	41842			
			10	1				
			20	0				

Appendix 2.2 – Signal density versus incubation time data for lettuce leaves infiltrated with water

Incubation time (hr)	Leaf	Infection site	Relative depth (μm)	Number of signals	Tissue area (μm^2)	Average signals per mm^3 tissue	Mean average signals per mm^3 tissue	Standard deviation of average signals per mm^3 tissue
1	1	1	0	0		0	112	194
			10	0				
			20	0				
		2	0	0				
			10	0				
			20	0				
		3	0	0				
			10	0				
			20	0				
	2	1	0	0	45985	336		
			10	0				
			20	0				
		2	0	0	43785			
			10	0				
			20	0				
		3	0	0	49587			
			10	1				
			20	0				
	3	1	0	0		0		
			10	0				
			20	0				
		2	0	0				
			10	0				
			20	0				
		3	0	0				
			10	0				
			20	0				

Note: tissue area measurements were not required to calculate signal density in samples that had no signals above the intensity threshold.

Appendix 2.2 continued

Incubation time (hr)	Leaf	Infection site	Relative depth (μm)	Number of signals	Tissue area (μm^2)	Average signals per mm^3 tissue	Mean average signals per mm^3 tissue	Standard deviation of average signals per mm^3 tissue
24	1	1	0	0	58358	673	569	525
			10	0				
			20	0				
		2	0	0	52494			
			10	0				
			20	1				
		3	0	1	46881			
			10	0				
			20	0				
	2	1	0	0		0		
			10	0				
			20	0				
		2	0	0				
			10	0				
			20	0				
		3	0	0				
			10	0				
			20	0				
	3	1	0	0	55085	1035		
			10	0				
			20	0				
		2	0	0	48291			
			10	3				
			20	0				
		3	0	0	50550			
			10	0				
			20	0				

Note: tissue area measurements were not required to calculate signal density in samples that had no signals above the intensity threshold.

Appendix 2.2 continued

Incubation time (hr)	Leaf	Infection site	Relative depth (μm)	Number of signals	Tissue area (μm^2)	Average signals per mm^3 tissue	Mean average signals per mm^3 tissue	Standard deviation of average signals per mm^3 tissue
48	1	1	0	0	44244	753	251	435
			10	1				
			20	0				
		2	0	0	55521			
			10	0				
			20	1				
		3	0	0	55573			
			10	0				
			20	0				
	2	1	0	0		0		
			10	0				
			20	0				
		2	0	0				
			10	0				
			20	0				
		3	0	0				
			10	0				
			20	0				
	3	1	0	0		0		
			10	0				
			20	0				
		2	0	0				
			10	0				
			20	0				
		3	0	0				
			10	0				
			20	0				

Note: tissue area measurements were not required to calculate signal density in samples that had no signals above the intensity threshold.

Appendix 2.2 continued

Incubation time (hr)	Leaf	Infection site	Relative depth (μm)	Number of signals	Tissue area (μm^2)	Average signals per mm^3 tissue	Mean average signals per mm^3 tissue	Standard deviation of average signals per mm^3 tissue
72	1	1	0	0		0	288	276
			10	0				
			20	0				
		2	0	0				
			10	0				
			20	0				
		3	0	0				
			10	0				
			20	0				
	2	1	0	0	60379	549		
			10	0				
			20	0				
		2	0	1	61070			
			10	0				
			20	0				
		3	0	1	60259			
			10	0				
			20	0				
	3	1	0	0	58679	316		
			10	0				
			20	0				
		2	0	1	52783			
			10	0				
			20	0				
		3	0	0	57687			
			10	0				
			20	0				

Appendix 2.3 – GUS activity versus time post-infiltration data

Hours post-infiltration	Volume of infiltrated suspension (ml)	Leaf area with GUS activity (mm^2/ml infiltrated bacterial suspension)	Mean leaf area with GUS activity (mm^2/ml infiltrated bacterial suspension)	Standard deviation of leaf area with GUS activity (mm^2/ml infiltrated bacterial suspension)
0	0.0095	0.00	0	0
		0.00		
		0.00		
24	0.00743	396.11	150	215
		0.00		
		54.08		
48	0.00618	3723.7	5048	1524
		6712.8		
		4706.0		
72	0.0151	4707.2	3635	2050
		4925.9		
		1271.0		

Appendix 2.4 – Infiltrated liquid and leaf viability versus surfactant concentration data

Surfactant concentration (ppm, v/v)	Infiltrated liquid volume (ml/g leaf)	Number of putrefied leaf disks
1	0.269230769	0
1	0.271883289	0
1	0.259385666	0
10	0.311871227	0
10	0.2858122	0
10	0.274672188	0
100	0.392663043	0
100	0.453306067	0
100	0.445887446	0
1000	0.400140647	3
1000	0.451314854	1
1000	0.425876011	1

Appendix 2.5 – Density of attached bacteria versus surfactant concentration data

Surfactant concentration (ppm)	Leaf	Infection site	Relative depth (μm)	Number of signals (bacteria)	Tissue area (μm^2)	Average bacteria per mm^3 tissue
1	1	1	0	34	49872	144364
			10	18		
			20	24		
		2	0	87	41890	
			10	61		
			20	44		
		3	0	59	54413	
			10	49		
			20	31		
	2	1	0	10	48154	36943
			10	8		
			20	7		
		2	0	10	59540	
			10	10		
			20	13		
		3	0	22	48988	
			10	16		
			20	18		
	3	1	0	48	46550	67071
			10	42		
			20	23		
		2	0	11	42560	
			10	15		
			20	6		
		3	0	8	41427	
			10	18		
			20	9		

Appendix 2.5 continued

Surfactant concentration (ppm)	Leaf	Infection site	Relative depth (μm)	Number of signals (bacteria)	Tissue area (μm^2)	Average bacteria per mm^3 tissue
1	4	1	0	26	56318	51979
			10	47		
			20	36		
		2	0	19	51868	
			10	4		
			20	8		
		3	0	9	44399	
			10	8		
			20	9		
	5	1	0	15	35269	61558
			10	10		
			20	15		
		2	0	18	34622	
			10	11		
			20	12		
		3	0	26	45088	
			10	20		
			20	16		
	6	1	0	4	53892	58146
			10	5		
			20	1		
		2	0	17	40423	
			10	15		
			20	5		
		3	0	25	35597	
			10	34		
			20	26		

Appendix 2.5 continued

Surfactant concentration (ppm)	Leaf	Infection site	Relative depth (μm)	Number of signals (bacteria)	Tissue area (μm^2)	Average bacteria per mm^3 tissue
10	1	1	0	40	43626	55943
			10	5		
			20	7		
		2	0	16	42276	
			10	6		
			20	2		
		3	0	17	38825	
			10	24		
			20	21		
	2	1	0	10	51545	36060
			10	7		
			20	2		
		2	0	18	39770	
			10	8		
			20	8		
		3	0	16	41487	
			10	14		
			20	9		
	3	1	0	7	45176	37031
			10	4		
			20	3		
		2	0	10	47820	
			10	19		
			20	13		
		3	0	15	37731	
			10	13		
			20	11		

Appendix 2.5 continued

Surfactant concentration (ppm)	Leaf	Infection site	Relative depth (µm)	Number of signals (bacteria)	Tissue area (μm^2)	Average bacteria per mm^3 tissue
10	4	1	0	23	50937	60760
			10	18		
			20	10		
		2	0	16	50642	
			10	29		
			20	19		
		3	0	38	60843	
			10	25		
			20	21		
	5	1	0	7	41625	46621
			10	15		
			20	10		
		2	0	17	43810	
			10	19		
			20	15		
		3	0	18	42806	
			10	7		
			20	12		
	6	1	0	33	46530	81926
			10	35		
			20	14		
		2	0	10	53297	
			10	13		
			20	11		
		3	0	59	58044	
			10	46		
			20	41		

Appendix 2.5 continued

Surfactant concentration (ppm)	Leaf	Infection site	Relative depth (μm)	Number of signals (bacteria)	Tissue area (μm^2)	Average bacteria per mm^3 tissue
100	1	1	0	13	42970	60017
			10	7		
			20	4		
		2	0	29	36191	
			10	31		
			20	19		
		3	0	20	41881	
			10	8		
			20	8		
	2	1	0	16	50112	63989
			10	15		
			20	12		
		2	0	20	40379	
			10	18		
			20	14		
		3	0	38	50783	
			10	27		
			20	21		
	3	1	0	10	42535	79982
			10	19		
			20	9		
		2	0	27	31668	
			10	16		
			20	14		
		3	0	35	33245	
			10	18		
			20	17		

Appendix 2.5 continued

Surfactant concentration (ppm)	Leaf	Infection site	Relative depth (µm)	Number of signals (bacteria)	Tissue area (μm^2)	Average bacteria per mm^3 tissue
100	4	1	0	23	39931	81521
			10	20		
			20	12		
		2	0	12	41446	
			10	20		
			20	9		
		3	0	26	41194	
			10	43		
			20	35		
	5	1	0	17	41903	73547
			10	14		
			20	20		
		2	0	13	49216	
			10	13		
			20	10		
		3	0	23	38145	
			10	34		
			20	37		
	6	1	0	30	54454	65653
			10	33		
			20	27		
		2	0	29	44965	
			10	11		
			20	13		
		3	0	25	42429	
			10	15		
			20	7		

Appendix 2.5 continued

Surfactant concentration (ppm)	Leaf	Infection site	Relative depth (μm)	Number of signals (bacteria)	Tissue area (μm^2)	Average bacteria per mm^3 tissue
1000	1	1	0	44	33998	107761
			10	38		
			20	37		
		2	0	15	28381	
			10	14		
			20	21		
		3	0	22	38216	
			10	11		
			20	13		
	2	1	0	57	30029	159985
			10	43		
			20	28		
		2	0	23	35092	
			10	21		
			20	16		
		3	0	61	35293	
			10	37		
			20	30		
	3	1	0	22	38911	67846
			10	18		
			20	11		
		2	0	17	40863	
			10	18		
			20	17		
		3	0	26	38319	
			10	17		
			20	14		

Appendix 2.5 continued

Surfactant concentration (ppm)	Leaf	Infection site	Relative depth (µm)	Number of signals (bacteria)	Tissue area (µm^2)	Average bacteria per mm^3 tissue
1000	4	1	0	27	44763	75772
			10	10		
			20	5		
		2	0	25	48715	
			10	22		
			20	25		
		3	0	40	46477	
			10	33		
			20	26		
	5	1	0	32	43085	112297
			10	25		
			20	10		
		2	0	41	50715	
			10	42		
			20	28		
		3	0	57	51768	
			10	59		
			20	39		
	6	1	0	34	42998	107778
			10	24		
			20	19		
		2	0	34	44511	
			10	32		
			20	32		
		3	0	40	46076	
			10	36		
			20	38		

Appendix 2.6 – Density of attached bacteria versus vacuum infiltration pressure data

Pressure (kPa)	Leaf	Infection Site	Relative depth (μm)	Number of signals (bacteria)	Tissue Area (μm^2)	Average bacteria per mm^3 tissue	Mean average bacteria per mm^3 tissue	Standard deviation of average bacteria per mm^3 tissue
5	1	1	0	70	44073	181356	86896	81805
			10	80				
			20	56				
		2	0	44	42656			
			10	26				
			20	12				
		3	0	80	47608			
			10	64				
			20	60				
	2	1	0	23	44704	39866		
			10	19				
			20	11				
		2	0	11	42539			
			10	15				
			20	4				
		3	0	9	45894			
			10	8				
			20	6				
	3	1	0	16	50551	39467		
			10	16				
			20	11				
		2	0	8	49057			
			10	14				
			20	11				
		3	0	22	43803			
			10	9				
			20	6				

Appendix 2.6 continued

Pressure (kPa)	Leaf	Infection Site	Relative depth (μm)	Number of signals (bacteria)	Tissue Area (μm^2)	Average bacteria per mm^3 tissue	Mean average bacteria per mm^3 tissue	Standard deviation of average bacteria per mm^3 tissue
25	1	1	0	16	52884	31294	30882	1017
			10	15				
			20	3				
		2	0	10	50491			
			10	9				
			20	7				
		3	0	14	52793			
			10	14				
			20	10				
	2	1	0	10	50387	31628		
			10	8				
			20	2				
		2	0	12	39336			
			10	19				
			20	6				
		3	0	9	39274			
			10	4				
			20	9				
	3	1	0	9	43868	29725		
			10	6				
			20	6				
		2	0	12	41222			
			10	9				
			20	4				
		3	0	8	37234			
			10	10				
			20	8				

Appendix 2.6 continued

Pressure (kPa)	Leaf	Infection Site	Relative depth (μm)	Number of signals (bacteria)	Tissue Area (μm^2)	Average bacteria per mm^3 tissue	Mean average bacteria per mm^3 tissue	Standard deviation of average bacteria per mm^3 tissue
45	1	1	0	8	49376	27744	37850	23661
			10	9				
			20	1				
		2	0	11	61110			
			10	13				
			20	12				
		3	0	11	52039			
			10	15				
			20	11				
	2	1	0	30	39935	64886		
			10	28				
			20	23				
		2	0	18	42358			
			10	17				
			20	6				
		3	0	14	41253			
			10	18				
			20	5				
	3	1	0	9	54370	20920		
			10	2				
			20	6				
		2	0	17	61657			
			10	12				
			20	6				
		3	0	6	50689			
			10	8				
			20	5				

Appendix 2.7 - Density of attached bacteria versus density of infiltrated bacteria data

Density of infiltrated bacteria (CFU/ml)	Leaf	Infection site	12-bit signal intensity threshold	Relative depth (µm)	Number of signals (bacteria)	Tissue area (μm^2)	Average attached bacteria per mm^3 tissue	Mean average attached bacteria per mm^3 tissue	Standard deviation of average attached bacteria per mm^3 tissue
1.0E+08	1	1	250	0	0	55366	3638	1625	1850
				10	0				
				20	0				
		2	250	0	1	52909			
				10	1				
				20	0				
		3	250	0	6	55400			
				10	2				
				20	2				
	2	1	230	0	0	54717	0		
				10	0				
				20	0				
		2	230	0	0	57253			
				10	0				
				20	0				
		3	230	0	0	58607			
				10	0				
				20	0				
	3	1	230	0	0	45425	1235		
				10	1				
				20	1				
		2	230	0	0	42805			
				10	0				
				20	0				
		3	230	0	1	33241			
				10	0				
				20	0				

Appendix 2.7 continued

Density of infiltrated bacteria (CFU/ml)	Leaf	Infection site	12-bit signal intensity threshold	Relative depth (µm)	Number of signals (bacteria)	Tissue area (μm^2)	Average attached bacteria per mm^3 tissue	Mean average attached bacteria per mm^3 tissue	Standard deviation of average attached bacteria per mm^3 tissue
1.0E+09	1	1	230	0	22	43953	52741	73299	20169
				10	26				
				20	14				
		2	250	0	13	52428			
				10	12				
				20	3				
		3	250	0	28	57388			
				10	23				
				20	19				
	2	1	250	0	46	51918	93055		
				10	21				
				20	33				
		2	230	0	19	47307			
				10	29				
				20	25				
		3	240	0	50	52032			
				10	34				
				20	26				
	3	1	240	0	7	52926	74101		
				10	12				
				20	14				
		2	250	0	37	54887			
				10	41				
				20	41				
		3	250	0	29	47145			
				10	28				
				20	21				

Appendix 2.7 continued

Density of infiltrated bacteria (CFU/ml)	Leaf	Infection site	12-bit signal intensity threshold	Relative depth (µm)	Number of signals (bacteria)	Tissue area (µm^2)	Average attached bacteria per mm^3 tissue	Mean average attached bacteria per mm^3 tissue	Standard deviation of average attached bacteria per mm^3 tissue
1.0E+10	1	1	280	0	54	55387	237086	202677	67541
				10	76				
				20	60				
		2	300	0	121	43511			
				10	103				
				20	82				
		3	300	0	49	40669			
				10	60				
				20	44				
	2	1	280	0	40	52712	124861		
				10	39				
				20	44				
		2	260	0	50	48412			
				10	46				
				20	40				
		3	280	0	38	47680			
				10	36				
				20	38				
	3	1	300	0	72	51363	246083		
				10	62				
				20	64				
		2	300	0	82	48454			
				10	83				
				20	79				
		3	300	0	100	45962			
				10	88				
				20	82				

Appendix 2.8 - MATLAB script for estimating parameters in saturation model describing average bacterial attachment to leaf tissue versus infiltrated bacterial density

Script:

```
% Script for fitting saturation function to attached bacteria versus
infiltration density data
% Written by Christopher Simmons
% March 14, 2011

global dI0

% Infiltrated bacteria concentrations (CFU/ml)
dI=[1E8 1E8 1E8 1E9 1E9 1E9 1E10 1E10 1E10];

% Maximum average pixel intensity values observed in experiment
dI0=1E8;

% Difference between dI and dI,0
ddI=dI-dI0;

% Average density of attached bacteria at infection sites (cells/mm^3
tissue)
dA=[3638.449522 0 1235.192467 52740.70012 93055.11417 74100.99486
237086.0959 124860.8378 246083.4051];

% Initial estimates for parameters dAmax and alpha in saturation model
beta=[1 1];

% Call nlinfit function to estimate parameter values for saturation
model
[betahat1,f1,J1]=nlinfit(ddI,dA,'nlinfit_dA_vs_ddI',beta);

% Display parameter estimates for saturation model
dAmax=betahat1(1);
alpha=betahat1(2);
fprintf('dAmax = %3.1f\n cells/mm^3 tissue and alpha = %3.1f\n
cells/mm^3 tissue', dAmax, alpha)

% Call nlparci function to determine 95% confidence intervals for
maximum average pixel intensity per object vs stain concentration
parameter estimates
beta1ci=nlparci(betahat1,f1,J1);
fprintf('The 95 percent confidence intervals for parameter estimates
are %3.2f\n <= dAmax <= %3.2f\n cells/mm^3 tissue, %3.2f\n <= alpha <=
%3.2f\n cells/mm^3 tissue', beta1ci(1,1), beta1ci(1,2), beta1ci(2,1),
beta1ci(2,2))
```

Appendix 2.8 continued

Function files:

```
function dAhat=nlinfit_dA_vs_dI(beta,ddI)

global dI0
dAmax=beta(1);
alpha=beta(2);
dAhat=dAmax*ddI./((alpha-dI0)+ddI);

end
```

Output:

dAmax = 246118.4 cells/mm^3 tissue and alpha = 2221961897.8 cells/mm^3 tissue

The 95 percent confidence intervals for parameter estimates are

144432.53 <= dAmax <= 347804.34 cells/mm^3 tissue,

-792550963.11<= alpha <= 5236474758.63 cells/mm^3 tissue

Appendix 2.9 – GUS activity versus infiltrated bacterial density data

Density of infiltrated bacteria (CFU/ml)	A405 measurements for stopped samples after various reaction times				
	0 min	15 min	30 min	45 min	60 min
1.E+08	0.215 0.218 0.214	0.236 0.237 0.234	0.256 0.252 0.250	0.273 0.271 0.271	0.289 0.293 0.288
1.E+08	0.209 0.210 0.208	0.243 0.238 0.234	0.266 0.264 0.265	0.296 0.295 0.293	0.323 0.327 0.326
1.E+08	0.237 0.239 0.236	0.268 0.266 0.266	0.304 0.308 0.306	0.334 0.333 0.332	0.368 0.369 0.369
1.E+09	0.221 0.219 0.218	0.256 0.257 0.254	0.293 0.291 0.294	0.331 0.329 0.331	0.372 0.371 0.348
1.E+09	0.227 0.225 0.223	0.256 0.258 0.254	0.288 0.292 0.283	0.329 0.325 0.321	0.346 0.351 0.348
1.E+09	0.197 0.197 0.196	0.221 0.219 0.218	0.247 0.247 0.245	0.270 0.273 0.272	0.296 0.296 0.299
1.E+10	0.211 0.209 0.203	0.218 0.213 0.210	0.218 0.215 0.218	0.223 0.226 0.224	0.234 0.232 0.232
1.E+10	0.210 0.214 0.210	0.217 0.216 0.219	0.225 0.227 0.229	0.237 0.236 0.235	0.238 0.237 0.237
1.E+10	0.231 0.234 0.237	0.259 0.258 0.259	0.251 0.252 0.247	0.257 0.255 0.255	0.256 0.256 0.257

Appendix 2.9 continued

Density of infiltrated bacteria (CFU/ml)	Infiltrated leaf mass (g)	GUS activity (U/g infiltrated leaf tissue)	Average GUS activity (U/g infiltrated leaf)	Standard deviation of GUS activity (U/g infiltrated leaf)
1.E+08	0.1551	62.5	91.8	27.1
1.E+08	0.1567	97		
1.E+08	0.1481	116		
1.E+09	0.1554	129	109	22.0
1.E+09	0.147	112		
1.E+09	0.1566	85.2		
1.E+10	0.1587	20.1	19.9	5.06
1.E+10	0.1488	24.8		
1.E+10	0.1482	14.7		

Appendix 3.1 – Infiltrated liquid volume and leaf viability versus infiltrated surfactant concentration data

Concentration of surfactant (ppm)	Pre-infiltration leaf mass (g)	Post-infiltration leaf mass (g)	Volume of infiltrated liquid (ml/g leaf)	Number of yellowed or putrefied leaves
1	0.0884	0.0910	0.0294	0
1	0.0830	0.0880	0.0602	0
1	0.0936	0.0989	0.0566	0
10	0.0952	0.1007	0.0578	0
10	0.0877	0.0922	0.0513	0
10	0.0844	0.0880	0.0427	0
100	0.1005	0.1062	0.0567	0
100	0.0931	0.0993	0.0666	0
100	0.0756	0.0786	0.0397	0
1000	0.0987	0.1041	0.0547	0
1000	0.0910	0.0933	0.0253	0
1000	0.0780	0.0826	0.0590	0

Appendix 3.2 - Density of attached bacteria versus surfactant concentration data

Surfactant concentration (ppm)	Leaf	Infection site	Relative depth (μm)	Number of signals (bacteria)	Tissue area (μm^2)	Average bacteria per mm^3 tissue
1	1	1	0	4	30188	47230
			10	6		
			20	5		
		2	0	13	33275	
			10	8		
			20	4		
		3	0	13	30902	
			10	25		
			20	11		
	2	1	0	3	35421	8041
			10	1		
			20	5		
		2	0	2	47604	
			10	2		
			20	1		
		3	0	3	48650	
			10	2		
			20	1		
	3	1	0	2	28549	13433
			10	1		
			20	0		
		2	0	4	32101	
			10	6		
			20	3		
		3	0	3	30416	
			10	5		
			20	1		

Appendix 3.2 continued

Surfactant concentration (ppm)	Leaf	Infection site	Relative depth (μm)	Number of signals (bacteria)	Tissue area (μm^2)	Average bacteria per mm^3 tissue
1	4	1	0	12	25169	70758
			10	20		
			20	16		
		2	0	24	27613	
			10	17		
			20	9		
		3	0	7	24637	
			10	2		
			20	4		
	5	1	0	7	26829	47115
			10	6		
			20	2		
		2	0	5	26910	
			10	4		
			20	4		
		3	0	25	29696	
			10	17		
			20	11		
	6	1	0	28	26009	66972
			10	16		
			20	8		
		2	0	2	23896	
			10	2		
			20	0		
		3	0	24	23763	
			10	9		
			20	11		

Appendix 3.2 continued

Surfactant concentration (ppm)	Leaf	Infection site	Relative depth (μm)	Number of signals (bacteria)	Tissue area (μm^2)	Average bacteria per mm^3 tissue
10	1	1	0	6	24615	24903
			10	10		
			20	8		
		2	0	3	23638	
			10	1		
			20	2		
		3	0	5	26384	
			10	1		
			20	1		
	2	1	0	4	24154	30356
			10	1		
			20	0		
		2	0	5	23522	
			10	9		
			20	7		
		3	0	4	20788	
			10	6		
			20	5		
	3	1	0	2	24987	20609
			10	2		
			20	1		
		2	0	2	27305	
			10	4		
			20	2		
		3	0	3	22867	
			10	7		
			20	7		

Appendix 3.2 continued

Surfactant concentration (ppm)	Leaf	Infection site	Relative depth (μm)	Number of signals (bacteria)	Tissue area (μm^2)	Average bacteria per mm^3 tissue
10	4	1	0	1	23251	24475
			10	1		
			20	1		
		2	0	6	23273	
			10	4		
			20	4		
		3	0	2	23038	
			10	7		
			20	8		
	5	1	0	8	22847	46320
			10	11		
			20	10		
		2	0	7	22210	
			10	7		
			20	9		
		3	0	6	23193	
			10	3		
			20	2		
	6	1	0	3	24031	33141
			10	2		
			20	3		
		2	0	9	21511	
			10	8		
			20	10		
		3	0	1	22477	
			10	3		
			20	5		

Appendix 3.2 continued

Surfactant concentration (ppm)	Leaf	Infection site	Relative depth (μm)	Number of signals (bacteria)	Tissue area (μm^2)	Average bacteria per mm^3 tissue
100	1	1	0	7	24562	35523
			10	5		
			20	1		
		2	0	4	22871	
			10	1		
			20	0		
		3	0	10	22407	
			10	10		
			20	11		
	2	1	0	11	21431	94884
			10	9		
			20	11		
		2	0	12	21162	
			10	49		
			20	17		
		3	0	6	21404	
			10	4		
			20	2		
	3	1	0	14	24645	133181
			10	26		
			20	11		
		2	0	29	19313	
			10	24		
			20	14		
		3	0	17	23244	
			10	17		
			20	23		

Appendix 3.2 continued

Surfactant concentration (ppm)	Leaf	Infection site	Relative depth (µm)	Number of signals (bacteria)	Tissue area (µm^2)	Average bacteria per mm^3 tissue
100	4	1	0	3	19855	138664
			10	10		
			20	14		
		2	0	25	20226	
			10	19		
			20	12		
		3	0	22	18371	
			10	23		
			20	32		
	5	1	0	6	22501	28887
			10	7		
			20	0		
		2	0	n/a	n/a	
			10	n/a		
			20	n/a		
		3	0	n/a	n/a	
			10	n/a		
			20	n/a		
	6	1	0	7	26546	47731
			10	15		
			20	12		
		2	0	5	26596	
			10	3		
			20	1		
		3	0	12	28923	
			10	13		
			20	11		

Note: Only one infection site could be located in leaf explant number 5.

Appendix 3.2 continued

Surfactant concentration (ppm)	Leaf	Infection site	Relative depth (μm)	Number of signals (bacteria)	Tissue area (μm^2)	Average bacteria per mm^3 tissue
1000	1	1	0	1	27161	12145
			10	6		
			20	2		
		2	0	2	28234	
			10	1		
			20	3		
		3	0	2	27055	
			10	2		
			20	1		
	2	1	0	14	24968	31222
			10	13		
			20	6		
		2	0	2	25089	
			10	6		
			20	2		
		3	0	1	19603	
			10	1		
			20	1		
	3	1	0	8	25039	26601
			10	10		
			20	15		
		2	0	1	24517	
			10	2		
			20	2		
		3	0	1	26951	
			10	1		
			20	0		

Appendix 3.2 continued

Surfactant concentration (ppm)	Leaf	Infection site	Relative depth (μm)	Number of signals (bacteria)	Tissue area (μm^2)	Average bacteria per mm^3 tissue
1000	4	1	0	6	22626	80896
			10	1		
			20	1		
		2	0	34	24621	
			10	25		
			20	21		
		3	0	11	24781	
			10	14		
			20	6		
	5	1	0	47	19379	235096
			10	52		
			20	41		
		2	0	41	20938	
			10	38		
			20	50		
		3	0	6	22202	
			10	6		
			20	4		
	6	1	0	6	22273	76419
			10	5		
			20	3		
		2	0	29	22677	
			10	15		
			20	18		
		3	0	9	22085	
			10	11		
			20	7		

Appendix 3.3 – Infiltrated liquid volume versus infiltration pressure data

Infiltration pressure (kPa)	Pre-infiltration leaf mass (g)	Post-infiltration leaf mass (g)	Infiltrated liquid volume (ml/g leaf)
5	0.0950	0.1020	0.0737
5	0.0769	0.0807	0.0494
5	0.0908	0.0977	0.0760
25	0.0872	0.0886	0.0161
25	0.0871	0.0887	0.0184
25	0.0951	0.0973	0.0231
45	0.0878	0.0888	0.0114
45	0.0925	0.0952	0.0292
45	0.0898	0.0913	0.0167

Appendix 3.4 – Density of attached bacteria versus vacuum infiltration pressure data

Pressure (kPa)	Leaf	Infection site	Relative depth (µm)	Number of signals (bacteria)	Tissue area (μm^2)	Average bacteria per mm^3 tissue	Mean average bacteria per mm^3 tissue	Standard deviation of average bacteria per mm^3 tissue
5	1	1	0	8	27396	47608	38388	8400
			10	7				
			20	4				
		2	0	7	25198			
			10	9				
			20	12				
		3	0	11	28525			
			10	11				
			20	8				
	2	1	0	7	29580	31169		
			10	4				
			20	4				
		2	0	4	33487			
			10	6				
			20	5				
		3	0	7	26227			
			10	9				
			20	8				
	3	1	0	6	25719	36387		
			10	5				
			20	8				
		2	0	6	24724			
			10	7				
			20	3				
		3	0	5	25083			
			10	7				
			20	8				

Appendix 3.4 continued

Pressure (kPa)	Leaf	Infection site	Relative depth (µm)	Number of signals (bacteria)	Tissue area (μm^2)	Average bacteria per mm^3 tissue	Mean average bacteria per mm^3 tissue	Standard deviation of average bacteria per mm^3 tissue
25	1	1	0	43	33904	74545	86310	11430
			10	16				
			20	10				
		2	0	31	35613			
			10	11				
			20	10				
		3	0	14	33764			
			10	10				
			20	9				
	2	1	0	50	31294	97371		
			10	38				
			20	47				
		2	0	20	33120			
			10	10				
			20	4				
		3	0	11	31888			
			10	3				
			20	2				
	3	1	0	10	18981	87016		
			10	9				
			20	4				
		2	0	32	24824			
			10	24				
			20	12				
		3	0	6	19687			
			10	11				
			20	8				

Appendix 3.4 continued

Pressure (kPa)	Leaf	Infection site	Relative depth (μm)	Number of signals (bacteria)	Tissue area (μm^2)	Average bacteria per mm^3 tissue	Mean average bacteria per mm^3 tissue	Standard deviation of average bacteria per mm^3 tissue
45	1	1	0	7	19636	47305	42796	27749
			10	5				
			20	0				
		2	0	11	19655			
			10	10				
			20	11				
		3	0	4	18363			
			10	4				
			20	3				
	2	1	0	2	22523	13069		
			10	3				
			20	4				
		2	0	1	27690			
			10	2				
			20	0				
		3	0	0	25344			
			10	3				
			20	4				
	3	1	0	7	29404	68014		
			10	8				
			20	5				
		2	0	22	26318			
			10	22				
			20	15				
		3	0	11	26751			
			10	10				
			20	10				

Appendix 3.5 – Density of attached bacteria versus density of infiltrated bacteria data

Concentration of infiltrated bacteria (CFU/ml)	Leaf	Infection site	Relative depth (µm)	Number of signals (bacteria)	Tissue area (μm^2)	Average bacteria per mm^3 tissue	Mean average bacteria per mm^3 tissue	Standard deviation of average bacteria per mm^3 tissue
1.00E+08	1	1	0	1	24501	4533	5282	2921
			10	0				
			20	0				
		2	0	2	26120			
			10	1				
			20	1				
		3	0	1	25629			
			10	1				
			20	0				
	2	1	0	3	23296	8504		
			10	2				
			20	2				
		2	0	2	28546			
			10	3				
			20	0				
		3	0	1	28916			
			10	0				
			20	0				
	3	1	0	1	35229	2808		
			10	0				
			20	1				
		2	0	0	32118			
			10	0				
			20	0				
		3	0	2	35807			
			10	1				
			20	1				

Appendix 3.5 continued

Concentration of infiltrated bacteria (CFU/ml)	Leaf	Infection site	Relative depth (µm)	Number of signals (bacteria)	Tissue area (μm^2)	Average bacteria per mm^3 tissue	Mean average bacteria per mm^3 tissue	Standard deviation of average bacteria per mm^3 tissue
1.00E+09	1	1	0	3	25379	10112	21846	24649
			10	1				
			20	0				
		2	0	4	26294			
			10	3				
			20	2				
		3	0	3	28077			
			10	0				
			20	0				
	2	1	0	9	27327	50170		
			10	7				
			20	4				
		2	0	18	28787			
			10	20				
			20	15				
		3	0	3	27447			
			10	4				
			20	5				
	3	1	0	3	27156	5255		
			10	2				
			20	0				
		2	0	1	24484			
			10	0				
			20	0				
		3	0	1	22135			
			10	1				
			20	0				

Appendix 3.5 continued

Concentration of infiltrated bacteria (CFU/ml)	Leaf	Infection site	Relative depth (μm)	Number of signals (bacteria)	Tissue area (μm^2)	Average bacteria per mm^3 tissue	Mean average bacteria per mm^3 tissue	Standard deviation of average bacteria per mm^3 tissue
1.00E+10	1	1	0	92	23559	315008	370332	55523
			10	85				
			20	80				
		2	0	27	27970			
			10	25				
			20	12				
		3	0	80	29980			
			10	55				
			20	36				
	2	1	0	34	23204	369936		
			10	25				
			20	23				
		2	0	63	22271			
			10	66				
			20	42				
		3	0	86	23307			
			10	87				
			20	83				
	3	1	0	119	27086	426051		
			10	130				
			20	102				
		2	0	34	25534			
			10	29				
			20	32				
		3	0	71	25664			
			10	82				
			20	75				

Appendix 3.6 *In planta* GUS activity versus infiltrated bacterial density data from spectrophotometric activity assay

Strain	Infiltrated bacterial density (CFU/ml)	Mass of infiltrated leaves (g)	GUS activity (U/g leaf)
C58C1	1.00E+08	7.17E-02	3.49E-01
C58C1	1.00E+08	6.67E-02	9.35E-02
C58C1	1.00E+08	6.87E-02	5.36E-01
C58C1	1.00E+09	7.23E-02	2.61E-01
C58C1	1.00E+09	7.13E-02	2.85E-01
C58C1	1.00E+09	7.09E-02	7.88E-02
C58C1	1.00E+10	7.18E-02	8.86E-02
C58C1	1.00E+10	6.85E-02	4.82E-01
C58C1	1.00E+10	7.23E-02	4.82E-01
none	0.00E+00	5.82E-02	1.01E-01
none	0.00E+00	5.97E-02	-2.07E-01
none	0.00E+00	6.06E-02	3.89E-01
C58	1.00E+09	5.78E-02	1.82E-01
C58	1.00E+09	6.07E-02	-1.33E-01

Appendix 3.7 – *In planta* GUS activity versus infiltrated bacterial density data from histochemical staining

Concentration of infiltrated bacteria (CFU/ml)	Replicate	Leaf	Expression site	Number of stain regions	Average number of stain regions per mm^2 tissue	Mean average number of stain regions per mm^2 tissue	Standard deviation of average number of stain regions per mm^2 tissue
1.00E+08	1	1	1	44	57.0	48.2	18.2
			2	22			
			3	26			
		2	1	59	70.1		
			2	15			
			3	39			
		3	1	23	37.2		
			2	23			
			3	14			
	2	1	1	20	45.3		
			2	27			
			3	26			
		2	1	22	44.6		
			2	24			
			3	26			
		3	1	32	63.2		
			2	37			
			3	33			
	3	1	1	6	19.8		
			2	9			
			3	17			
		2	1	28	69.4		
			2	44			
			3	40			
		3	1	11	26.7		
			2	15			
			3	17			

Note: all micrographs contained 0.5376 mm^2 leaf tissue.

Appendix 3.7 continued

Concentration of infiltrated bacteria (CFU/ml)	Replicate	Leaf	Expression site	Number of stain regions	Average number of stain regions per mm^2 tissue	Mean average number of stain regions per mm^2 tissue	Standard deviation of average number of stain regions per mm^2 tissue
1.00E+09	1	1	1	51	87.4	57.6	25.3
			2	48			
			3	42			
		2	1	51	84.3		
			2	36			
			3	49			
		3	1	17	31.0		
			2	22			
			3	11			
	2	1	1	18	26.7		
			2	14			
			3	11			
		2	1	29	50.2		
			2	24			
			3	28			
		3	1	21	26.7		
			2	9			
			3	13			
	3	1	1	41	68.2		
			2	32			
			3	37			
		2	1	25	59.5		
			2	38			
			3	33			
		3	1	62	84.3		
			2	47			
			3	27			

Note: all micrographs contained 0.5376 mm^2 leaf tissue.

Appendix 3.7 continued

Concentration of infiltrated bacteria (CFU/ml)	Replicate	Leaf	Expression site	Number of stain regions	Average number of stain regions per mm^2 tissue	Mean average number of stain regions per mm^2 tissue	Standard deviation of average number of stain regions per mm^2 tissue
1.00E+10	1	1	1	31	52.1	76.7	30.6
			2	26			
			3	27			
		2	1	36	64.5		
			2	40			
			3	28			
		3	1	56	109.1		
			2	66			
			3	54			
	2	1	1	26	47.1		
			2	31			
			3	19			
		2	1	17	30.4		
			2	18			
			3	14			
		3	1	40	97.3		
			2	49			
			3	68			
	3	1	1	67	112.2		
			2	72			
			3	42			
		2	1	57	107.3		
			2	55			
			3	61			
		3	1	35	70.7		
			2	35			
			3	44			

Note: all micrographs contained 0.5376 mm^2 leaf tissue.

Appendix 3.7 continued

Concentration of infiltrated bacteria (CFU/ml)	Replicate	Leaf	Expression site	Number of stain regions	Average number of stain regions per mm^2 tissue	Mean average number of stain regions per mm^2 tissue	Standard deviation of average number of stain regions per mm^2 tissue
1.00E+09 (strain C58)	1	1	1	16	18.6	27.0	22.5
			2	9			
			3	5			
		2	1	0	3.1		
			2	1			
			3	4			
		3	1	21	24.8		
			2	6			
			3	13			
	2	1	1	13	19.8		
			2	12			
			3	7			
		2	1	15	38.4		
			2	36			
			3	11			
		3	1	0	0.6		
			2	0			
			3	1			
	3	1	1	26	45.3		
			2	27			
			3	20			
		2	1	4	19.2		
			2	8			
			3	19			
		3	1	52	73.2		
			2	30			
			3	36			